CO_2 Sensor based on Lithium Ion Conductor

Dissertation

Zur Erlangung des akademischen Grades

Doktor der Ingenieurwissenschaften

(Dr. –Ing.)

der Technischen Fakultät

der Christian – Albrechts – Universität zu Kiel

Yongming Zhu

Kiel

2007

1. Gutachter: Prof. Dr. Franz Faupel
2. Gutachter: Prof. Dr. Werner Weppner
3. Gutachter: Prof. Dr. Wolfgang Jäger

Datum der mündlichen Prüfung: 07.06.2007

Acknowledgements

The author would like to express his sincere appreciation to the following for their contribution to this thesis.

I would foremost like to thank my thesis advisor Professor W. Weppner for his constant guidance, support and readiness for stimulating scientific discussions during accomplishment of this work. From the very first ideas to this final version of the text he has been a constant source advise and inspiration. His analytical approach to scientific problems has been essential to make this thesis possible.

I express special thanks to Professor Eckhard Quandt for his kindly support.

I would also thank Dr. W.F.Chu for his assistance in useful discussions and sharing his valuable experience on experimental aspects.

I would like to thank Dr. C. Dietz for his experience on LiSiPO preparation method.

I am also grateful to Dr. V. Thangadurai and Dr. R. Murugan for encouragement and assistance in preparing Garnet.

I would like to thank Dr. M. Sakthivel for his assistance with the SEM investigation.

I want to thank Q. P. Fang and for being always open for technical and general discussions.

I would also like to thank T. Metzing for providing countless technical assistance, and J. Dahmke for her assistance in ICP.

I would like to thank the members of the Sensors and Solid State Ionics group for an excellent atmosphere, and the library team for being always helpful.

I thank my parents and my wife for their continuous moral support and encouragement throughout my studies.

Yongming Zhu

Kiel, June 2007

Contents

1. Introduction……1

1.1 Solid state ionic materials and sensor devices…….…….1

1.2 Objective of the work……5

Reference to Chapter 1……...7

2. Background and present state of the art of electrochemical sensors.8

Reference to Chapter 2…….……12

3. Fundamental theoretical aspects……..15

3.1 Classification of electrochemical gas sensors…….……15

3.1.1 Potentiometric sensors…….……16

3.1.1.1 Type I sensors…….……..16

3.1.1.2 Type II sensors…….…….17

3.1.1.3 Type III sensors……19

3.1.2 Amperometric sensors……..21

3.2 Fundamental aspects of Galvanic Cell…….……..23

3.2.1 Formation of galvanic cell voltages…….23

3.2.2 Galvanic cell current……24

3.3 Solid State Electrolyte……27

3.3.1 Conductivity of major charge carriers (ions)……..28

3.3.2 Conductivity of minority charge carriers (electrons, holes)……29

3.4 Electrode kinetics……...31

3.4.1 Adsorption……34

3.4.2 Charge transfer……35

3.4.3 Diffusion……...36

3.5 Interfaces of electrode-electrolyte……..39

3.6 Impedance spectroscopy…….…….44

3.7 Phase diagrams……..51

3.8 Components of CO_2 sensor……54

3.8.1 LiSiPO and Garnet as electrolyte……54

3.8.2 Li_2CO_3 as gas sensing electrode……..55

3.8.3 Li, $Li_4Ti_5O_{12}$, HgLi, Li_xWO_3, $LiMn_2O_4$, 3PE ($LiMn_2O_4$ - Li_2MnO_3 - $LiMnO_2$) as reference electrodes…….……..56

3.9 Fundamental aspects on electrochemical CO_2 sensors……..59

Reference to Chapter 3…….……..63

4. Experimental aspects……...70

4.1 Measuring apparatus (Kiel Cell)……70

4.2 Preparation of cells and experimental setup……...71

4.3 Experimental methods……79

Reference to Chapter 4…….……...82

5. Results……83

5.1 Performance of CO_2 gas concentration cell……...83

5.1.1 Cell characteristics…….……..84

5.1.2 EMF measurements……..86

5.2 Solid reference electrodes for Potentiometric CO_2 sensor…….…89

5.2.1 Li as reference electrode……..90

5.2.2 $Li_4Ti_5O_{12}$ as reference electrode…….……..92

5.2.3 HgLi as reference electrode……99

5.2.4 Li_xWO_3 as reference electrode……...102

5.2.5 $LiMn_2O_4$ as reference electrode…….106

5.2.6 *3PE ($LiMn_2O_4$ - Li_2MnO_3 - $LiMnO_2$) as reference electrode*……..111

Reference to Chapter 5……..115

6. Discussion……116

6.1 Discussion on the sensing electrode…….…….116

6.2 Discussion on reference electrodes……...121

6.3 Discussion on cell performance……...……..122

Reference to Chapter 6…….……..125

7. Summary and Outlook……...126

7.1 Summary……126

7.2 Outlook……127

List of Symbols…….128

List of Abbreviations……...130

List of Figures……...131

List of Tables……135

Physical constants…….……...136

CHAPTER 1

Introduction

1.1 Solid state ionic materials and sensor devices:

Ionics is the science and technology of the motion of ions alone or together with electrons within the bulk of materials and across interfaces. The phenomenon of ionic transport in solids has been subject of scientific research over many years. At the end of 19th century Warburg and Tegetmeier [1] carried out transference measurements, showing the validity of Faraday's law for solid ionic conductors which also called solid electrolytes. Ionic motion in solids raised interest to scientific studies on understanding the mechanisms of ion transport in solid materials, but also for technological applications of solid electrolytes in galvanic cells. Several ionic conductors have been discovered with electrical conductivity at elevated temperatures comparable to those of liquid electrolytes. The first application of solid electrolytes demonstrated by Nernst [2] making use of zircondioxide in a device known as ´´Nernst Glower´´ whereas at high temperatures the resistance decreased and current could be passed through the material. Due to the passage of current, heat is produced causing a further decrease in the resistance and light is emitted. However, it took long time until the detailed aspects of ionic motion in solids understood well. The combination of knowledge emanating from many scientific fields in order to study the physics and chemistry of materials with ionic motion resulted to study the physics and chemistry of materials with ionic motion resulted to the interdisciplinary field of solid state ionics.

In solid electrolytes the conductivity stems from mobile ions rather than electrons. Typically the conductivity is dominated by one type of ion only. Solid electrolytes already play an important role in commercial gas and ion sensors. In these applications solid electrolytes are used as nonporous membranes separating two compartments containing chemical species at different concentrations on either side. By measuring the potential across such a membrane, one can determine the concentration of the chemical species on one side if the concentration on the other side (i.e., the reference side) is known. In general, we will see that solid electrolytes

allow the quantitative determination of the concentration of those species that are ionically transferred in the electrolyte.

There are some similarities between ionics and electronics since both technologies are based on the local displacement of electrical charges across interfaces which results in electrical fields. While only electrons move in the case of electronics, both electrons and ions move in the case of ionics [3]. The most prominent applications for ionics are:

- Fuel and water electrolysis cells based on solid electrolytes.
- Batteries with high energy and power densities with fast ionically conducting electrolytes and mixed ionically and electronically conducting electrodes for mobile and stationary energy storage.
- Supercaps with high capacities obtained from ionic charge relocations at interfaces between an electrolyte and electronically conducting materials for fast storage and delivery of electrical energy.
- Photogalvanic solar cells with interfaces between ionic conductors and semi-conductors with the generation of electrical fields for the separation of the electron-hole pairs generated by light.
- Chemical sensors for environmental protection and process control for oxygen, CO_x, NO_x etc. based on electrolytes for the direct conversion of partial pressures or concentration of chemical species into electrical signals.
- Electrochromic systems with variable coloration of thin films by the electrochemical variation of the concentration of electronic charge carriers.

In those devices, fast ionic motion in the solid electrolyte is a requirement. The formation of electrical junctions or transitions between materials with different electrical properties is a key aspect for the successful performance of the electrochemical devices. Interfaces in solid ionic galvanic cells are the important regions where the voltage drop occurs while typically the materials bulk is commonly free on internal electrical fields. In this view the performance of the total cell is dependent and may governed by the interfacial processes in a narrow region at the junction electrolyte-electrode. Since at the interface electrolyte-electrode there are various physicochemical phenomena involved, the electrode kinetics is a significant parameter for the overall behavior of the system under real operating conditions. Thus, the electrical performance of electrochemical devices is directly related to appropriate fabrication of junctions between solid electrolytes and electrodes. In ionic devices,

often current is flowing though junctions between materials with different Fermi levels resulting into deviations from the equilibrium state underlying the importance of the system kinetics with respect to the device characteristics.

Gas analysis with electrochemical sensors is a research area of increasing interest. Sensors find large applicability areas such as process plant, environmental and pollution monitoring, military applications, laboratory-based analysis, clinical diagnosis, automotive, indoor air quality (IAQ), aerospace, and agriculture. Overview of the application fields and markets for electrochemical gas sensors are given in [4,5]. The continuous concentration increase of " greenhouse gases" such as carbon dioxide made CO_2 an important target gas. Carbon dioxide gas emitted from automobiles and factories burning coal and hydrocarbons is recognized as a major cause of the global warming of the earth. The atmospheric CO_2 concentration has risen since the industrialization about 30% of its pre-industrial value, and continues to increase even nowadays, enhancing the natural greenhouse effect. European Union has set attention and alarm levels with regard to air pollution monitoring in indoor as well as in outdoor environments. In Germany, the maximum allowable concentration of gases in indoor working environments is given by the index MAK (Maximale Arbeitsplatzkonzentration) which for CO_2 has the value of 5×10^3 ppm [6]. Hence monitoring CO_2 in the atmosphere is important to track the status of the environment. Monitoring CO_2 plays an important role in the storage of fresh agricultural products such as fruits and meats (e.g., Modified Atmosphere Packaging (MAP)). MAP system prevents the drip loss problem and improves the color stability of meat. Moreover, decreased oxygen and increased CO_2 concentrations reduce the respiration rate of fruit. Furthermore, CO_2 plays important role in controlling corrosion rate in chemical processing and carbonation of concrete.

The general principle of electrochemical gas sensors is the direct conversion of chemical energy of the reaction involving species from the galvanic cell and the gaseous species under detection, into electrical energy. Or vice versa, by the application of electrical energies to a galvanic cell forcing the chemical reaction to occur. In both cases, chemical information is directly transduced into electrical information e.g. voltages or currents. The performance of gas sensors is determined by several characteristic variables. In the following, the most considerable variables such as the sensitivity, speed of response, selectivity and choice of electrode material are briefly presented.

Sensitivity to a specific gas is the change of the sensor signal over the change of the concentration of these gaseous species. If the sensor output varies linearly with the concentration of the species under detection, that means obey the Nernst's law, the sensitivity can be calculated from the slope of this line. For potentiometric sensors where typically the voltage varies with the logarithm of the gas partial pressure it is useful to refer the sensitivity to the change of the gas partial pressure by one order of magnitude, thus having units [mV / dec].

The speed of response is also a considerable variable since it may limit the applicability of the sensor device. In potentiometric devices where the output voltage obeys Nernst's law, rapid change in the partial pressure of gas under detection should provide a new voltage value consistent to the Nernst's law in thermodynamic equilibrium. However, in reality a time delay is always observed until the final steady state equilibrium voltage is reached. The response time is a measure of how fast the sensor may respond to the changes in the partial pressure of the detecting gas. The factors contributing to a short response time appear to be [7]:

(a) Rapid transmission of the new chemical potential level across the boundary layer and establishment of local equilibrium at the electrolyte surface;

(b) A high diffusion coefficient of the conducting species in the electrolyte;

(c) A rapid adjustment of the reference electrode to a change in temperature.

The equilibration at the sensing electrode is commonly not rapid and there are several processes involved. A frequently used parameter is the response time t_{90}, which is defined as the time taken to achieve 90% of the final change in the sensor signal upon a variation the gas partial pressure. From a practical point of view it is very useful since complete equilibration may require very long time with quite small signal changes.

The selectivity is a variable indicating ability of the sensor to respond or not on various gaseous species. In many cases it is desirable that the sensor resists to poisoning with other gases, thus remaining sensitive only to the gaseous species under detection. Since electrochemical gas sensors may show cross sensitivities to gases other than those under detection, it is useful to identify how selective is the response of the device to various gaseous species.

Selection of electrode material is essential in many cases because the sensor performance may be improved by choosing appropriate electrode material. The electrode material and morphology should in general be considered at electrochemical

gas sensors, since the electrode reaction determines the sensing characteristics of such a device. Parameters such as composition, microstructure, porosity, particle size and inhomogeneities may lead to localization of the electrode reaction or affect the kinetic behavior of the system.

Beside electrochemical sensors there are also other techniques providing the possibility of gas detection such as infrared analysis, semiconducting oxide sensors and surface acoustic wave sensors. These principles are summarized below.

An alternative method for monitoring gas concentrations is by infrared gas analysis (IR sensors) based on the ability of certain gas molecules to absorb infrared radiation at wavelengths that are characteristic of the chemical structure of the molecule. This method may require complicated electronic systems with often calibrations and is sensitive to small temperature changes.

Semiconducting oxide sensors is another method in which electronic properties such as the resistance of a metal oxide semiconductor material, changes when it is exposed to the target gas. However in this method, the sensor performance depends strongly on the presence of trace impurities and is limited to specific gases.

Surface acoustic wave sensors (SAW), for monitoring atmospheric gases have been also investigated. The principle of operation of SAW sensors is based on the transmission of a periodic deformation across the surface of a piezoelectric material, typically quartz. Changes in frequency of the transmitted wave are monitored as a function of the gas concentration. Disadvantage of this method is the commonly short device lifetime.

The above techniques require in general complicated manufacturing processes in comparison to the electrochemical sensors and are limited to a number of detectable gases. In contrast, electrochemical techniques can be applied in a variety of extreme experimental conditions thus being advantageous for a wide range of applications. Furthermore, electrochemical gas sensors provide directly electrical quantities, which may be easily measured.

1.2 Objective of the work

Objective of the work is the investigation of the interfaces gas – solid and solid – solid (in this work is electrode - electrolyte) in electrochemical gas sensors, especially type III potentiometric sensor, by systematic studies applying

potentiometric principles. Solid electrolytes are employed as membranes, selectively transporting one kind of ionic species, and appropriate solid electrodes are used as sensing and reference electrodes. The kinetics of the interface electrolyte – electrode is of complex nature involving several processes and is of significance regarding the overall behavior of the sensor device leading in many cases to sluggish response times or deviation from thermodynamic equilibrium. The characterization of interfacial kinetics in systems type III sensors should reveal the critical parameters responsible for the electrode kinetics. Furthermore it should be investigated if dynamic measurements combined with a model for the interfacial processes involved may allow to reveal information for the electrical performance of the interface solid – gas under the presence of gaseous species.

In this work, type III potentiometric CO_2 gas sensors based on lithium ion conducting electrolytes were constructed. The structure of the sensor is complex involving solid – solid and solid – gas interfaces. The gaseous species equilibrate with the electrolyte through an intermediate layer, so called gas sensitive layer, which forms a solid – solid interface in contact with the electrolyte. Thus, it is of interest to study potential of electrode materials as gas sensitive layers with regard to the kinetics of the sensing interface. Additionally, a solid reference electrode is establishing a constant reference potential forming another solid – solid interface at the reference side of the electrochemical type III gas sensor. There are ionic junctions with exchange of both electrons and ions across interfaces between solid ionic conductors and mixed ionic – electronically conducting electrodes. To investigate and characterize properly the kinetic behavior of that system, the interfacial properties should be investigated carefully with separate experiments. Additionally, it should be investigated if kinetic processes at the interfaces are responsible for controversies in the results and deviation from thermodynamic equilibrium reported on type III structures for potential detection of carbon dioxide.

References to Chapter 1

[1] E. Warburg, *Wiedemann Ann. Phys.* **21**, 622 (1884); E. Warburg, F. Tegetmeier, *Wiedemann Ann. Phys*. **32**, 455 (1888)

[2] W. Nernst, German Patent 104872 (6 July 1897); *Z. Elektrochem*. **6**, 41 (1899)

[3] W. Weppner, *Ionics*. **9**, 444-464 (2003)

[4] M. J. Madou, S. R. Morrison, ´´Chemical Sensing with Solid State Devices``, Academic Press Inc., San Diego, London (1989)

[5] J. R. Stetter, W. R. Penrose, and S. Yao, *J. Electrochem. Soc.* **150** [2], S11-S16 (2003)

[6] ´´MAK-und BAT-Werte-Liste 1997``, Deutsche Forschungsgemeinschaft, Wiley-VCH (1997)

[7] C.B. Alcock, *Solid State Ionics* **53-56**, 3-17 (1992)

CHAPTER 2

Background and present state of the art of solid state electrochemical sensor

This chapter includes the present state of the art regarding scientific investigations reported in literature for the solid state electrochemical sensors, electrochemical type III sensors for possibility of CO_2 detection and cells which use lithium ion systems.

Chemical sensors have been widely used in such applications as critical care, safety, industrial hygiene, process control, product quality controls e.g. In these applications, chemical sensors have resulted in both economics and social benefits. The range of detection for sensors can be percent levels in process streams with O_2 sensors to single molecule or unique organism detection with carbon nanotubes.

Solid electrolyte sensors are typically designed to operate at high temperature and can operate in either a potentiometric or amperometric mode. An example of a potentiometric sensor is the well known yttria-stabilized zirconia (YSZ) based oxygen sensors that have been widely used for air/fuel ratio control in internal combustion engines. The sensor response is described by the Nernst equation at equilibrium. Over the past ten years, two potentiometric designs have evolved: surface-modified solid electrolyte gas sensor [1-3] and mixed potential gas sensors [4,5]. In the former, the surface of a solid electrolyte is coated with an auxiliary phase which will react electrochemically and reversibly with the analyte and generate an interfacial potential. Sensitivity and selectivity to the analyte are provided by the auxiliary phase, e.g., the Na_2CO_3/NASICON system can be used for CO_2 sensing because the carbonate can introduce the electrochemical reaction:

$$CO_3^{2-} = CO_2 + \frac{1}{2}O_2 + 2e^- \tag{2.1}$$

This approach allows the use of several conventional ceramic solid electrolyte, including YSZ, β-alumina, or NASICON to construct sensors for many gases [6-8] especially the environmental gaseous pollutants. An important advantage of this approach is the development of detection methods that survive harsh conditions where typical liquid electrochemical sensors would be inappropriate.

In a mixed potential sensor design [6-8] more than one electrochemical reaction takes place at the electrodes so that a mixed potential is established by competing reactions. The catalytic activity of the electrode material is particularly important, e.g., the Pt/YSZ/Au sensor can measure CO and hydrocarbons due to the difference in catalytic activities between the Pt and Au electrodes.

CO_2 sensors which contain galvanic solid electrolyte cell have been offered commercially since about 1998 [9-11]. The devices with CO_2 sensors developed until now show considerable differences in their structure and properties. In several papers on galvanic solid electrolyte cells for CO_2 measurement, earlier recommended systems have been discussed [12-16]. In 1977, Gauthier and Chamberland [17] showed the possibility to measure CO_2 concentrations with solid electrolyte cells, using the hygroscopic K^+ conductor K_2CO_3. However, detailed investigations did not lead to a stable reference with silver [18]. The K^+ conductivity could be increased considerably by admixture of $SrCO_3$. With composites of Na and Ba carbonates, solid electrolytes were obtained which were gastight, not hygroscopic and suitable for long term stable CO_2 concentration cells [19,20]. Equipment with such cells is, however, awkward and expensive, and the necessary gastight separation of the electrode chambers only lasts if the cell is kept constantly at the operational temperature. With the investigations of Maruyama et al. [21,22,23] the development of CO_2 sensors using NASICON or β-alumina started in 1987. For CO_2 measurements in reducing gaseous phases, gas concentrations cells were used, in which NASICON served as a Na^+ membrane between electrodes with Na_2CO_3 [21,22]. An essential simplification was reached with an arrangement [23] without dependence of the signals on the O_2 partial pressure, in which the alkali oxide activity in the NASICON or β-alumina at the interface with the reference electrode should serve as a stable basis for measurement. Sensors of this type were prepared with thick and thin film techniques [24]. It was tried to reduce the drifting of the signals of these planar sensors by covering the reference electrode with glass. However, the preparation, particularly with melting process, led to quite different Na_2O activities in the reference electrodes. In addition, the signals were dependent on the O_2 partial pressure again. Non-stoichiometric phases like Na_xCoO_{2-y} yield reference potentials dependent on x and y [25].

Long term stable signals that follow an easily calculable thermodynamic relation were expected for a sensor with liquid sodium as the reference substance [26]. However, apart form the problems of handling liquid sodium and evaluating the resulting signal, which is very high compared to the changes caused by variation of the CO_2 concentration, a side reaction to give Na_2O_2 interferes and the dependence on the O_2 partial pressure was unfavorable as well. Alloys of sodium were also checked [27].

It was tried repeatedly to make sensors in which stabilized ZrO_2, an oxide ion-conducting solid electrolyte, is sandwiched between the electrodes and carbonate, NASICON or β -alumina. The quite different results of the different authors are based on the reactions at the interfaces between the anion and cation conductors that were used. These reactions depend on whether the cation conductor covers the anion conductor in a gastight manner or is porous and thus the interface is exposed to the gas which surrounds the sensor. A third case is present when the same gas surrounds the contact between the ion conductors and the electors on the oxide ion conductor. The gas sensitivity of the contacts between a potassium and an oxide ion conductor was already recommended for the measurement of SO_x and CO_2 and discussed in papers from 1978 to 1985 [28,29,30,31].

Recent years several studies report the utilization of lithium ion compounds used in CO_2 gas sensors. Miura [32] have studied the electrode reaction in electrochemical cells with MSZ electrolytes coated with pre – molten Li_2CO_3 auxiliary phase. The authors considered the possible formation of an intermediate layer at the sensing interface acting as an ionic bridge. Zhang [33] employed Li_2CO_3 – Li_3PO_4 – $LiAlO_2$ solid electrolytes for lithium ions, in contact with two phase $LiCoO_2$ – Co_3O_4 or one phase pure $LiCoO_2$ solid reference electrodes. The electromotive force of such cells was found to vary logarithmically with the CO_2 partial pressure in CO_2 – O_2 gas mixtures at temperatures between 350 – 400 °C, with response times in the order of 1 min at 400 °C. The cell voltage was reported to decrease with time during long term experiments when pure $LiCoO_2$ was used as reference. Kim [34] investigated the characteristics of electrochemical cell with Li_2CO_3 – Li_3PO_4 – Al_2O_3 electrolytes and $LiMn_2O_4$ solid reference electrode. The cell sensitivity to CO_2 was found to be in agreement with the calculated one in the carbon dioxide range from 10^2 ppm to 10^4 ppm above 350 °C, and a small effect in the sensing behavior was

observed when water vapor was present in the gas phase. Schäf [35] concluded that a metastable phase is formed at the reference side of electrochemical cells with Li^+ conducting ceramics as electrolytes and Li_2CO_3 as sensitive auxiliary electrode. The reproducibility of the cell signal employing different solid electrolyte glasses was found to be within 30 mV at 600 °C. Li^+ ion conducting electrolytes such as lithium phosphorous oxynitride ($Li_{2.88}PO_{3.73}N_{0.14}$) [36] and $LiTi_2(PO_4)_3 + 0.2Li_3PO_4$ [37] are also used in CO_2 sensors.

Reference to chapter 2

[1] W.Weppner, in *Proceedings of the Second IMCS*, 59 (1996)

[2] N.Yamazoe and N.Miura, *Solid State Ionics* **86-88**, 987 (1996)

[3] W.Göpel, G.Reinhardt, and M.Rosch, *Solid State Ionics* **136-137**, 533 (2000)

[4] N.Miura, G. Lu and N.Yamazoe, *Solid State Ionics*, **136-137**, 533 (2000)

[5] R.Mukundan, E.L.Brosa, D.R.Brown and F.H.Garzon, *Electrochem. Solid-State Lett.*, **2**, 412 (1999)

[6] S.Yao,Y.Shimizu, N.Miura and N.Yamazoe, *Chem. Lett.,* 2033 (1990)

[7] S.Yao, Y.Shimizu, N.Miura and N.Yamazoe, *Chem. Lett.,* 587 (1992)

[8] H.Aono and Y.Sadaoka, *J.Electrochem.Soc.,* **147**, 4363 (2000)

[9] C.Voit, *Elektron Ind* **11**, 56-61 (2000)

[10] Figaro, Figaro Engineering, Mino.Osaka, Japan (2002)

[11] Zirox, Zirox Sensoren & Elektronik,Greifswald, Germany (2002)

[12] J. Maier, *Solid State Ionics* **62**, 105-111 (1993)

[13] J. Maier, M.Holzinger, W.Sitte, *Solid State Ionics* **74**, 5-9 (1994)

[14] M.Holzinger, J.Maier, W.Sitte, *Solid State Ionics* **86-88**, 1055-1062 (1996)

[15] H.H.Möbius, P.Shuk, W.Zastrow, *Fresunius J. Anal. Chem*., **356**, 221-227 (1997)

[16] V.Brüser, W.Klingner, H.H.Möbius, U.Guth, *Proc. Sensor 97*, **III**, 209-214 (1997)

[17] M.Gauthier, A.Chamberland, *J.Electrochem. Soc.,* **124** 1579-1583 (1977)

[18] F.Barwisch, Thesis, University of Greifswald (1984)

[19] S.Brosda, Thesis, University of Greifswald (1992)

[20] N.Miura, S.Yao, Y.Shimizu, N.Yamazoe, *J.Eletrochem. Soc.,* **139** 1384-1388 (1992)

[21] T.Maruyama, X.Y.Ye, Y.Saito, *Solid State Ionics* **23** 113-117 (1987)

[22] T.Maruyama, X.Y.Ye, Y.Saito, *Solid State Ionics* **24** 281-287 (1987)

[23] T.Maruyama, X.Y.Ye, Y.Saito, *Solid State Ionics* **23** 107-112 (1987)

[24] W.F.Chu, D.Fischer, H.Erdmann, M.Ilgenstein, H.Köppen, V.Leonhard, *Solid State Ionics* **53-56**, 80-84 (1992)

[25] H.Schettler, J.Liu, W.Weppner, R.A.Huggins, *Appl.Phys.* **A57** 31-35 (1993)

[26] J.Liu, W.Weppner, *Eur. J.Solid State Inorg. Chem.,* **28** 1151-1160 (1991)

[27] W.Weppner, Proc. Sensor 93, **VI** 65-72 (1993)

[28] M.Gauthier, A.Belanger, M.Y.Kleitz, Solid-state potentiometric gauges for gaseous species. Academic Press, New York, 497-517 (1978)

[29] M.Kleitz, A.Pelloux, M.Gauthier, New types of solid-electrolyte gas sensors. Elsevier North-Holland, Amsterdam, 69-73 (1979)

[30] A.Belanger, M.Gauthier, D.Fauteux, *J.Electrochem. Soc.,* **131**, 579-586 (1984)

[31] H.H.Möbius, Proc. Int. Symp.Syst.Fast Ionic Transport, Smolenice, CSSR. CSTVS, Bratislava, 26-30 (1985)

[32] N.Miura, Y.Yan, S.Nonaka and N.Yamazoe, *J.Mater.Chem*. **5** [9], 1391-1394 (1995)

[33] Y.Zhang, H.Tagawa, S.Asakura, J.Mizusaki and H.Narita, *J. Electrochem. Soc.* **144** [12], 4345-4350 (1997)

[34] D.Kim, J.Yoon, H.Park and K.Kim, *Sensors and Actuators* **B** 76, 594-599 (2001)

[35] O.Schäf, *Ionics* **2**, 274-281 (1996)

[36] C.Lee, S.A.Akbar and C.O.Park, *Sensors and Actuators* B **80**, 234 (2001)

[37] G.Adachi and N.Imanaka, in Proc. Symp'on Chemical Sensors II*, J. Electrochem. Soc.*, Vol 93, p. 182 (1998)

CHAPTER 3

Fundamental theoretical aspects

3.1 Classification of electrochemical gas sensors

The general principle of electrochemical gas sensor is the direct conversion of chemical energies from reaction between the gas and another phase into an electrical energy, or the application of electrical energies to force a chemical reaction to occur. It is thus a common feature of all-solid-state electrochemical sensors that the measuring quantities are of electrical nature, voltages or currents. However, the specific characteristics of each one of those vary with the sensor structure and sensing principle. It is therefore necessary to distinguish them into smaller groups with common characteristics. They may be primary divided into potentiometric devices operated under open circuit voltage conditions and amperometric devices where current is flowing through the cell. The various branches of electrochemical gas sensors are schematically shown in figure 3.1.

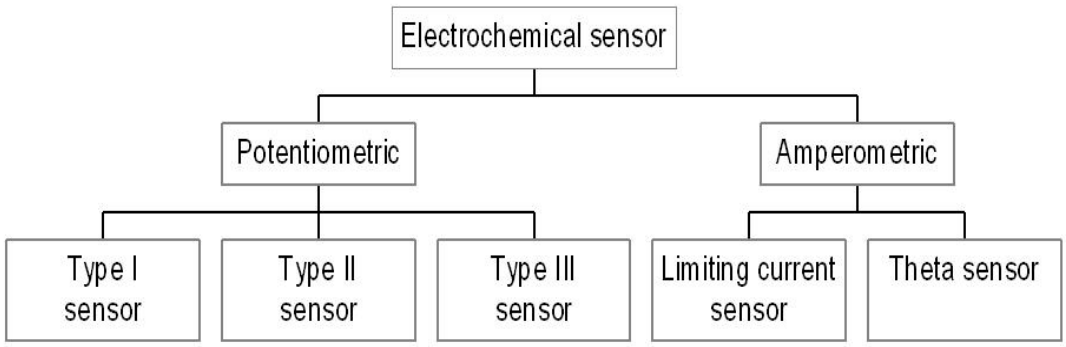

Figure 3.1: Schematic representation of the classification of electrochemical gas sensors.

3.1.1 Potentiometric sensors

A fundamental classification of potentiometric electrochemical gas sensors into three categories was made by Weppner [1]. Depending on the type of interfaces employed for sensing, the sensor can be separated into type I, type II and type III. In potentiometric sensors of any of these types, an equilibrium potential drop at the

electrode – electrolyte interfaces is being related to the activity or partial pressure of species under detection. The sensor output voltage is proportional to the logarithm of partial pressure of gas to be detected. The essential aspects of type I, type II and type III sensors will be analyzed in the following sections.

3.1.1.1 Type I Sensors

Main characteristic of type I sensors is that the gas equilibrates with the mobile component in the electrolyte. The most well known example of type I gas sensors is the ´ *λ – probe* ´ that is used as an oxygen sensor for automobile exhaust control. The name ´ *λ – sensor* ´originates from the shape of the voltage versus fuel to air ratio, in a Nernst electrochemical cell where the reference electrode exposed to ambient air and the measuring electrode to the exhaust gas of a gasoline engine [2]. Sensors of this type take advantage of the equilibration of the gas with the ionic conductor that conducts ions of the neutral species to be measured. The potential difference between the two electrodes is given by Nernst's law:

$$E = \frac{kT}{zq} \ln\left(\frac{P_A^{(l)}}{P_A^{(r)}}\right) \tag{3.1}$$

Where $P_A^{(l)}$ and $P_A^{(r)}$ the partial pressure of the gaseous species under detection at the left and right hand side, respectively. k is Boltzmann's constant, T the absolute temperature, z the charge number of the mobile ions A and q the elementary charge. According to equation (3.1) if the reference gas partial pressure is kept constant the sensor output quantity (voltage) is proportional to the logarithm of partial pressure of the gas to be measured. The structure of type I gas sensors is schematically shown in figure 3.2.

The gas equilibrates with the electrolyte, and the chemical potential of electrons is measured at an inert metallic probe on the surface of the electrolyte, since only electrons may be exchanged across the interface. The exchange of electrons across the interface between the solid electrolyte and the electrode is similar to the semiconductor-metal junction. Beside the lambda probe, other examples of type I sensors are gauges for hydrogen [3-5], for Cl_2 [6] and for NO sensing [7].

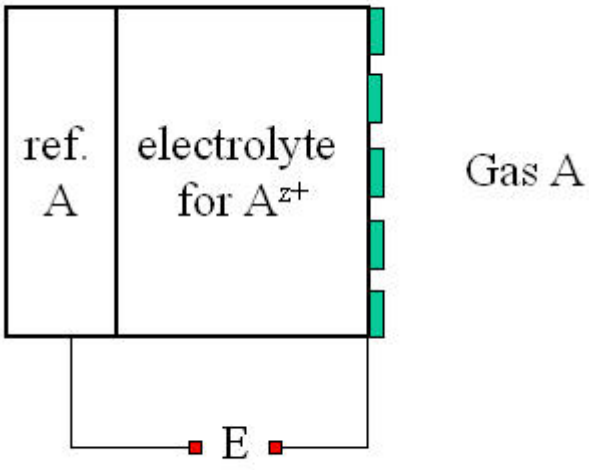

Figure 3.2: Schematic arrangement of a type I gas sensor for measurement of the partial pressure of gas A.

3.1.1.2 Type II sensors

In type II electrochemical gas sensors, the gas equilibrates with a component of the electrolyte that is different from the predominantly mobile species. That is the principal characteristic of type II sensors, and main difference to type I electrochemical gas sensors. An advantage in comparison with the type I sensors is that it avoids the problem that for detecting species A_i an electrolyte conducting those species has to be known and employed. Thus, it expands the applicability of solid electrolytes to the possibility of detection of complex gases. Across the interface between the electrode and the electrolyte only electrons are exchanged establishing thermodynamic equilibrium. The cell assembly of a type II gas sensor employing an electrolyte conducting A^{z+} for the measurement of partial pressure of gas B is showing in figure 3.3. The gas equilibrates with the immobile species of the electrolyte and the chemical potential of electrons is measured at an inert metal on the surface of the electrolyte. Since what is measured is the chemical potential of electrons at the interface between the electrolyte and the electrode, it is not relevant which type of ions is mobile within the ionic conductor.

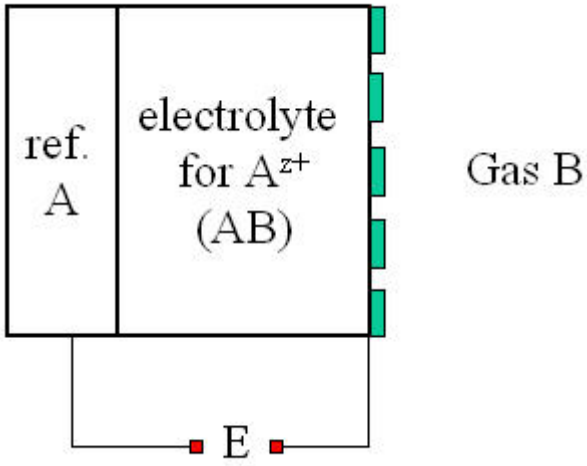

Figure 3.3: Measurement of the partial pressure of gas B employing a type II gas sensor.

Rather, an additional equilibrium is established between the measured immobile and mobile component according to the Duhem-Margules relationship:

$$SdT - VdP + \sum_i n_i d\mu_i = 0 \qquad (3.2)$$

Where S, T, V, n_i and μ_i are the entropy, temperature, volume, total pressure, number of species i and chemical potential of the neutral component i, respectively. At typical experimental conditions of constant total pressure and temperature equation (3.2) reduces to the following:

$$\sum_i n_i d\mu_i = 0 \qquad (3.3)$$

Relationship (3.3) includes all chemical components of the electrolyte. The absolute values of the chemical potentials of all neutral components i are related by Duhem - Gibbs equation through the Gibbs energy G of the electrolyte.

$$G = \sum_i n_i \mu_i \qquad (3.4)$$

Assuming an electrolyte with N independent components, that requires equilibration with N-1 gases. The relationship between the gas partial pressures and the open circuit voltage is obtained by solving Duhem - Gibbs equation for the standard Gibbs energy of formation of the electrolyte from the pure elements (a_j = 1), for the measurable activity of the electroactive component i. Inserting this expression into Nernst's law for a reference electrode of defined activity a_i^{ref} of the mobile component, provides:

$$\Delta G_f^0 = kT\sum_j n_j \ln a_j \tag{3.5}$$

$$E = -\frac{kT}{n_i z_i q}\left[\frac{\Delta G_f^0}{kT} - \sum_{j\neq i} n_j \ln a_j - n_i \ln a_i^{ref}\right] \tag{3.6}$$

An example of type II sensors is the application of AgBr solid ionic conductor for silver ions to the detection of Br_2 gas [8] where according to what discussed above, bromine gas equilibrates with the immobile component of the electrolyte. Other investigations in type II electrochemical gas sensors involve studies on for O_2 [9], SO_2 [10-12], SO_x [13-17], Cl_2 [19] and CO_2 [20] sensing.

3.1.1.3 Type III sensors

Limitations of type I or type II gas sensors are that materials with specific electrical properties at the desired operating temperatures have to be employed, this may be overcame by the concept of type III gas sensors [21]. In this approach, the gas is being equilibrated with the solid electrolyte through an auxiliary phase on top of the electrolyte. The auxiliary phase should preferably be a mixed ionic-electronic conductor and must contain both the mobile species of the solid electrolyte and the species to be detected. This layer is being used instead of a metallic contact with the electrolyte and forms an ionic junction with the solid ionic conductor allowing the equilibration of both mobile ions and electrons across the interface. Thus, in contrast to type I and type II sensors, both ions and electrons are exchanged across the electrode - electrolyte interface in type III sensors.

The formation of ionic junction is the main feature of type III gas sensors allowing to expand the number of gaseous species that may be detected with type I or type II sensors. Gas species may be detected with a type III electrochemical gas sensor even if they are not included as either mobile or immobile components of an electrolyte. Figure 3.4 shows schematically the arrangement of a type III gas sensor where the gas C equilibrates with an additional auxiliary phase AC containing the mobile species of the electrolyte. The gas C may in general be also a complex one composed of more than one atomic constituent. The chemical potential of species A is measured at the reference electrode remains constant. Application of Duhem - Gibbs equation and Nernst's law for the mobile component results in the following relation for response to gas C in the case of an electrolyte for the mobile electroactive component A [22]:

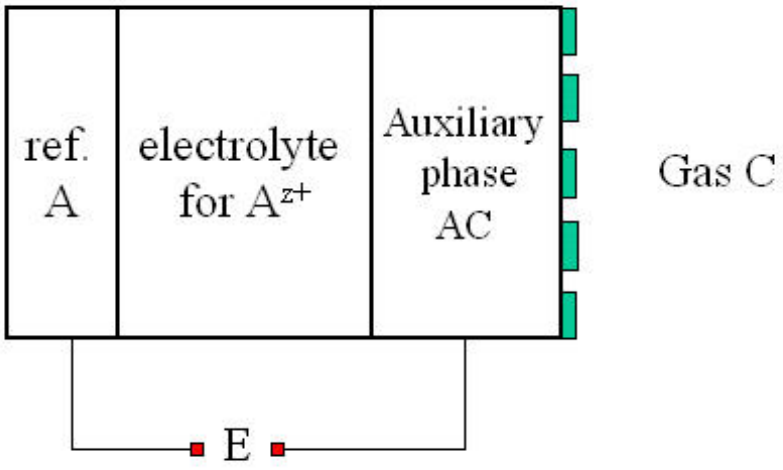

Figure 3.4: Schematic arrangement of a type III gas sensor for the measurement of partial pressure of gas C.

$$E = \frac{kT}{zqd}\ln p_C^g \sum_{p=1}^{k-1}(-1)^{p+1} n_{pC} d_{pA} - \frac{1}{zqd}\sum_{p=1}^{k-1}(-1)^{p+1}\Delta G_{f,p}^0 d_{pA} + \frac{kT}{zq}\ln a_A^r \qquad (3.7)$$

Where the sum runs over all k-1 solid phases p. The determinant formed by the stoichiometric numbers n_{ij} of the ith phase and the jth component excluding those stoichiometries of the gaseous species B denoted as d. The minor formed by eliminating the column of the stoichiometries of the mobile component A and the pth row of the determinant d, denoted as d_{pA}.

$$d = \begin{vmatrix} X_{11} & X_{12} & \dots & X_{1k} \\ X_{21} & X_{22} & \dots & X_{2k} \\ & & & \\ X_{k1} & X_{k2} & \dots & X_{kk} \end{vmatrix}, \qquad d_{pA} = \begin{vmatrix} X_{11} & \dots & X_{1A} & \dots & X_{1k} \\ X_{21} & \dots & X_{2A} & \dots & X_{2k} \\ & & & & \\ X_{p1} & \dots & X_{pA} & \dots & X_{pk} \\ & & & & \\ X_{k1} & \dots & X_{kA} & \dots & X_{kk} \end{vmatrix}$$

An example of type III sensors is the measurement of oxygen partial pressure at significantly lower temperatures than conventionally required by type I oxygen

sensors [23]. Other investigations on type III sensors involve studies for the possibility of detection of complex gases such as NO_x [23-25], Cl_2 [26-27], CO_2 [28-37] and SO_2 [38-39].

3.1.2 Amperometric sensors:

Instead of measuring potential differences under open circuit conditions, partial gas pressures may be also determined by measuring currents under the application of appropriate voltages in electrochemical cells. The major practical importance of passing currents through solid state galvanic cells used for gas sensors lies in the chance to control or influence the kinetics and therefore the cell reaction. Amperometric electrochemical gas sensors can be mainly divided into limiting – current and kinetic $\theta - sensors$.

Limiting current sensors were originally introduced in combination with liquid electrolytes using various types of membranes such as Teflon [40]. With respect to selectivity, it turned out to be very successful to use a membrane that limits the access of the gas to the electrolyte. This step is assumed to be controlled by diffusion:

$$J_i = -\tilde{D}_i \, dc_i / dx = -\tilde{D}_i \, \Delta c_i / d \tag{3.8}$$

where Δc is the concentration difference across the membrane of thickness d and $\tilde{D}$ is the effective diffusion coefficient. Each type of gaseous species has a distinct diffusion coefficient $\tilde{D}_i$ in the membrane. If a voltage is applied to the electrolyte in such a way that the concentration of the mobile component decreases more and more between the electrolyte and the membrane, the current may not increase any more above a certain voltage limit. The applied voltage has produced such a small concentration compared to the gas that the concentration difference may be considered to be constant. With the knowledge of the diffusion coefficient $\tilde{D}_i$ and the thickness d, it is thus possible to determine the concentration in the gas independent of the type of reference electrode. The principle is schematic illustrated by figure 3.5. One example of the limiting – current is the application of tetragonal zirconia polycrystal electrolytes to the detection of oxygen gas [41]. An additional ceramic disc with a small hole in it, limits the access of oxygen to the solid electrolyte and the current is controlled by gas diffusion through the barrier of the diffusion hole.

Accordingly, the current is linearly related to the oxygen partial pressure within the limiting current plateau regime. The other example is the measurement of chlorine partial pressure employing this principle on electrochemical cells with $Ag-\beta^{"}-$ alumina electrolytes [42]. Limiting current sensors may be operated under lower temperatures [43] but generally have smaller detection ranges than the potentiometric ones.

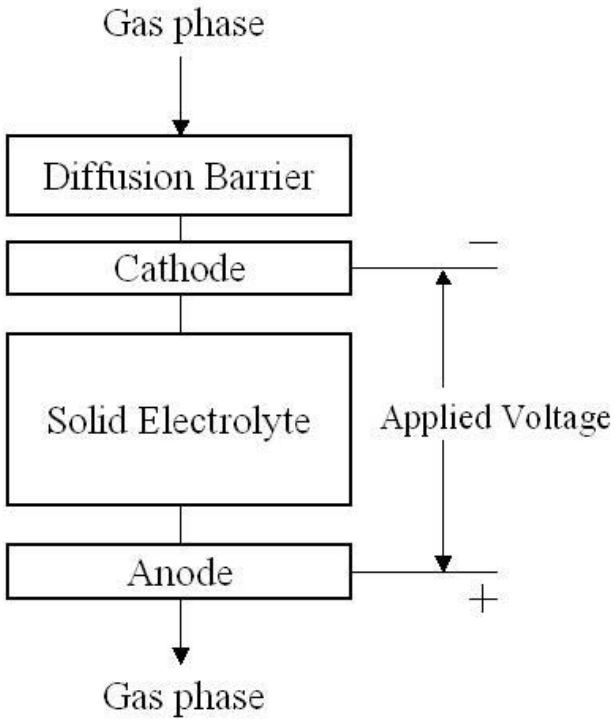

Figure 3.5. Principle of the limiting-current sensor.

The $\theta-sensor$ concept [44] for the detection of gas species, based on kinetic principles and utilizes a periodical with time electrical perturbation applied to the electrochemical system. This method may allow to overcome several problems of the potentiometric sensors such as cross sensitivities to species other than the datable ones. The advantages of this technique in comparison to other sensing principles was also discussed by E.D.Tsagarakis [45].

3.2 Fundamental aspects of Galvanic Cell

3.2.1 Formation of galvanic cell voltages

The application of a voltmeter even with very high input impedance (electrometer) requires a small current. A chemical reaction will occur in the galvanic cell by the transfer of the ions. The chemical energy of this process at constant total pressure and temperature, the Gibbs energy of reaction, ΔG_r, corresponds to the electrical work that accompanies the electrical current:

$$\Delta G_r = -nqE \tag{3.9}$$

where n,q, and E are the number of charges that are transferred for the reaction, the elementary charge, and open-circuit cell voltage (emf), respectively. The charge of the Gibbs energy with the number of atoms in the electrodes corresponds to the chemical potential μ of this component. Accordingly, the transfer of ions A^{z+} corresponds to the cell voltage

$$E = \frac{1}{zq}(\mu_A^l - \mu_A^r) \tag{3.10}$$

l and r stand for the left- and right-hand electrodes, respectively. The chemical potential μ may be written in terms of the activity a or the equilibrium partial pressure p_A,

$$\mu_A = \mu_A^0 + kT \ln a_A = \mu_A^0 + kT \ln p_A \tag{3.11}$$

μ^0, k, and T are the chemical potential in the standard state, Boltzmann's constant, and absolute temperature, respectively. Substitution of Equation (3.11) into (3.10) results in

$$E = \frac{kT}{zq} \ln \frac{a_A^l}{a_A^r} = \frac{kT}{zq} \ln \frac{p_A^l}{p_A^r} \tag{3.12}$$

The voltage is determined by the reaction that really occurs by the application of the voltmeter.

3.2.2 Galvanic Cell Current

If an electric current is forced or permitted to pass through the galvanic cell, the partial current density i_n of any species n (ions A^{z+}, electrons e, holes h) is, in general, proportional to the overall transport force acting upon that species. If the transport is isothermal and involves no volume change, we can neglect all but chemical and electrostatic forces. Correlations with the fluxes of other particles may also often be neglected [46]. The proportionality constant between the current and the electrochemical potential gradient is given by the partial electrical conductivity σ_n,

$$i_n = -\frac{\sigma_n}{z_n q}\frac{\partial \eta_n}{\partial x} \tag{3.13}$$

where η_n is the electrochemical potential of species n which is composed of an electrostatic potential ϕ and a chemical potential μ_n contribution according to the relation

$$\eta_n = \mu_n + z_n q \phi \tag{3.14}$$

The conductivity σ_n may be written in terms of the product of the concentration c_n and the diffusivity D_n of the mobile species n [47]:

$$\sigma_n = \frac{c_n D_n z_n^2 q^2}{kT} \tag{3.15}$$

where D_n is the diffusivity, which is related to the electrical mobility u_n or the general mobility b_n by the Nerst-Einstein relation [47] regardless of whether the material may be considered to be an ideal or a nonideal solution:

$$D_n = u_n \frac{kT}{|z_n| q} = b_n kT \tag{3.16}$$

This quantity describes the random motion of species n in the absence of concentration gradients. It is related to the tracer diffusion coefficient $D_{Tr,n}$, which is determined by the use of radioactive isotopic tracers according to $D_{Tr,n} = f D_n$, where f is the correlation factor or, more generally, the Haven ratio [48].

With the help of Equations (3.11), (3.14), and (3.15), Equation (3.13) can be cast into the form:

$$i_n = -\sigma_n \frac{\partial \phi}{\partial x} - z_n q D_n \frac{\partial \ln a_n}{\partial \ln c_n}\frac{\partial c_n}{\partial x} \tag{3.17}$$

The first term of the right-hand side is Ohm's law for the migration of species n under the influence of an electrical field. The second term is Fick's first law for

diffusion under the influence of a concentration gradient. Equation (3.17) holds in general for isothermal conditions and is valid at any position in a galvanic cell, assuming that there is no volume change and no other forces are involved in the transport, e.g., correlation effects.

Equation (3.17) holds both in electrolyte phases, in which the transport of change is primarily due to the motion of ionic species, and in mixed ionic and electronic conducting electrode phases. In most cases of interest one may assume that practically useful ionic conductors in galvanic cells are characterized by a very large concentration of mobile ionic defects. As a result, the chemical potential of the mobile ions may be regarded as being essentially constant within the material. Thus any ionic transference in such phases must be predominantly due to the influence of an internal electrostatic potential gradient:

$$i_{ion(electrolyte)} = -\sigma_{ion} \frac{\partial \phi}{\partial x} \tag{3.18}$$

On the other hand, for the electronic species, which may be considered to be comparatively dilute in an electrolyte, the concentration gradient is the more important driving force.

A different situation holds in the case of electrodes that transport both electrons and ions, but predominantly electronic species. In that case the chemical potentials of the electrons or holes may be regarded as practically independent of location within the solid, due to their high concentrations. Thus, their transport is primarily due to the effect of an internal electric field in such materials. Because of the large concentrations as well as the high mobilities, this field will be very small.

If an ionic flux occurs across an electrode/electrolyte interface in connection with the current flow by the motion of ions in the electrolyte, the ionic transport within the electrode material must be predominantly determined by the presence of a local ionic concentration gradient:

$$i_{ion(electrode)} = -z_{ion} q D_{ion} \frac{\partial \ln a_{ion}}{\partial \ln c_{ion}} \frac{\partial c_{ion}}{\partial x} \tag{3.19}$$

The ´´thermodynamic`` factor $\frac{\partial \ln a_{ion}}{\partial \ln c_{ion}}$ (which is a special case of the Wagner factor, as described later) is sometimes very large and enhances the ionic flux above that which would be expected from the concentration gradient alone. In a predominantly electronic conductor in which the concentrations of electrons or holes

are very large, i.e., the chemical potentials of the electronic species are essentially uniform throughout the material, the gradients of the chemical potentials of neutral atoms and their respective ions are identical. The transport of ions may be considered to be the same as the net transport of neutral species in this case.

If an electrode material is not overwhelmingly an electron or hole conductor, the internal electric field may not be completely neglected with regard to the movement of ions. The transport of ionic species occurs under the combined influence of electrostatic and chemical potential gradients. This situation can be expressed by an equation similar to Equation (3.19) by replacing $\frac{\partial \ln a_{ion}}{\partial \ln c_{ion}}$ by the more general Wagner factor W [49]:

$$i_{ion(mixedconductor)} = -z_{ion} q D_{ion} W \frac{\partial c_{ion}}{\partial x} \tag{3.20}$$

The total charge transport within a solid (especially in an electrode) may be composed of several partial currents whose relative contributions vary with position. In the external circuit only the total current that is passed through the overall cell may be observed. However, an electrolyte serves as an ion-pass filter and only ionic species can cross phase boundaries between electrodes and such an electrolyte. Since under steady-state conditions the ionic current must be continuous, the total externally measurable current must be equal to the partial ionic current, as expressed in Equation (3.20), within the electrode material just at the interface.

It is possible that the most mobile ions within the electrolyte are not those that are predominantly transferred in the electrode. In such a case, the overall cell current is given by Equation (3.20) when it is written in terms of the ionic species that are most mobile in the electrode phase.

3.3 Solid state electrolyte

Ionic transport under an applied field takes place to some extent in all ionic solids but generally comprises the movement of ions into vacant sites over substantial energy barriers that result in very low mobilities, even at high temperatures. Certain materials, known as ´´fast-ion conductors´´, ´´solid electrolytes´´ or ´´superionic conductors´´, exhibit higher ionic mobilities and have opened up the possibility of practical applications. In most cases, these applications require that the electronic

conductivity should be at least an order of magnitude less than the ionic conductivity. In solid electrolytes, one component of the structure, cationic or anionic, is not confined to specific lattice sites but is essentially free to move throughout the structure. Solid electrolytes are, therefore, intermediate in structure and property between, on the one hand, normal crystalline solids with regular three-dimensional structures and immobile atoms or ions and, on the other, liquid electrolytes which do not have regular structures but do have mobile ions. Often solid electrolytes are stable only at high temperatures. At lower temperatures they may undergo a phase transition to give a polymorph with a low ionic conductivity and a more usual type of crystal structure (Fig.3.6).

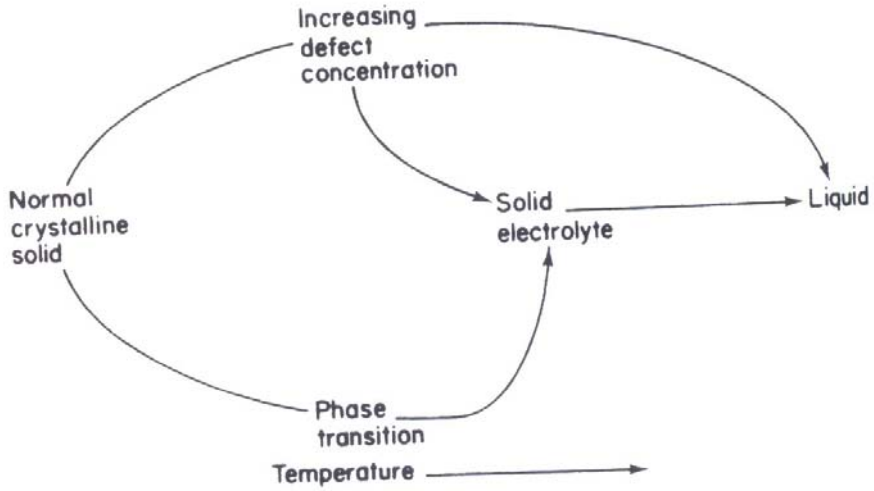

Fig 3.6: Solid electrolytes as intermediate between normal crystalline solids and liquids [50].

The motion of ions in solid state materials occurs because of imperfections of the crystalline lattice, so called crystal defects. Lattice defects may be point defects also called zero-dimensional defects, edge or screw dislocations also called one-dimensional defects, grain boundaries or surfaces also called two-dimensional defects, and cavities also called three-dimensional defects. The formation of thermally activated point defects in ionic crystals is mainly accomplished via the Schottky and the Frenkel mechanisms. In the first one mechanism, ionic motion occurs by the motion of vacancies (Schottky defects) which are missing particles from lattice positions. In the second one mechanism, electrical charge is transported by the motion of interstitial species (Frenkel defects) which are particles additional to the ideal

crystal. In solid materials with more than one mobile species，the conductivities are discussed by following:

3.3.1 Conductivity of majority charge carriers (ions)

The ionic conductivity in an electrolyte with negligible electronic conduction may be determined by using Ohm's law, provided that nonpolarizable reversible electrodes are employed which allow unimpeded delivery of the mobile ions on one side and their removal on the other side. To overcome the limitation, separate voltage probes, in the form of identical electronic leads connected to the electrolyte at positions separated by a distance L, are employed. Under these conditions the ionic conductivity is given by

$$\sigma_{ion} = -\frac{iL}{E} \tag{3.21}$$

This technique is called the four-point dc technique [51]. An alternative that may be used to overcome polarization problems is the use of alternating current techniques using a wide range of frequencies, commonly from 10^{-2} to 10^{+6} Hz. This technique (impedance spectroscopy) is discussed in detail elsewhere (section 3.6).

The identity of the mobile ionic species may be determined in simple cases from the changes in the mass of the ionic sink and source electrodes after a defined charge-flux through the cell. Electrodes must be used that are able to exchange all potential ionic species involved in the transport within the solid ionic conductor. If one species dominates the total charge transport, Faraday's law can be used to relate the mass change $|\Delta m|$ of either one of the electrodes per unit time and unit current by

$$\frac{|\Delta m|}{\int Idt} = \frac{A}{|z|F} \tag{3.22}$$

where A is the atomic weight of the particles transferred as ions of charge z through the electrolyte. The atomic weight divided by the charge number relates to the mobile species.

3.3.2 Conductivity of Minority Charge Carriers (electrons, holes)

In spite of the small electronic conductivity in a practically useful solid electrolyte, electrons and holes are responsible for many materials properties. For example, electronic conductivity acts as an internal short circuit within a galvanic cell, thus reducing the energy available to do useful work in an external circuit. In addition, electronic conductivity reduces the cell voltage. Furthermore, the transport of electrons or holes controls the rate of equilibration of the composition within an electrolyte, since the condition of local charge flux neutrality requires equivalent amounts of different charged species to be transported within the solid.

The minority electronic properties of solid electrolytes may vary considerably with changes in composition. It is therefore often necessary to study the minority charge carrier transport as a function of the activity of the components. Because no current is allowed to pass through the external electric circuit, the charge neutrality condition demands that the current densities i_n of the different kinds of species n, i.e., all ions, electrons, and holes, are electrically compensated by each other:

$$\sum_n i_n = 0 \tag{3.23}$$

substitution of Equation (3.13) for the current densities and making use of the equilibrium relation between ion, neutral atoms, and electrons, $\mu_A = \eta_{A^{z+}} + z\eta_{e^-}$, integration over the length of the electrolyte yields the following equation for the difference in the electrochemical potentials of the electrons between the two electrodes:

$$E = \frac{1}{q}\sum_{ions}\frac{1}{z_n}\int_{electrolyte} t_n d\mu_n \tag{3.24}$$

where μ_n is the chemical potential of the neutral species n.

In general, one has to assume that the ionic transference number is strongly dependent on the chemical potential of the components. The transference numbers of the species n may be determined as a function of their activities from the change in the cell voltage with the variation of the chemical potential of the neutral n-th component at one electrode while all other chemical potentials are held constant. Differentiation of Equation (3.24) with regard to the upper limit of the integral, μ_n^r, yields

$$t_n(\mu_n^r) = -z_n q \frac{\partial E}{\partial \mu_n^r} \tag{3.25}$$

while in the experiments described so far both ionic and electronic species are transferred, it is also possible to determine the partial electronic conductivity by using ionically blocking electrodes to suppress the ionic transport so that only electrons and holes can pass. This technique is known as the asymmetric polarization or Hebb-Wagner technique [52, 53]. By using a chemically inert electronic conducting material, no ions will be delivered to the electrolyte when a voltage is applied with such a polarization that the mobile ions tend to be depleted at the inert electrode. An electrode used on the other side fixes the chemical potential of the mobile component of the electrolyte by the applied voltage at that phase boundary.

If the electrolyte has large ionic disorder and since the blocked ionic current i_{ion} is zero, Equation (3.13) and (3.14) indicate that no gradient can exist in the electrostatic potential within the sample. Then the steady-state transport of electrons and holes occurs only due to diffusion under the influence of gradients in their concentrations. These gradients must be uniform if the diffusion coefficient does not depend markedly on the concentration. From Equation (3.10) and (3.11) and the ionization equilibrium, the cell voltage determines the ratio of the activities of the electronic species at both sides of the electrolyte:

$$E = \frac{kT}{q} \ln \frac{a_e^r}{a_e^l} = -\frac{kT}{q} \ln \frac{a_h^r}{a_h^l} \tag{3.26}$$

integration of the diffusion part of the general transport over the length L of the sample, differentiation of the result with regard to the lower limit of the integral, $\ln a_e^r$, and consideration of equation (3.26) yields

$$\frac{di}{dE} = -\frac{1}{L}(\sigma_e^r + \sigma_h^r) \tag{3.27}$$

this equation allows the determination of the total electronic conductivity $\sigma_e^r + \sigma_h^r$ within the electrolyte adjacent to the interface with the inert electrode. The corresponding chemical potential of the electroactive component at that location is given by the cell voltage according to Nernst's equation. Thus, by varying the applied voltage, $\sigma_e + \sigma_h$ may be obtained as a function of the component activities or the composition of the sample. Usually, the electronic conductivity depends significantly

upon the cell voltage because of changes in the defect concentration within the material. In certain potential ranges either the hole or the electron conductivity may be dominant. Then σ_e or σ_h may be studied separately as a function of the composition.

The relation between the current and the voltage in a dc polarization experiment may be obtained by assuming that ratios of the activities of electrons and holes can be replaced by ratios of their concentrations. Such an assumption is valid up to concentrations of about 10^{19} particles per cubic centimeter. Then, integration of Equation (3.27) (assuming that the diffusion coefficients of electrons and holes are concentration independent) yields

$$i = \frac{kT}{qL}\{\sigma_e^r\left[1-\exp\left(\frac{Eq}{kT}\right)\right]+\sigma_h^r\left[\exp\left(-\frac{Eq}{kT}\right)-1\right]\} \tag{3.28}$$

Equation (3.28) includes one term that approaches a plateau of the current and another term shows an exponential increase of the current with increasing voltage. The relative contributions depend on the magnitudes of the prefactors which are the partial conductivities at the activity imposed by the reversible electrode. The shape of the log (current) vs. voltage curves allows one to determine the type of minority charge carriers and to derive their conductivities from the plateau value and the intersection with the log (current) axis of the extrapolated straight line.

3.4 Electrode kinetics

The processes, applications and characterization at electrodes were discussed in this subchapter. The electrode processed considered are charge transfer and diffusion limitation. The applications of electrodes are presented for both current-carrying contacts and voltage probes.

Electrodes can serve as current-carrying contacts or as voltage probes where the total current vanishes. Current-carrying electrodes introduce into or remove from a sample, in general, both electric charge and material. When the material is supplied from the gas phase an auxiliary conducting material must also be present on the surface to supply or remove electrons. (an exception is when the surface is electronically conducting.) For example, the introduction of oxygen into the solid electrolyte, Y_2O_3-doped ZrO_2 (YSZ, or yttrium-stabilized zirconia), in the form of

ions can be achieved by using, as electrodes, porous platinum layers applied onto the YSZ.

The transfer of material and charge at the electrodes can consist of a series of elementary processes. Each one may include the motion of neutral species (molecules, atoms, or neutral point defects), or the motion of charged species (ions, charged point defects, electrons, or holes). The path for the motion of the species occurs within single phases, parallel to phase boundaries, and across interface, following kinds of electrodes are commonly considered:

- Reversible Electrode

  Electrodes are defined as reversible ones if they transfer electrons and ions with negligible impedance. Then also under current, the electrochemical potential of electrons, μ_e, and ions, μ_i, do not change across the different interfaces which may exist in an electrode. As a result, the chemical potential of the neutral species is also constant across the interface.

- Irreversible Electrodes

  Plates of inert metals such as platinum, gold and graphite serve in solid state electrochemical cells to supply electrons to the sample, but block the passage of material and ions for voltages below the thermodynamic decomposition voltage of the SE. The ionic current is blocked since the metals do not contain the required material that can provide the ions. In addition, the metal blocks are applied in a way that blocks the exchange of material with, e.g., the surrounding atmosphere, as well. Not only inert metal can serve for that purpose, but also any electron conductor, whether metal or semiconductor, that stays chemically intact and is impermeable to the material flow either in the form of ions or neutral species. One important use of ion-blocking electrodes is in selective measurements of the partial electronic conductivities of mixed ionic-electronic conductors.

  Electrodes that transmit ions and block electrons are SEs. In the ideal case they exhibit an infinitely high resistance to electronic current. Then the electronic current through the SE vanishes. Contrary to common belief, the voltage drop on the blocking electrode need not be equal, in the general case, to the applied voltage [54].

From a microscopic point of view, there are several-kinetic processes occurring at the electrolyte – electrode interface. Of great importance for electrochemical gas

sensors are the processes occurring at the solid – gas interface where interaction of species from the gas ad the solid phases is taking place. Therefore, the kinetic properties of this interface in an electrochemical cell for gas detection will depend on the presence of the specific gas on the surrounding. Specific adsorption of gas at the electrode surface, surface of bulk diffusion and charge transfer across the interface are kinetic processes involved in the sensing mechanism in an all-solid state sensor. Fast electrode kinetics may accelerate the equilibration process on the sensing electrode but on the other hand side slow kinetics may have the opposite effect, namely hindering the electrode reaction thus slowing down the equilibration of the gas with the solid. A comprehensive analysis of the various processes involved is therefore essential on understanding the kinetics of the solid – gas interface. These processes may be described in a phenomenological way by governing equations and therefore allowing evaluation of the kinetic parameters for the interface under investigation. This may also permit the identification of the possible kinetic rate determining steps at the interface solid – gas in electrochemical gas sensors.

3.4.1 Adsorption

Adsorption is the process of particle attachment to a surface, which may be generally regarded as a reaction process between the free sites at the electrode surface and the adsorbed gaseous species. It can be accomplished in two ways [55], by physisorption and chemisorption. The first one associated with weak long range Van der Waals dipole-dipole interaction forces between the adsorbate and the adsorbent. In the second one, the molecules or atoms stick to the surface by forming a strong chemical bond. The reverse process of adsorption may also occur, known as desorption. The fundamental phenomenological problem of adsorption has been treated by Langmuir [56] and Wagner [57].

There are various adsorption isotherms depending on the assumptions being made. The most common used one is the so called Langmuir adsorption where all surface sites are assumed to be equivalent between each other composing a uniform surface, The equilibrium between the bulk and the surface established by the formation of one monolayer, thus the adsorption can not proceed beyond monolayer surface coverage. Additionally, in Langmuir adsorption the interactions between the adsorbed particles are neglected. A useful parameter is the fraction of the surface covered by the

adsorbate, denoted as θ. For a completely covered surface θ equals to unity while for a completely uncovered surface is θ is zero. The surface fraction which is free from adsorbate is therefore $(1-\theta)$. The rate of reaction in adsorption, namely the rate of change of the surface coverage can be written in absolute rate theory in the case of non dissociative adsorption, and considering the adsorption of one type pf species:

$$\upsilon_{ad} = \frac{d\theta}{dt} = k_{ad} c(1-\theta) \tag{3.52}$$

Analogously for the rate of desorption we may write:

$$\upsilon_{des} = -\frac{d\theta}{dt} = k_{des}\theta \tag{3.53}$$

In equilibrium, the adsorption and desorption rates in equations (3.52) and (3.53) are the same, yielding for the equilibrium coverage:

$$\frac{\theta_0}{1-\theta_0} = K_C \tag{3.54}$$

$$\text{Whereas: } K = \frac{k_{ad}}{k_{des}} \tag{3.55}$$

Complex gas molecules may dissociate into their fragments. For dissociativ adsorption of a diatomic molecule the rates of adsorption and desorption are:

$$\upsilon_{ad} = \frac{d\theta}{dt} = k_{ad} c(1-\theta)^2 \tag{3.56}$$

$$\upsilon_{des} = -\frac{d\theta}{dt} = k_{des}\theta^2 \tag{3.57}$$

The equilibrium coverage results by equalizing adsorption and desorption rates:

$$\frac{\theta_0^2}{(1-\theta_0^2)} = K_C \tag{3.58}$$

The adsorption process is generally of importance with respect to the performance of electrochemical gas sensors. It may commonly involve several individual steps as the adsorption of carbon dioxide and oxygen on the surface of a type III electrochemical carbon dioxide sensor:

$$
\begin{aligned}
&O_{2,g} \leftrightarrow 2O_{ad} \\
&2O_{ad} + 2e^{-} \leftrightarrow 2O_{ad}^{-} \\
&CO_{2,g} \leftrightarrow CO_{2,ad} \\
&CO_{2,ad} + 2O_{ad}^{-} \leftrightarrow CO_{3,ad}^{-2} \\
&CO_{2,ad} + O_{ad}^{-} + e^{-} \leftrightarrow CO_{3,ad}^{-2}
\end{aligned}
\tag{3.59}
$$

3.4.2 Charge transfer

Charge transfer is the rate-determining step at low current densities. In a reversible interface and under thermodynamic equilibrium equal number of ion are neutralized and formed at unit surface area per unit time. These two processes are in dynamic equilibrium between each other establishing thermodynamic equilibrium at the interface. When an interface is not at equilibrium e.g. with current flowing trough it, the potential of the electrode is induced. Species that have to cross an interface have to overcome the energy barrier at the interfacial region resulting from the presence of an electrical field. The activation energy barrier at the interface depends on the potential difference across the interface, which is generally different from the equilibrium one. Under conditions of charge transfer control, the current density as a function of the electrode potential is given by the Butler-Volmer equation [58] which for both anodic and cathodic reaction currents involved, takes the form:

$$
I = I_0 \left[\exp\left(\frac{\alpha z F \eta}{RT} \right) - \exp\left(-\frac{(1-\alpha) z F \eta}{RT} \right) \right] \tag{3.60}
$$

Where I_0 is the exchange current density, α the transfer coefficient $(0 < \alpha < 1)$, and η the charge transfer overpotential. Two limiting cases of the equation (3.60) can be distinguished, a low overpotential and a high overpotential limit. For low overpotentials $|\eta| << \frac{RT}{zF}$, equation (3.60) can be expanded using the Taylor-MacClaurin expansion, therefore in this case holds:

$$
I = I_0 \frac{zF}{RT} \eta \tag{3.61}
$$

It is seen from this relationship that the current density varies linearly with the overpotential, similarly to the Ohm's law and its independent from the transfer

coefficient. In this view, the proportionality constant in (3.61) is defied as the charge transfer resistance:

$$R_{ch-tr} = \frac{d\eta}{dJ} = \frac{RT}{J_0 zF} \tag{3.62}$$

On the other limit, for high cathodic overpotentials, $|\eta| >> \frac{RT}{zF}$ holds:

$$I = -I_0 \exp\left(\frac{(1-\alpha)zF\eta}{RT}\right) \tag{3.63}$$

Taking the logarithm in this relationship we get:

$$\ln I = -\ln I_0 + \frac{(1-\alpha)zF\eta}{RT} \tag{3.64}$$

This relationship indicates that plotting $\ln J$ against the overpotential η provides in the high overpotential limit a straight line with slope of $\frac{(1-\alpha)zF}{RT}$ which is called Tafel slope.

3.4.3 Diffusion

The first treatment of a flux of particles in a concentration gradient has been carried out empirically by Fick in 1855 [59] proposing that the particle flux is proportional to the concentration gradient. In pure diffusion the molecules or ions move from a region of high concentration to a region of low concentration. For an isotropic diffusion coefficient D_i that may be expresses as:

$$\vec{J}_i = -D_i grad c_i \tag{3.65}$$

Where $\vec{J}_i$ is the number of particles i crossing a unit are perpendicular to the direction of $\vec{J}_i$ in unit time, and c_i the number of particles i in unit volume. The negative sign indicates that the flux is in opposite direction to the concentration gradient. In solid systems commonly the flux is within one dimension, thus equation (3.65) may be written for a particle flux over the x-axis:

$$J_x = -D\frac{\partial c}{\partial x} \tag{3.66}$$

Equation (3.66) is useful evaluating the current flowing through the interface electrolyte-electrode in electrochemical systems with diffusion as dominant. When current is flowing through an electrochemical cell, diffusion processes occurring at the electrode-electrolyte interface correspond to the motion of mobile species within the electrode just inside the phase boundary with the electrolyte (x=0), thus creating concentration gradient. According to (3.66) the current is:

$$I = zFAD(\frac{\partial c}{\partial x})_{x=0} \tag{3.67}$$

where A is the area of the electrolyte-electrode interface.

Equation (3.65) known as Fick's first law. It provides information for the spatial variation of the particle concentration. The variation of particle concentration with time is given by Fick's second law. For one dimensional diffusion with concentration independent diffusion coefficient D, this can be written as:

$$\frac{\partial c(x,t)}{\partial t} = D\frac{\partial^2 c(x,t)}{\partial x^2} \tag{3.68}$$

where time t and distance x are independent variables. Equation (3.68) may therefore utilize to describe particle concentration changes with time and distance within an electrochemical cell. It is a partial differential equation involving order partial derivative with respect to time and second order partial derivative with respect to distance. Solution of this equation requires therefore one initial and two boundary conditions for the concentration c=c (x, t). Depending on how suitable these conditions are, solution of (3.68) may be relative simple, but it can also be rather complicated requiring the application of numerical methods. Solutions of this equation for a variety of initial and boundary conditions are given by Crank [60]. A statistical approach for the diffusion problem incorporating the concept of particle mean square displacement in the so called random walk model is discussed by [61]. In a type III sensor the equilibration process includes the diffusion of electroactive species within the modifying compound [62].

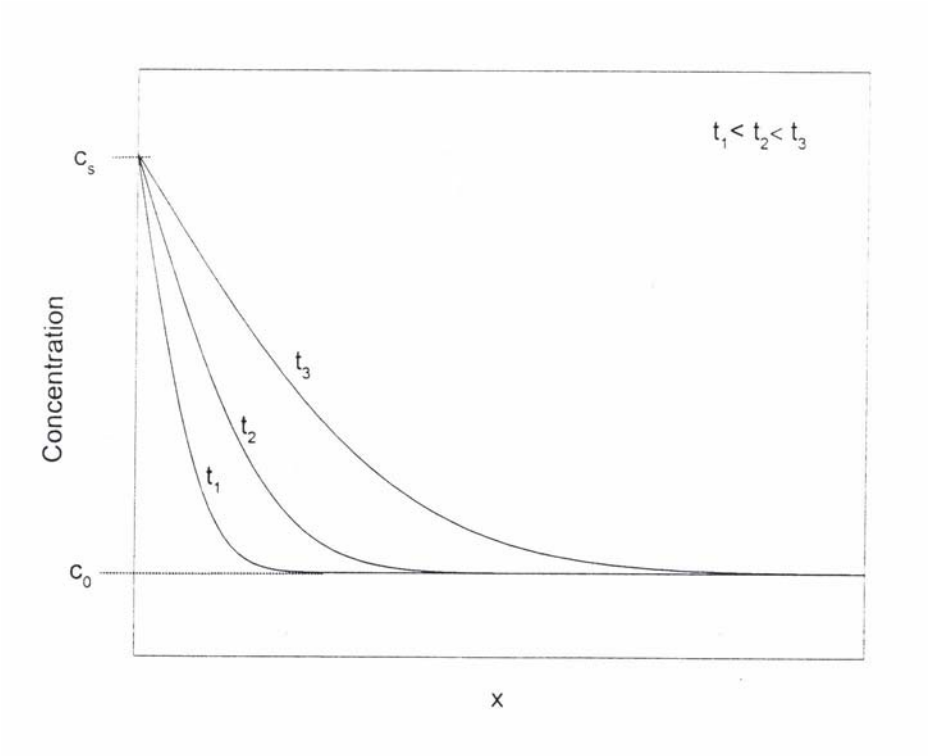

Figure 3.7: Concentration profiles according to the solution of diffusion equation subjected to the conditions given above.

Ignoring backward diffusion effects, the diffusion of one electroactive species within the modifying compound may be mathematically described by the diffusion equation (3.68) under the following conditions:

Initial condition:

$$t = 0, x \geq 0 : c = c_0 \tag{3.69}$$

Boundary conditions:

$$t > 0, x = 0 : c = c_s \tag{3.70}$$

$$t > 0, x \to \infty : c = c_0 \tag{3.71}$$

Solution of the diffusion equation satisfying the conditions (3.69)-(3.71) can be obtained by application of the Laplace transformation [60]:

$$\frac{c - c_0}{c_s - c_0} = erfc\left(\frac{x}{2\sqrt{Dt}}\right) \tag{3.72}$$

Where $erfc\left(\frac{x}{2\sqrt{Dt}}\right)$ is the complementary error function of $\frac{x}{2\sqrt{Dt}}$. Figure 3.7 shows concentration profiles of the electroactive component at different times, according to solution (3.72).

3.5 Interfaces of electrode-electrolyte

Electrolytes have a definite voltage range of stability in a galvanic cell before they are decomposed by electrolysis in which one component is oxidized, the other reduced, provided the electrodes themselves remain inert in this voltage range. These voltage limits can be controlled by the solvent itself, which may be oxidized at the anode instead of the anion and/or be reduced at the cathode instead of the cation. The electrodes behave beyond these limits like a capacitor with a definite capacity for the storage of electric charge. This capacitive behavior can be studied by polarizing an inert electrode in contact with a suitable electrolyte in a galvanic cell, the potential being measured vs. a reference electrode. The main information pertaining to capacities comes from such experiments, which are summarized in the following.

The simplest model is that of a plate capacitor developed very early by Helmholtz [63]. The idea is that the ions of the electrolyte, which form the excess charge there, can approach the metal surface only up to the distance of the radius which includes the inner salvation sphere in liquid solutions. Measurements of the differential capacity of smooth electrodes yielded values for the Helmholtz double-layer capacity, C_H, on the order of 20 to 30 μF cm^{-2}. The model of a plate capacitor gives for the differential capacity

$$\frac{\partial Q}{\partial \Delta\varphi} = C_H = \frac{\varepsilon_H \cdot \varepsilon_0}{d} \tag{2.43}$$

where Q is the charge in C cm^{-2}, ε_H the dimensionless dielectric constant relative to vacuum, ε_0 the permittivity in vacuum ($\varepsilon_0 = 8.85 \times 10^{-14} CV^{-1}cm^{-1}$), and d the distance between the plates in centimeters. For d $\approx$ 2x10^{-8} cm, the capacity is $C_H \approx \varepsilon_H \times 4.4 \mu F$ cm^{-2}. The effective dielectric constant therefore has to be on the order of 5 to 7. That ε_H is much smaller than in the bulk of the electrolyte solution is reasonable, since the molecules of the salvation shell are oriented and no solvent layer exists between the ion and the metal surface, except when the solvent molecules strongly adsorb thereon. In such a case, however, these molecules will also be oriented and much less polarizable than in the bulk of the solution. Assuming a variability of ε_H and a variability of d, depending on the field strength in the double

layer, which changes the orientation of the polar molecules and can distort the salvation shell or even break up part of it, this crude model can to some extent explain the dependence of C_H on the voltage applied. The real situation is, however, much more complex in the molecular picture, and still open to debate.

It has been observed that the capacity is usually larger on the branch where the metal has a positive excess charge than on the negative branch. There are two reasons for this behavior. On the positive branch, the counter ions are anions which have a larger radius and a more weakly bound salvation shell. They will come closer to the interface at higher positive field strength by losing part of their salvation shell. Cations have less distortable salvation shells, and their distance should remain less affected by the field strength. Another effect with consequences in the same direction is connected with the excess charge distribution on the metal. The negative charge of electrons extends somewhat over the last layer of the positive atomic nuclei, the more the higher the negative excess charge. The repulsive forces between these electrons and the solvent or ion molecules increase the average distance of the counter charge from the surface. On the positive branch, the electrons are drawn back into the bulk while the nuclei remain fixed [64]. The counter ions can come closer to the surface, and the capacity increases. Aside from such effects, the dipole formed between the surface electrons and the ionic atom cores varies also with the potential, and this can contribute considerably to the differential capacity in some potential ranges [65].

The adsorption of specific ions from the electrolyte has an important influence upon the charge distribution in the double layer. Such ions, which are stabilized in solution by a salvation shell, can lose part of their salvation shell and come into direct contact with the metal surface. This happens when the adsorption forces overcompensate the loss of interaction energy with the solvent molecules. The counter ions will remain at a larger distance from the surface and can form part of the opposite charge if the charge of the adsorbed ions is not fully compensated by the excess charge on the metal.

The amount of adsorbed ions varies with the voltage applied. The adsorption of anions increase with positive excess charge on the metal and is completely suppressed at some critical negative excess charge on the metal. Cations behave in the opposite way. The differential capacity increases if specific ion adsorption contributes to the charge distribution across the interface. The quantitative relations are very complex because the local position of the adsorbed ions and structure of their remaining

solvation shell varies with the field strength in the inner Helmholtz double layer. In addition to this, a partial charge transfer between the ions and the metal is often connected with the adsorption which is equivalent to the formation of a polar bond between adsorbed ions and the metal surface. The amount of charge transfer (or the dipole moment of the adsorption bond) also varies with the field strength. The quantitative interpretation of capacity data is therefore in such cases extremely model dependent, and is not discussed her in more detail.

Another situation which can be analyzed more clearly is important for the understanding of the electrode interface. This is a contact to an electrolyte with a small concentration of mobile ions as in dilute electrolyte solutions. In this case, the counter charge in the electrolyte cannot be represented by a layer of ions in the outer Helmholtz plane, but extends over some distance into the space of the electrolyte. The reason is that the accumulation of the excess charge in the Helmholtz double layer leads to a relatively large local increase in the concentration which, in turn, exerts a chemical driving force for back diffusion into the bulk of the electrolyte. Therefore, the excess ions and with it the electric field extend into the bulk until the electric and chemical forces are balanced. This situation was analyzed by Gouy [66] and by Chapman [67]. Stern [68] combined their ideas with the Helmholtz model. His model is represented by two capacitors in series.

In this model, it is assumed that the space of the extension of the Helmholtz double layer, d, with the averaged dielectric constant ε_H is free of charge while the counter charge Q balancing the surface charge Q_M on the metal is in the diffuse layer $x \geq d$.

$$Q = \int_{\infty}^{d} \rho(x)dx = -Q_M \tag{2.44}$$

the charge distribution in this layer is controlled by a combination of the Poisson equation and the Boltzmann distribution function

$$\frac{d^2\varphi}{dx^2} = -\frac{1}{\varepsilon\varepsilon_0}\rho(x) \tag{2.45}$$

$$\rho(\varphi) = e_0\left[z^+ N_c^0 \exp\left(-z^+ e_0\varphi / kT\right) - z^- N_a^0 \exp\left(-z^- e_0\varphi / kT\right)\right] \tag{2.46}$$

where z^+ and z^- are the charges of the cations and anions, N_c^0 and N_a^0 are their concentrations per cubic centimeter in atomic units, and e_0 the elementary charge. Electroneutrality requires

$$z^+ N_c^0 = z^- N_A^0 \tag{2.47}$$

The charge distribution in the diffuse double layer can be calculated from the Poisson-Boltzmann model explicitly for the case $z^+ = z^- = z$. For asymmetric electrolytes the solution of these differential equations requires numerical methods. For the simpler case above where $N_c^0 = N_a^0 = N^0$, the relation between charge density and potential, Equation (2.46), becomes

$$\rho(\varphi) = -2ze_0 N^0 \sinh(ze_0\varphi / kT) \tag{2.48}$$

Integration of Equation (2.45) with the charge density of Equation (2.48) yields a connection between the excess charge Q in the space charge layer and the field strength at x=d

$$-\varepsilon\varepsilon_0 \int_{\infty}^{d} \frac{d^2\varphi}{dx^2} dx = -\varepsilon\varepsilon_0 \frac{d\varphi}{dx} dx \Big|_{x=d} = \int_{\infty}^{d} \rho(x) dx = Q \tag{2.49}$$

After some transformations one obtains

$$Q = \left(\varepsilon_s \varepsilon_0 kTN^0\right)^{\frac{1}{2}} 4 \sinh\left(\frac{ze_0}{kT}\varphi_d\right) = -Q_M \tag{2.50}$$

with $\varphi_d = \varphi(x = d)$

It is possible to calculated the local distribution of φ in the space charge layer by a second integration of $d\varphi / dx$ up to φ_d, but this cannot be checked by direct measurements. However, the relation between space charge and differential capacity can be derived form this model and gives a tool to compare measurements with the theory.

The potential drop between the metal and the bulk of the electrolyte is $\Delta\varphi = \Delta\varphi_H + \Delta\varphi_d$ according to the model. $\Delta\varphi_H$ is determined by

$$\Delta\varphi_H = \frac{Q_M}{\varepsilon_H \varepsilon_0} d \tag{2.51}$$

and $\Delta\varphi_d = \varphi_d$ is related to Q by Equation (2.50).

The differential capacity is

$$C = \frac{dQ_M}{d\Delta\varphi} \tag{2.52}$$

which can be related to Equation (2.50) and (2.51) by

$$\frac{1}{C} = \frac{d\Delta\varphi_H}{dQ_M} + \frac{d\Delta\varphi_d}{dQ_M} = \frac{1}{C_H} + \frac{1}{C_d} \tag{2.53}$$

One sees that the capacity can be represented by a series of two capacities, the Helmholtz capacity $C_H = \varepsilon_H \times \varepsilon_0 / d$ and a capacity of the diffuse layer $C_d = dQ_M / d\Delta\varphi_d$

$$C_d = 2\left(\frac{\varepsilon_s \varepsilon_0 N^0}{kT}\right)^{\frac{1}{2}} ze_0 \cosh\left(\frac{ze_0}{kT}\Delta\varphi_d\right) \tag{2.54}$$

C_d has a minimum for $\Delta\varphi_d = 0$ or Q_M=0.

$$_{\min} C_d = 2ze_0\left(\frac{\varepsilon_s \varepsilon_0 N^0}{kT}\right)^{\frac{1}{2}} = 1.5\times 10^{-9} z\sqrt{\varepsilon N^0}\,\mu F \cdot cm^{-2} \tag{2.55}$$

Since the capacity of the diffuse double layer is in series with the Helmholtz double layer, the best chance to see it in the measurements requires $C_d \le C_H$. Equation (2.50) and (2.54) indicate that C_d increases rapidly with Q_M. In accordance with this conclusion, a minimum of the differential capacity was found in measurements on metals in very dilute electrolyte solutions, which is an indication for the absence of excess charge on the electrode, provided that there is also no specific adsorption of ions.

The description of the double layer properties by the Stern-Gouy model is a very crude one. A very weak point is the assumption that the dielectric contact suddenly changes from that of the solution to that of the Helmholtz double layer. The main information comes, therefore, from the minimum which indicates the potential of zero excess charge on the metal. That is, however, only correct in the absence of specific adsorption of ions. If ions are adsorbed, the counter charge for the diffuse double layer is the sum of the surface charge in the metal and of the adsorbed ion. Since the concentration of adsorbed ions also varies with the applied potential, this effect increase the apparent capacity of the Helmholtz double layer.

The potential of zero charge (pzc) can in such a situation be determined by the maximum of the interfacial tension between a metal and the electrolyte, because its potential dependence is dominated by the interaction between the excess charge on the metal and the ions of the electrolyte. The adsorption of ions reduces the interfacial energy. This causes a shift of the potential where the interfacial tension reaches its maximum. In this situation the adsorbed ions and the counter charge in the electrolyte

form a dipole layer. Therefore, anion adsorption results in a shift of the pzc into negative direction; cation adsorption has the opposite effect.

3.6 Impedance spectroscopy

A useful tool for evaluation of many electrical properties of materials and interfaces is impedance spectroscopy. This method involves the application of a small periodical voltage perturbation, typically sinusoidal, whereas the magnitude and phase shift of the corresponding current are registered over a wide range of frequencies. Historically, the first application of this technique to solid electrochemical systems goes back to the work of Bauerle [69] at 1969 studying the polarization behavior of zirconia-yttria solid electrolytes with various Pt electrodes. He presented a general equivalent circuit to explain electrical properties of ceramic polycrystalline electrolytes, consisting of a series combination of RC branches corresponding to grain interiors, grain boundaries, and electrode polarization. In view of this approach, the application of impedance spectroscopy offers the possibility to separate several physicochemical processes involved in an all-solid state electrochemical system. The overall electrical behavior is a result of several contributions:

a) Bulk electrolyte and grain boundary impedance
b) Electrode-electrolyte interfacial impedance
c) Measuring lead impedance

A survey of the measurement method principles is given in [70-73]. For the following analysis it is assumed that the electrical system under investigation is linear, that is the impedance is independent of the perturbation magnitude. Impedance spectroscopy utilizes a potential function that is harmonically periodic with time, namely monochromatic. For a sinusoidal varying voltage perturbation of the form:

$$\vec{V}(t) = V_0 \exp(i\omega t) \tag{3.73}$$

where the symbol $\vec{V}$ represents a vector quantity. The resulting current response has in general the form:

$$\vec{I}(t) = I_0 \exp(i\omega t - i\varphi) \tag{3.74}$$

the complex admittance $\vec{Y}$ is defined as the ratio of complex current $\vec{I}(t)$ over the complex voltage perturbation $\vec{V}(t)$ applied to the system, and the complex impedance $\vec{Z}$ as the reciprocal of the complex admittance. Thus considering relations (3.73) and (3.74):

$$\vec{Y} = \frac{\vec{I}(t)}{\vec{V}(t)} \tag{3.75}$$

$$\vec{Z} = (\vec{Y})^{-1} = \frac{\vec{V}(t)}{\vec{I}(t)} = \frac{V_0}{I_0}\exp(i\varphi) \tag{3.76}$$

Therefore complex admittance and impedance are time independent. Since the impedance is a complex quantity it may be written in terms of a real and an imaginary part:

$$\vec{Z} = Z' + iZ'' \tag{3.77}$$

In the complex plane plot shown in figure 3.8 the admittance and impedance vectors are well defined if the real and imaginary parts of admittance respectively are known. Alternatively the admittance and impedance vectors are also well defined if the phase angle and modulus are known. The real and imaginary parts of impedance $\vec{Z}$ are:

$$\mathrm{Re}(\vec{Z}) = Z' = \left|\vec{Z}\right|\cos\varphi \tag{3.78}$$

$$\mathrm{Im}(\vec{Z}) = Z'' = \left|\vec{Z}\right|\sin\varphi \tag{3.79}$$

And the phase angle and modulus are:

$$\varphi = \tan^{-1}\left(\frac{Z''}{Z'}\right) \tag{3.80}$$

$$\left|\vec{Z}\right| = \sqrt{(Z')^2 + (Z'')^2} \tag{3.81}$$

If we consider a series combination of k complex impedances the overall impedance is given by the sum of the individual impedances $Z_1, Z_2, \ldots Z_k$, whereas for a parallel connection the corresponding overall admittance is equal to the sum of the individual admittances $Y_1, Y_2, \ldots, Y_k$.

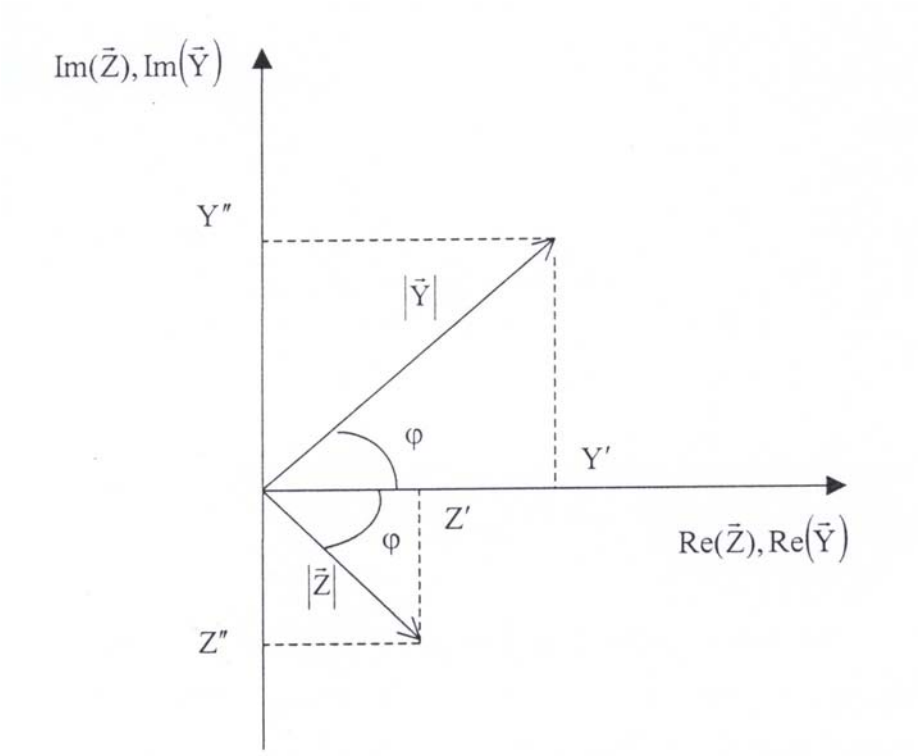

Figure 3.8: Complex plane representations of impedance and admittance vectors.

Impedance is according to (3.76) in general a complex quantity and is only real when $\varphi = 0$, that is for purely resistive behavior. In that case its also frequency independent. Table 3.1 summarizes typical electrical components for equivalent circuit and the corresponding impedance including pure resistive, capacitive, inductive and RC elements.

Circuit element	Admittance	Impedance
 Ohmic resistance	$\frac{1}{R}$	R
 Capacity	$i\omega C$	$-\frac{i}{\omega C}$
 Inductivity	$-\frac{i}{\omega L}$	$i\omega L$
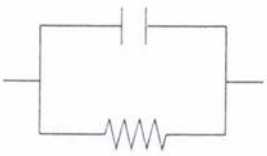 RC	$\frac{1}{R}+i\omega C$	$\frac{R}{1+\omega^2C^2R^2}-\frac{i\omega CR^2}{1+\omega^2C^2R^2}$

Table 3.1: Basic electrical elements of equivalent circuit representation.

From space charge theory the interface electrolyte-electrode can be as a first approximation modeled as a parallel plate capacitor. The rate of charging this capacitor is determined by the bulk ionic resistance of the electrolyte. In solid electrochemical systems where an ionic conductor is sandwiched between two electrodes two equivalent circuits commonly used to describe the frequency dispersion of the cell, dependent on the type of electrodes employed. Figure 3.9 shows the equivalent circuit and the corresponding complex plane impedance plots for an electrochemical cell consisting of a solid electrolyte in between two (a) reversible electrodes and (b) blocking electrodes. Circuit (b) has been used to describe the frequency response of linear systems with a single time constant known as Debye equivalent circuit [70]. The electrical resistance of the sample denoted as R, C_g is the geometric capacitance of the sample between two parallel electrodes and C_{dl} the double layer capacitance. The point where the semicircle touches the real axis provides the electrolyte ohmic resistance.

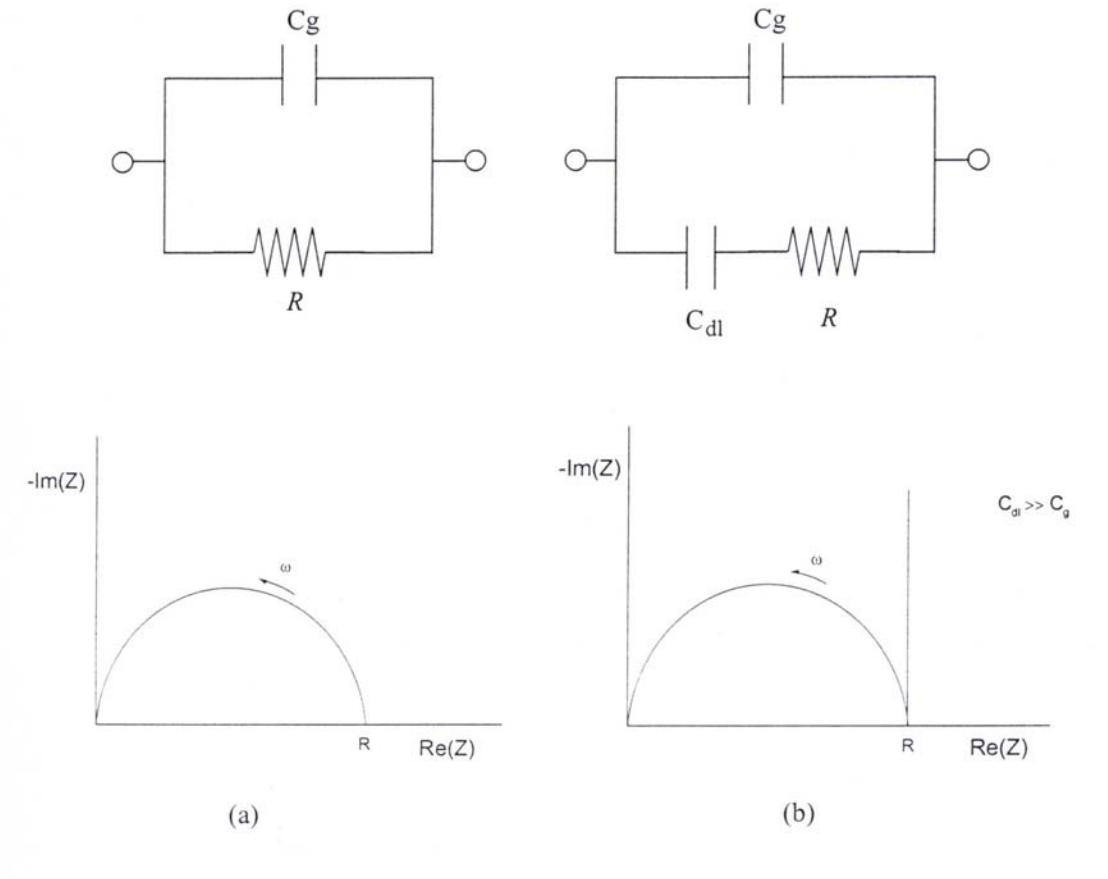

Figure 3.9: Equivalent circuits for the frequency dispersion of a solid ionic conductor with single time constant in between a) reversible (left-hand side) and b) blocking electrodes (right hand-side).

The geometrical capacitance can be calculated in a complex plane plot from the point where –Z'' reaches its maximum value. At that point holds:

$$\varpi RC_g = 1 \tag{3.82}$$

The geometrical capacitance C_g is typically in the order of pico-Farad. The double layer capacitance can be evaluated from the variation of $\left|\vec{Z}\right|$ with frequency in a Bode plot format whereas $\left|\vec{Z}\right|$ is plotted against frequency in a log-log plot. Typical values for the double layer capacitance are in the order of micro-Farad. The equivalent circuits shown in figure 3.9 may be also expand to describe the frequency dependence

of the impedance in systems involving polycrystalline solid electrolytes with either reversible or blocking electrodes [9].

The equivalent circuit representing from an electrical point of view the interfacial electrolyte-electrode impedance is shown in figure 3.10. This equivalent circuit has been proposed by Randles [74] and applied to solid electrochemical systems by Ho et al. [75] and Franceschetti et al. [76] to describe the a.c. frequency response. It includes the uncompensated ohmic resistance of the electrolyte and electrode R_1, the double layer capacitance of the electrode-electrolyte interface C_{dl}, the charge transfer resistance R_{CT} and the Warburg complex impedance $\vec{Z}_W$ arising from the diffusion of the electroactive species towards or from the electrode-electrolyte interface. The complex impedance plane plot corresponding to Randles equivalent circuit is also shown in figure 3.10. Solution of the diffusion equation (3.68) under appropriate initial and boundary conditions combined with the Buttler –Volmer equation for the small overpotential limit provides the complex Warburg impedance [70]:

$$\vec{Z}_W = \frac{RT}{z^2F^2A}\frac{1-i}{c^0\sqrt{2D\varpi}} \tag{3.83}$$

Thus imaginary and real parts are identical. In he complex plane plot Warburg impedance is represented by a straight line inclined 45^o between the real and imaginary parts as shown in figure 3.10. Typically however in real systems the straight line may not incline exactly 45^o to the real axis. This common experimental observation has been attributed to surface roughness [77] or because the conditions for this specific solution may not in reality exactly fulfilled. Under these circumstances the frequency dispersion of the complex Warburg impedance obeying the Kramers-Kronig transformation is:

$$\vec{Z}_i = A_i\varpi^{-a} - iB_i\varpi^{-a} \tag{3.84}$$

Where $\frac{A_i}{B_i} = \tan(\frac{a\pi}{2})$ (3.85)

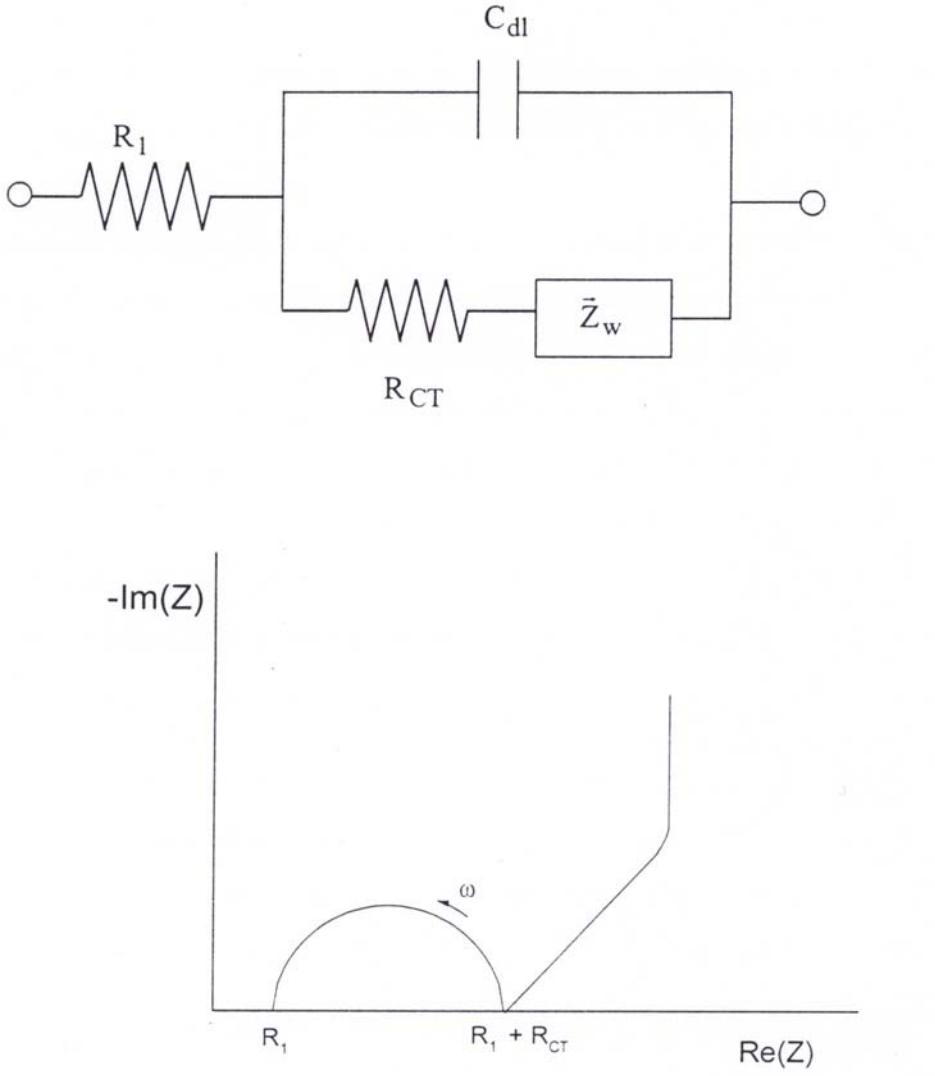

Figure 3.10: Complex plane representation of the impedance of the Randles equivalent circuit for the electrochemical interface.

With A_i, B_i and a to be constants for constant temperature and independent of frequency. At very low frequencies as shown in the complex impedance plane plot of figure 3.10, capacitive behavior becomes dominant thus the frequency dispersion follows a straight line perpendicular to the real axis.

3.7 Phase diagrams

The subject of phase equilibria and phase diagrams is one of the cornerstones of solid state chemistry. Phase diagrams can be seen as the primary thinking tool for understanding properties of multiphase, multicomponent systems in thermodynamic equilibrium. Phase diagrams are plots of temperature (occasionally pressure) against composition. They summarize in graphical form the ranges of temperature and composition over which certain phases or mixtures of phases exist under conditions of thermodynamic equilibrium. They provide information regarding how many and which phases exist in thermodynamic equilibrium and the voltage between them. A phase diagram may be thus regarded as a map presenting the domains of stability of phases and their combinations. With respect to the performance of ionic devices, it is important to know the thermodynamic stability of the different phases involved in the electrochemical cell as electrodes and electrolyte. In this way, the stability ranges of the various phases in a multicomponent system can be recognized and the optimum operating conditions of the device based on material combinations may be revealed. Even if in reality in many cases thermodynamic equilibrium is difficult to achieve due to slow kinetics, its important to know how many phases exist in ideal equilibrium conditions. A system is considered to be in equilibrium if the chemical potential of a component is the same throughout the system.

The fundamental rule on which phase diagrams are based is the phase rule, derived by W.J.Gibbs. If constant temperature and total pressure are kept constant it may written [78] as:

$$P+F=C+2 \tag{3.86}$$

Where F the degrees of freedom available in the system, P the number of phases, and C the number of components (e.g. elements or electrically neutral entities). While for binary systems the situation is commonly simple, for ternary or quaternary systems it is rather complex since typically many phases are involved. However, ternary compounds are of major importance because they are commonly used as gas sensitive layers for the detection of complex gases in type III sensors, Considering that most electrochemical systems are under operation at or near constant temperatures, two-dimensional figures may be used to describe phase diagrams of ternary electrodes under isobaric and isothermal conditions, For representation of composition, the isothermal Gibbs triangle may be used where the three elements lie at the corner, and

the position of each point within the triangle represents a fraction of each of the elements present, thus a fixed composition of the material. In two-phase regions of a ternary system one compositional parameter is fixed for temperature and total pressure constant, thus the activity of an electroactive species within a two-phase region may vary. Lines of constant intensive variables such as the potential within the two phase regions of a ternary system, so called tie lines are approximately parallel and may not cross each other. In reality tie lines within the two-phase regions are not exactly parallel and may be slightly bent but not crossed. Three phase regions in a ternary system are invariant triangles with no degree of freedom representing regions of constant intensive variables. Assuming a hypothetical ternary diagram A – B – C, in any of the three phase isobaric-isothermal triangles the activities of all components related to each other by the Gibbs-Duhem equation:

$$\sum_i n_i d\mu_i = 0 \Rightarrow n_A d\mu_A + n_B d\mu_B + n_C d\mu_C = 0 \tag{3.87}$$

where i is A, B and C. Application of Gibbs-Duhem relationship to obtain thermodynamical parameters for electrode materials conducted in [79,80]. Figure 3.11 (a) shows enlarged the single-phase region $A_xB_yC_z$ of a ternary diagram A- B- C. Within this region holds:

$$x d\mu_A + y d\mu_B + z d\mu_C = 0 \tag{3.88}$$

Tie lines such as those from (a) to (b) or from (c) to (d) representing lines of constant potential within the two phase regions are also shown. The variation of the activity of species i along the path $(a) \rightarrow (b) \rightarrow (c) \rightarrow (d)$ is also schematically illustrated. Paths $(a) \rightarrow (b)$ and $(c) \rightarrow (d)$ lying on tie lines of different potentials, within two phase region, while path $(b) \rightarrow (c)$ lies on a s single phase region with composition $A_xB_yC_z$. The evaluation of tie triangle equilibrium potentials in ternary systems may be accomplished employing the method of determinants [81] for a three component system A – B – C:

$$E = \frac{1}{2qd} \sum_{i=1}^{3} (-1)^i d_{i1} \Delta G_f^0 (A_{\alpha i} B_{\beta i} C_{\gamma i}) \tag{3.89}$$

Where q is the elementary charge, ΔG_f^0 the Gibbs energy of formation per mole and d is the determinant formed by the stoichiometric numbers of the three coexisting phases:

$$d = \begin{vmatrix} \alpha_1 & \beta_1 & \gamma_1 \\ \alpha_2 & \beta_2 & \gamma_2 \\ \alpha_3 & \beta_3 & \gamma_3 \end{vmatrix}$$

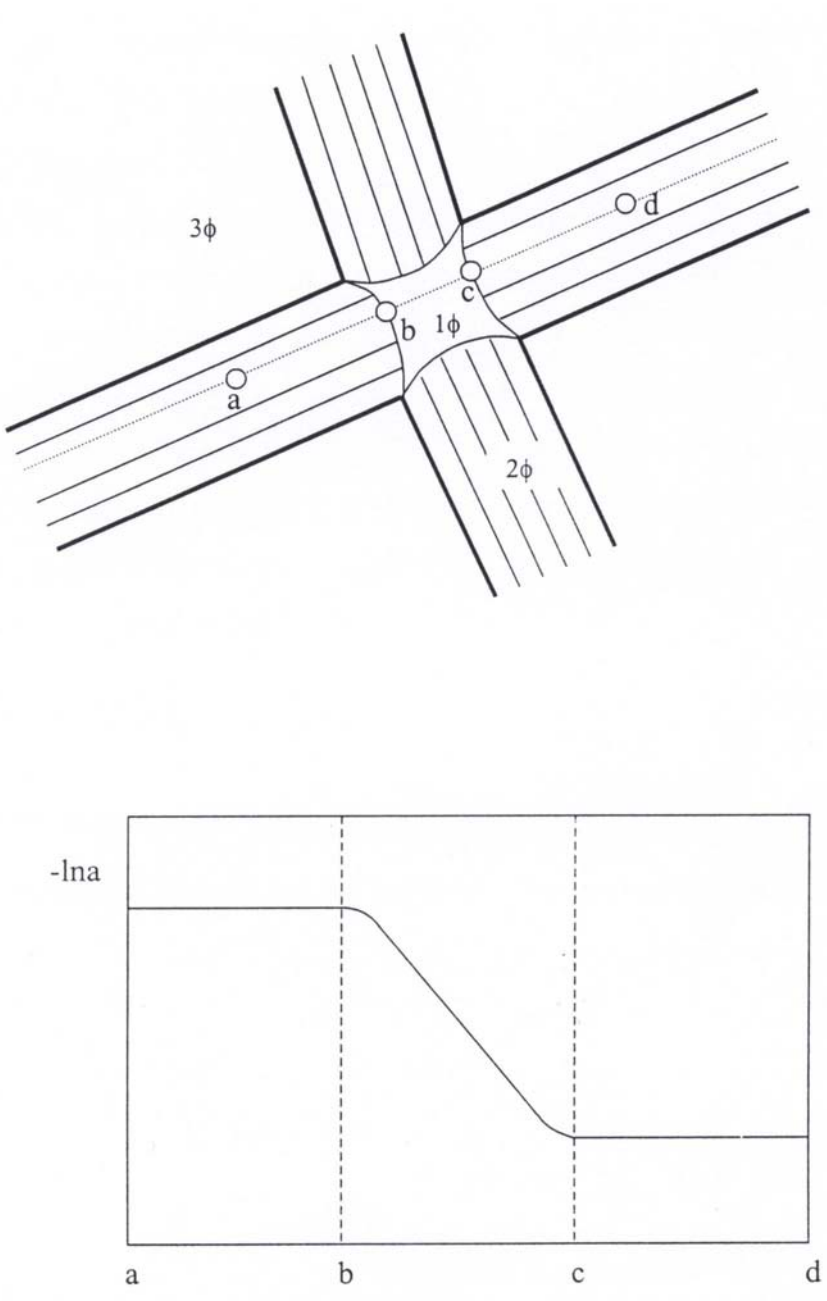

Figure 3.11: a) The region $A_xB_yC_z$ of a hypothetic ternary phase diagram A-B-C is shown enlarged 1ϕ, 2ϕ and 3ϕ indicate one, two or three phase regions. And b) variation in the activity of species i along the path a to b to c to d.

And d_{il} is the minor of d, formed by eliminating the first row and the i-th line of the determinant d. Thus knowing the Gibbs energy of formation of the coexisting phases allows the evaluation of tie triangle equilibrium potentials.

3.8 Components of CO_2 sensor

The electrochemical cell was based on Li^+ conductor for detecting different CO_2 gas concentration based on three components. As LiSiPO or Garnet were used as electrolytes since they both exhibit high lithium ion conductivity. The other two compartments of the cell are the electrodes, namely sensing and reference electrode. Whereas the property of the electrolyte is to transport sodium ions, at the electrodes there are electrochemical processes involved.

3.8.1 LiSiPO and Garnet as electrolyte

LiSiPO is the solid solution of Li_3PO_4 with 50 mole % Li_4SiO_4 [82,83]. In Li_3PO_4 two kinds of tetrahedral lithium sites are present, and they are both fully occupied at room temperature, in Li_4SiO_4 there are 8 Li ions distributed over 18 sites [84]. As soon as Li_4SiO_4 is added to the Li_3PO_4, however, interstitial Li ions are introduced, which can contribute to the conductivity. In this work the composition has been prepared according to the solid state reaction. For LiSiPO the electrical conductivity is $3.6\times10^{-5}\,S/cm$ (100°C) with an activation energy of 0.43 eV, which is comparable to those values previously reported for the lithium ion conductor LISICON (0.56 eV) [85] and higher than that of Li_3N (0.25 eV) [86]. At 400 °C, the electrical conductivity is $0.1S/cm$ with an activation energy of 0.24 eV for LiSiPO.

Garnets are orthosilicates with the general structural formula, $A_3^{II}B_2^{III}(SiO_4)_3$, where A and B refer to eight-coordinated and six-coordinated cation sites [87], respectively. SiO_4 tetrahedral are isolated and connected to each other through ionic bonds with the interstitial B-cations. A large variety of complex oxides have also been found to crystallize in garnet-like structures with other elements replacing silicon, for example, $A_3B_5O_{12}$ (A=Ca, Mg, Y, or Ln=La, or rare earth; B= Al, Fe, Ga, Ge, Mn, Ni, V). The typical garnet-related structure of $Y_3Fe_5O_{12}$ (a=12.376 Å; space group: Ia3d;

No. 230, Z=8) is shown in figure 3.12. It is built up of a 3D framework consisting of FeO_6 octahedra and FeO_4 tetrahedra, in which each octahedron is joined to six others through corner-sharing tetrahedra. Each tetrahedron shares each corner with four octahedra [88]. Compounds with the chemical formula $Li_6ALa_2Ta_2O_{12}$ (A=Sr, Ba) were also found to have a garnet-like structure [89]. In this work, the composition $Li_6BaLa_2Ta_2O_{12}$ was prepared by a solid state reaction process. The electrical conductivity of the Garnet was found to be $4.0\times10^{-5}\,S/cm$ (25°C) with an activation energy of 0.40 eV.

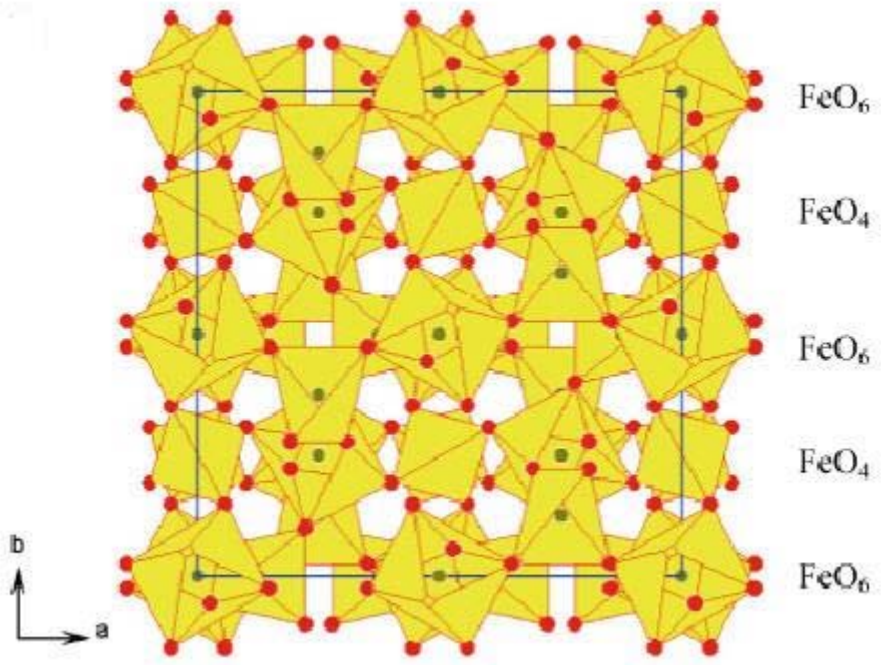

Fig. 3.12: Crystal structures of typical garnet $Y_3Fe_5O_{12}$. For clarity, the positions of Y in $Y_3Fe_5O_{12}$ is not shown [90].

3.8.2 Li_2CO_3 as gas sensitive electrode

Lithium carbonate is the simplest ternary compound that was used as gas sensitive material in a type III potentiometric sensor for carbon dioxide, based on a lithium ionic conductor. It contains both the mobile species of the electrolyte but also the species under detection as well. Lithium carbonate has a monoclinic structure with space group 12 / c. The lattice parameters are in the range of $a = 8.365 \pm 0.01\,\overset{0}{A}$, $b = 4.980 \pm 0.005\,\overset{0}{A}$, $c = 6.20 \pm 0.01\,\overset{0}{A}$, and $\beta = 114.7 \pm 0.1^0$ [91]. According to a

study by Janz [92] on the dependence of the melting point of Li_2CO_3 on its dissociation partial pressure, the material starts to decomposed into Li_2O and CO_2 at a temperature around 675 °C. This decomposition can, however, be prevented by enclosing the sample in a CO_2 atmosphere. A DTA study [93] has shown a phase transition at 410 °C and the melting point at 720 °C. Activation energy of the lithium carbonate for the temperature range 200 °C to 500 °C is 1.056 eV [94]. In alkali metal carbonates, Li_2CO_3 is unaffected by water vapor, Na_2CO_3 absorbs water vapor and K_2CO_3 dissolves in water vapor and eventually becomes an aqueous solution at room temperature [95]. In this work, Li_2CO_3 was used as sensing electrode.

3.8.3 Li, $Li_4Ti_5O_{12}$, HgLi, Li_xWO_3, $LiMn_2O_4$, 3PE ($LiMn_2O_4$ - Li_2MnO_3 - $LiMnO_2$) as reference electrodes

Reference electrodes in electrochemical sensor cells may be either solid or gas. Generally, in non-aqueous systems the potentials and thermodynamics of electrically neutral species in the electrodes are involved, while in liquid electrochemistry ions are measured. The pure element has the standard activity which is the best choice for the reference electrode. Ternary compounds of the type A_xMO_y where alkali metal ions A may provide suitable phase equilibrium, thus become favorable for use as solid reference electrodes. However, several requirements have to be fulfilled for the applicability in type III electrochemical gas sensors. An essential property of the reference electrode is that its electrical potential should not change if the stoichiometry of the alkali species is slightly changed, increased or decreased. Considering the Gibbs phase rule, the material composition should be selected within a three-phase region, if temperature and total pressure are constant. In case where the ratio of M / O is constant e.g. fixed by preparation, this can be seen as a quasi binary system. In such case, within a two-phase region the degree of freedom is zero, thus the potential will be constant inside a two-phase region. If however by some reason the ratio M / O changes, ternary phase equilibrium should be considered to account. Another requirement for the reference electrode is mixed ionic-electronic conduction allowing fast ion exchanged and electron transfer at the interface electrolyte-electrode of the galvanic cell. The electrode reaction should be reversible thus providing a

reversible potential. Furthermore the electrode material should be mechanically compatible but also chemically stable with the electrolyte in contact in the galvanic cell. Not only for short times but also for longer periods of time the reference material should not chemically react with the electrolyte even if current is flowing through the cell, at the operating temperature ranges.

Lithium is a Group 1 (IA) element containing just a single valence electron ($1s^2 2s^1$). Group 1 elements are called "alkali metals". Lithium is a solid only about half as dense as water. Lithium also has the largest negative value of electrode potential. A freshly cut chunk of lithium is silvery, but tarnishes in a minute or oxides in air to give a grey surface. Lithium is mixed (alloyed) with aluminium and magnesium for light-weight alloys, and now is widely used in batteries.

Lithium titanate is one of transition metal oxides, which is a promising anode material for rechargeable lithium ion batteries. Its density is 3.5 g/cm^3. This material exhibited no expansion or shrinkage of lattice constant during lithium ion insertion and extraction. Therefore, both powder samples and thin film electrodes of $Li_4Ti_5O_{12}$ have been extensively studied by many researchers [96-98]. In this work, $Li_4Ti_5O_{12}$ was investigated as reference electrode.

Lithium tungsten oxide with the formula Li_xWO_3 is used well in electrochromic device such as displays for watches, calculators or video monitors and at present to large scale ´´smart windows´´ for cars and buildings. The structure of WO_3 is monoclinic at room temperature, with unit – cell dimensions: $a_M = 7.306\overset{0}{A}$, $b_M = 7.540\overset{0}{A}$, $c_M = 7.692\overset{0}{A}$, and $\beta = 90.881^o$ [99]. When lithium intercalates into Li_xWO_3, the structure becomes successively more simple as x increases. For example, the structure for $Li_{0.1}WO_3$ is tetragonal and the structure for $Li_{0.5}WO_3$ is cubic (ReO_3 - like). When $0.265 < x > 0.5$, Li_xWO_3 has a cubic structure. For $Li_{0.36}WO_3$, the density is 7.54 g/cm^3 [100] and conductivity is 7×10^{-2} S/cm at 27 °C [101].

Lithium manganese oxide with the formula $LiMn_2O_4$ is one of the most promising cathode materials for lithium rechargeable batteries of its low cost and low toxicity. It exhibits enhanced safety characteristics, excellent rate capability, high capacity, and long cycle life. At 25 °C, the open circuit voltage is around 4.4 V for $LiMn_2O_4$ versus elemental Li. The spinel $LiMn_2O_4$ is a cubic structure in which lithium is present at the 8a tetrahedral sites and Mn is present at the 16d octahedral

sites [102]. $LiMn_2O_4$ has Mn^{3+} ion (ionic radius is 0.65 $\overset{0}{A}$) and Mn^{4+} ion (ionic radius is 0.53 $\overset{0}{A}$). For cubic $Li_xMn_2O_4$, the lattice parameter varies from 1.8245 nm in $LiMn_2O_4$ to 0.8029 nm in Mn_2O_4 [103]. And it has a good electronic conductivity which shows in the order of 10^{-4} S/cm at 25 °C.

$LiMnO_2$ is known to exist in several phases. Two phases, whose crystal structures have been well characterized, are a high temperature orthorhombic phase (*pmnm*) and a tetragonal phase ($I4_1/amd$). Both structures involve cubic close packing but they differ in the arrangement of the ordering og the lithium and manganese cations. Davidson et al. [104] studied $LiMnO_2$ prepared at high (800 – 1000°C) temperatures from $\beta - MnO_2$ and Li_2CO_3 in argon. The prepared orthorhombic $LiMnO_2$ has the lattice parameters: $a = 2.8048(3)\overset{0}{A}$, $b = 4.5755(6)\overset{0}{A}$ and $c = 5.7494(7)\overset{0}{A}$.

The Li_2MnO_3 structure has a monoclinic cell with space group C2/m (Z=4) and cell parameters $a = 4.9246(1)\overset{o}{A}$, $b = 8.5216(1)\overset{o}{A}$, $c = 5.0245(1)\overset{o}{A}$ and $\beta = 109.398(1)^0$ [105]. The phase diagram of the system Li – Mn – O is illustrated in figure 3.13.

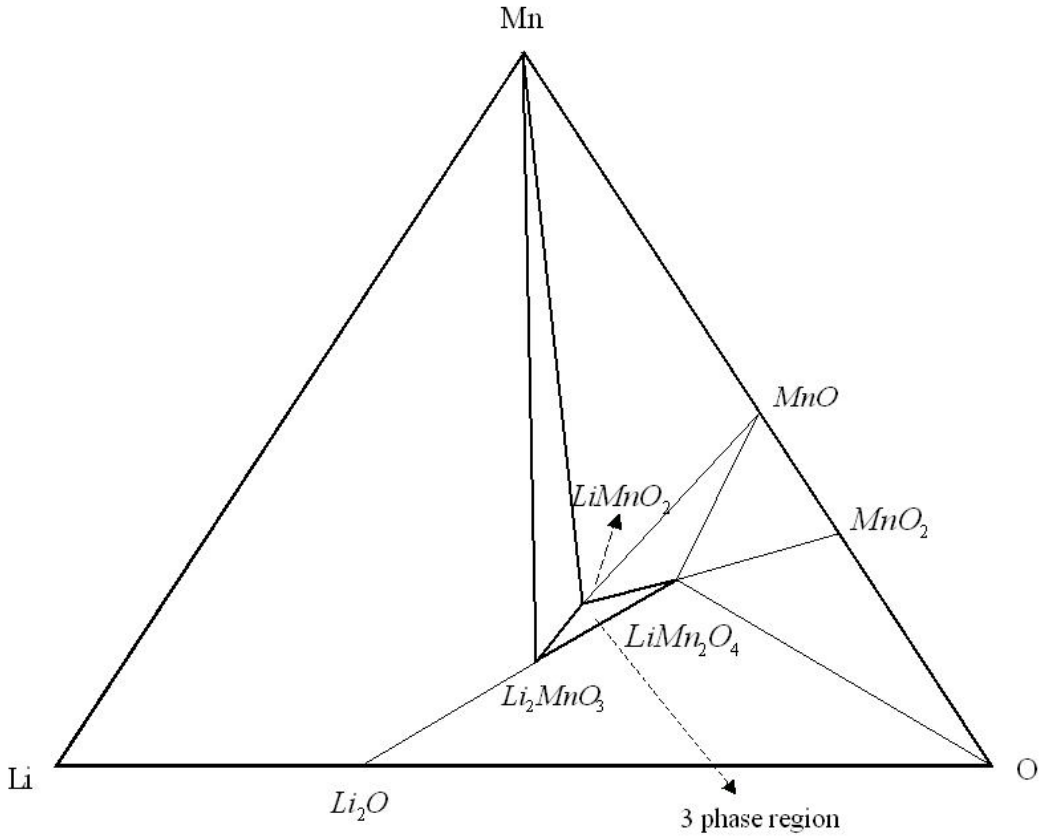

Figure 3.13: Phase diagram of the system Li – Mn – O.

3.9 Fundamental aspects on electrochemical CO_2 sensors

The fundamental thermodynamic relationships of electrochemical type III cells based on lithium ion conductor for the detection of CO_2 under equilibrium conditions will be analyzed here.

Describing thermodynamic properties of an electrochemical system consisting of a solid ionic conductor with two electrodes is commonly complicated especially if there are interaction between species from the electrochemical system and the surrounding gas, as in the electrochemical sensors. Under several simplifying assumptions however, thermodynamic relationships for the most important properties of the system under investigation may be derived. It should be underlined that the following treatment is valid only under the assumptions which have been made. We consider the following electrochemical cell:

$$Li \mid Li^{+} conductor \mid Au, Li_2CO_3, O_{2(gas)}, CO_{2(gas)} \quad (3.90)$$

The electrodes are assumed to act reversibly to the species under consideration and the electrolyte capable to transport only one type of species, namely lithium ions. This condition may be expressed in terms of transference numbers ($t_{Li^+} \to 1, t_{e^-} \to 0$). The sensing electrode reaction involving the mobile species from the electrolyte, electrons from the metal and species from the gas phase may be written as:

$$2Li^+ + 2e^- + \frac{1}{2}O_2 + CO_2 \leftrightarrow Li_2CO_3 \quad (3.91)$$

At the reference side, the electrode reaction is:

$$2Li \leftrightarrow 2Li^+ + 2e^- \quad (3.92)$$

If lithium carbonate is already present on the surface of the solid lithium ionic conductor as a gas sensitive compound, and additional equilibrium should be considered:

$$Li^+_{(Li^+ cond.)} \leftrightarrow Li^+_{(Li_2CO_3)} \quad (3.93)$$

Summing up reaction (3.91) and (3.92) leads to the overall cell reaction:

$$2Li + \frac{1}{2}O_2 + CO_2 \leftrightarrow Li_2CO_3 \quad (3.94)$$

In the three component system Li – C – O the activities of all components are fixed at the sensing electrode at given CO_2 and O_2 partial pressures, if the total pressure and temperature are kept constant. The lithium activity in lithium carbonate is then fixed according to Gibbs – Duhem relationship:

$$2\mu_{Li} + \frac{3}{2}\mu_{O_2} + \mu_C = G_f(Li_2CO_3) \quad (3.95)$$

The chemical potential μ_i of species i is related to the activity a_i or pressure p_i for ideal diluted systems as:

$$\mu_i = \mu_i^o + kT \ln a_i = \mu_i^o + kT \ln P_i \quad (3.96)$$

Where i is CO_2, O_2, Li

Considering that:

$$C + O_2 \leftrightarrow CO_2 \quad (3.97)$$

We may write for the chemical potentials of species shown in (3.97):

$$\mu_C + \mu_{O_2} = \mu_{CO_2} \Rightarrow \mu_C = \mu_{CO_2} - \mu_{O_2} \quad (3.98)$$

Replacing μ_C in (3.95) and solving for the lithium chemical potential in lithium carbonate μ_{Li} we get:

$$\mu_{Li} = \frac{1}{2}\left[\Delta G_f^o(Li_2CO_3) - \frac{1}{2}\mu_{O_2} - \mu_{CO_2}\right] \tag{3.99}$$

Assuming furthermore that Joule's heating and other irreversible energy losses are negligible, the galvanic cell voltage is related to the Gibbs energy of the galvanic cell reaction:

$$\Delta G_r = -2qE \tag{3.100}$$

The galvanic cell voltage may be expressed by the difference in the chemical potential of the neutral electroactive species at both electrodes, according to the Nernst's law:

$$E = -\frac{1}{q}\left[\mu_{Li(meas)} - \mu_{Li(ref)}\right] \tag{3.101}$$

where $\mu_{Li(meas)}$ and $\mu_{Li(ref)}$ denotes chemical potential of lithium at the sensing and reference electrode, respectively. Considering relations (3.96), (3.99) and (3.101) and that $\Delta G_{O_2}^o = 0$ [106] we get an expression for the variation of the open circuit voltage of the galvanic cell (3.90) with CO_2 partial pressure:

$$E = -\frac{1}{2q}\left[\Delta G_f^0(Li_2CO_3) - \Delta G_f^0(CO_2)\right] + \frac{kT}{2q}\ln P_{CO_2} + \frac{kT}{4q}\ln P_{O_2} \tag{3.102}$$

Relationship (3.102) for the electromotive force consists of three terms. The first term in the brackets includes thermodynamical information for the gas sensitive layer and the gas under detection, while the two other terms outside the brackets provide the partial pressure dependence of the open circuit voltage from the gas components. Assuming that temperature and oxygen partial pressure are kept constant, expression (3.102) can be written in the form:

$$E = E^0 + \frac{kT}{2q}\ln P_{CO_2} = E^0 + \frac{2.303kT}{2q}\log P_{CO_2} \tag{3.103}$$

where E^0 is constant for a constant temperature. From (3.103) the sensitivity of cell (3.90) may be obtained by derivation:

$$\frac{dE}{d(\log P_{CO_2})} = \frac{2.303kT}{2q} \tag{3.104}$$

Therefore, the open circuit voltage varies linearly versus $\log P_{CO_2}$ with a slope of $\frac{2.303kT}{2q}$. The sensitivity to the gas species under detection is therefore dependent on the number of electrons incorporated in the galvanic cell reaction, and the temperature. In the above consideration, elemental lithium has been assumed to be reference electrode. Similar treatment holds if a lithium based solid reference electrode with a lithium activity different than unity is employed. An extra term should be considered including the activity of the neutral electroactive species at the reference electrode. The expression for the open circuit voltage may be thus written as:

$$E = -\frac{1}{2q}\left[\Delta G_f^0(Li_2CO_3) - \Delta G_f^0(CO_2)\right] + \frac{kT}{2q}\ln P_{CO_2} + \frac{kT}{4q}\ln P_{O_2} + \frac{RT}{F}\ln a_{Li(ref)} \tag{3.105}$$

From (3.105) it can be deducted that at constant temperature and oxygen partial pressure the sensitivity to the species under detection is the same as the one calculated from (3.102) thus independent of the choice of the reference electrode material.

Reference to chapter 3

[1] W. Weppner, *Proc. Of the 2nd int. Meeting on chemical sensors*, Bordeaux (1986)

[2] J. Riegel, H. Neumann, H. M. Wiedenmann, *Solid State Ionics* **152-153**, 783-800 (2002)

[3] J. S. Lundsgaard, J. Malling, and M. L. S. Birchall, *Solid State Ionics* **7**, 53 (1982)

[4] S. B. Lyon, D. J. Fray, *Solid State Ionics* **9-10**, 1295 (1983)

[5] H. Iwahara, H. Uchida, *Anal. Chem. Symp. Ser.* **17**, 227 (1983)

[6] A. Pelloux, P. Farby, and P. Durante, *Sens. Actuators* **7**, 245 (1985)

[7] A. Huerland, R. Moos, R. Mueller, C. Plog, U. Simon, *Sensors and Actuators B* **77**, 287-292 (2001)

[8] W.Weppner, *Ionics* **7**, 404-424 (2001)

[9] G. Hötzel, *Ph. D. Thesis*, University of Stuttgart (1986)

[10] N.Imanaka, Y. Yamaguchi, G. Adachi, and J. Shiokawa*, J. Electrochem. Soc.* **134** (3), 725-728

[11] M. Gauthier and A. Chamberland, *J. Electrochem. Soc.* **124** (10), 1570-1583

[12] N. Imanaka, Y.Yamaguschi, G. Adachi, and J. Shiokawa, *J. Electrochem. Soc.* **132** (10), 2519-2520 (1985)

[13] V. Demuysere, C.W.Bale, *Solid State Ionics* **9-10**, 1285 (1983)

[14] K.T.Jacob and D.Bhogeswara Rao*, J. Electrochem.Soc.* **126** (11), 1842-1847 (1979)

[15] M.Gauthier, R.Bellemare, and A.Belanger, *J.Electrochem.Soc.* **128** (2), 371-378 (1981)

[16] M.Itoh and Z.Kozuka, *J.Electrochem. Soc.* **133** (7), 1512-1517 (1986)

[17] C.D.Eastman, T.H.Etsell, *Solid State Ionics* **136 / 137**, 639-645 (2000)

[18] T.Maruyama, Y.Saito, Y.Matsumoto and Y.Yao, *Solid State Ionics* **17**, 281-286 (1985)

[19] A.Menne and W.Weppner, *Solid State Ionics* **40 / 41**, 468-471 (1990)

[20] R.Cote, C.W.Bale, M. Gauthier, *J.Electrochem. Soc.* **131** (1), 63-67 (1984)

[21] W. Weppner, *Solid State Ionics* **40/41**, 369-374 (1990)

[22] W.Weppner, *Materials Science and Engineering* **B15**, 48-55 (1992)

[23] G. Hötzel and W.Weppner, *Proc. Of the 2nd int. Meeting on chemical sensors, Bordeaux*, 258-288 (1986)

[24] G.Hötzel and W.Weppner, *Solid State Ionics* **18/19**, 1223-1227 (1986)

[25] S.Yao and J.R.Stetter, *J.Electrochem. Soc.* **151** (4), H75-H80 (2004)

[26] Y.Yan, N.Miura, N.Yamazoe, *Sensors and Actuators* **B 24/25**, 287-290 (1995)

[27] H.Aono and Y.Sadaoka, *J.Electrochem. Soc.* **147** (11), 4363-4367 (2000)

[28] J.Liu and W. Weppner, *Solid State Communications* **76** (3), 311-313 (1990)

[29] J.Liu and W.Weppner, *Solid State Ionics,* Editors: M.Balkanski, T.Takahashi and H.L.Tuller (1992)

[30] J.Liu and W.Weppner, *Eur. J. Solid State Inorg. Chem.* **Tome 28**, 1151-1160 (1991)

[31] N.Miura, Y.Yan, S.Nonaka and N.Yamazoe, *J. Mater. Chem*. **5** (9), 1391-1394 (1995)

[32] Y.C.Zhang, M.Keneko, K.Uchida, J.Mizusaki and H.Tagawa, *J. Electrochem. Soc.* **148** (8) H81-H84 (2001)

[33] N.Miura, S.Yao, Y.Shimizu and N.Yamazoe, *J. Electrochem. Soc*. **139** (5), 1384-1388 (1992)

[34] Y.C.Zhang, H.Tagawa, S.Asakura, J.Mizusaki, H.Narita, *J. Electrochem, Soc.* **144** (12), 4345-4350 (1997)

[35] T.Maruyama, X.Ye and Y.Saito, *Solid State Ionics* **23**, 113-117 (1987)

[36] Y.Saito and Maruyama, *Solid State Ionics* **28/30**, 1644-1647 (1988)

[37] E.Steudel, P.Birke and W.Weppner, *Electrochimica Acta* **42** (20-22) 3147-3153 (1997)

[38] S.Choi, W.Chung, D.Lee, *Sensors and Actuators* **B 35-36**, 263-266 (1996)

[39] Y.Yan, N.Miura and N.Yamazoe, *J. Electrochem. Soc.* **143** (1), 609-613 (1996)

[40] D.L.Short and G.S.G.Shell, *J. Phys. E.* **17**, 1085 (1984)

[41] B.Y.Liaw and W.Weppner, *J. Electrochem. Soc.* **138** (8), 2478-2483 (1991)

[42] J.Liu and W.Weppner, *Appl. Phys.* **A 52**, 94-99 (1991)

[43] H. Dietz, *Solid State Ionics* **6**, 175-183 (1982)

[44] J.Liu and W.Weppner, *Appl. Phys.* **A 55**, 250-257 (1992)

[45] E.D.Tsagarakis, Ph.D.Thesis, University of Kiel (2004)

[46] C.Wagner, *Prog. Solid State Chem*. **10**, 3-16 (1975)

[47] H.Rickert, *Solid State Electrochemistry: an Introduction*, Springer-Verlag, Berlin, (1982)

[48] A. D. Claire Le, *Physical Chemistry*, Academic Press, New York, **10**, 261-330 (1970)

[49] W.Weppner and R.A.Huggins, *Electrochem. Soc.,* **124**, 1569-1578 (1977)

[50] Anthony R. West, Solid State Chemistry and its Applications, JOHN Wiley & Sons (1984)

[51] F.Kohlrauch, *Praktische Physik*, **2** 284, Teubner, Stuttgart (1968)

[52] M.H.Hebb, *J.Chem.Phys.,* **20**, 185-190 (1952)

[53] C.Wagner, *Z.Elektrochem.,* **60**, 4-7 (1956)

[54] I. Riess, *Solid State Ionics*, **80**, 129 (1995)

[55] Atkins, ``Physical Chemistry`` sixth edition, Oxford University Press, Oxford-Melbourne-Tokyo (1998)

[56] I.Langmuir, *Journal of the American Chemical Society* **54**, 2798-2832 (1932)

[57] C.Wagner, *Nachrichten der Akademie der Wissenshaften in Göttingen*, Nr. **3**, 1-27 (1973)

[58] C.H.Hamann, W.Vielstich, ``Elektrochemie``, Wiley-Vch Verlag (1998)

[59] A.Fick, *Pogg. Ann*. **94**, 59 (1855)

[60] J.Crank, ``the Mathematics of Diffusion`` Second Edition, Oxford University Press (1975)

[61] A.R.Allnatt and A.B.Lidiard, ``Atomic tranport in Solids``, Cambridge University Press (1993)

[62] W.Weppner, *Solid State Ionics* **40/41**, 369-374 (1990)

[63] H.von.Helmholtz, *Wied. Ann*. **7**, 337 (1879)

[64] D.Price and J.W.Halley, *J.Electroanal. Chem.* **150**, 347 (1983)

[65] S.Amokrane and J.P.Badiali, *J.Electroanal. Chem*. **21**, 266 (1989)

[66] G.Gouy, *J.Phys. (Paris)* **9**, 457 (1910)

[67] D.C.Chapman, *Philos. Mag*. **25**, 475 (1913)

[68] O.Stern, *Z.Elektrochem*. **30**, 508 (1924)

[69] J.E.Bauerle, *J.Phys.Chem.Solids* **30**, 265-2670 (1969)

[70] J.R.Macdonald, ``Impedance spectroscopy: emphasizing solid materials and systems``, Wiley-Interscience Publication, New York-Chichester-Brisbane-Toronto-Singapore (1987)

[71] P.Hagenmuller, W.Van Gool, ´´ Solid Electrolytes: General Principles, Characterization, Materials, Applications``, Academic Press Inc. New York London (1978)

[72] C.Ho, Ph.D. Thesis, Stanford University (1980)

[73] G.Popkirov, *Current Topics in Electrochemistry* **7**, 23-47 (2000)

[74] J.E.B.Randles, *Discussions of the Faraday Society* **1**, 11-19 (1947)

[75] C.Ho, I.D.Raistrick and R.A.Huggins, *J.Electrochem. Soc.,* **127** [2], 343-350 (1980)

[76] D.R.Franceschetti and J.R.Macdonald, *J.Electrochem. Soc.,* **129** [8], 1754-1756 (1982)

[77] R.D.Armstrong, T.Dickinson and J.Turner, *Electroanalytical Chemistry and Interfacial Electrochemistry* **44**, 157-167 (1973)

[78] D.V.Ragone, ´´Thermodynamics of Materials`` Vol. 1, J.Wiley and Sons, New York Chichester Brisbane Toronto Singapore (1995)

[79] N.A.Godshall, Ph.D.Thesis, Stanford University (1980)

[80] N.A.Godshall, I.D.Raistrick and R.A.Huggins, *J.Electrochem. Soc.,* **131** [3], 543-549 (1984)

[81] L.C.Chen and W.Weppner, *Naturwissenschaften* **65**, 595 (1978)

[82] Y – W. Hu, I. D. Raistrick, and R. A. Huggins, Mater. Res. Bull **11**, 1227 (1976)

[83] Y – W. Hu, I. D. Raistrick, and R. A. Huggins, J. Electrochem. Soc. **8**, 1240 – 1242 (1977)

[84] H.Völlenkle, A. Wittmann, and H. Nowotny, *Monatsh. Chem.,* **99**, 1360 (1968)

[85] U.Von Alpen, M.F.Bell, W.Wiechelhous, K.Y.Cheung and G.J.Dudley, *Electrochim. Actu.,* **23**, 1395 (1978)

[86] U.Von Alpen, A.Rabenau and G.H.Talat, *Appl. Pys. Lett.,* **30**, 621 (1977)

[87] A. F. Wells, Structural Inorganic Chemistry, 5th ed., Oxford Science Publications, Clarendon Press, Oxford, UK 1984

[88] C. Wagner, in: Proceedings of the 7th meeting of the International Committee on Thermodynamic and Kinetic Electrochemistry (CITCE), Germany, Butterworth Publication, Lindau, London, p. *361,* **1957**.

[89] V. Thangadurai, W, Weppner, *Adv. Funct. Mater*. **15**, No. 1, January 2005

[90] V. Thangadurai and W.Weppner, J. Am. Ceram. Soc., **88, 411** (2005)

[91] J.Mizusaki and H.Tagawa, *Solid State Ionics* **53-56**, 791-797 (1992)

[92] G.J.Janz and M.R.Lorentz, *J. Electrochem. Soc.* **108**, 1052 (1961)

[93] A.Reisman, *J. Am. Chem. Soc.* **80**, 3558 (1958)

[94] M.A.K.L.Dissanayake and B.-E.Mellander, *Solid State Ionics* **21**, 279-285 (1986)

[95] H.Narita, Y.C.Zhang, J.Mizusaki, H.Tagawa, *Solid State Ionics* **79**, 349-353 (1995)

[96] S.Scharner, W.Weppner, and P.Schmid-Beurmannb, *J.Electrochem. Soc.,* **146,** 857 (1999)

[97] K.Kanamura, T.Umegaki, H.Naito, Z.Takehara, and T.Yao, *J. Appl. Electrochem*., **31**, 73 (2001)

[98] Y.H.Rho and K.Kanamura, *J.Electrochem. Soc.*, **150**, A107 (2003)

[99] B.O.Loopstra and H.M.Rietveld, *Acta. Crystallogr.* **B 25**, 1420 (1969)

[100] M.J.Sienko, T.B.Truong, *J.Am.Chem. Soc.* **83**, 3939-3943 (1961)

[101] H.R.Shanks, P.H.Sidles, G.C.Danielson, *Advan.Chem.Soc.* **39**, 237-245 (1963)

[102] D.Guyomard, J.M.Tarascon, *Solid States Ionics* **69**, 222-237 (1994)

[103] Y.L.Lu, M.Wei, Z.Q.Wang, D.G.Evans and X.Duan, *Electrochim. Acta,* **49**, 2361 (2004)

[104] I.J.Davidson, R.S.McMillan, J.J.Murray, J.E.Greedan, *Journal of Power Sources* **54**, 232-235 (1995)

[105] V.Massarotti, M.Bini, D.Capsoni, A.Altomare, A.G.G.Moliterni, *J.Appl.Cryst.,* **30**, 123-127 (1997)

[106] I.Barin, ´´Thermochemical Data of Pure Substances``, VCH, Weinheim – New York (1993)

CHAPTER 4

Experimental aspects

This section contains the experimental details for the preparation of the investigated cells and the measurement apparatus and techniques that have been employed in this work.

4.1 Measuring apparatus (Kiel Cell)

The so called ``Kiel Cell`` has been used for electrochemical measurements at defined temperatures and gas partial pressures or gas mixtures. The apparatus is schematically shown in figure 4.1. It consists of two compartments, a double walled quartz glass cylinder with one end closed and a steal support. These two parts are binding each other using O-rings. Through its relatively small and defined volume, utilization of this apparatus allows to change relatively fast the gas atmosphere over the sample and thus a reasonable estimation for the response time of the cell under investigation.

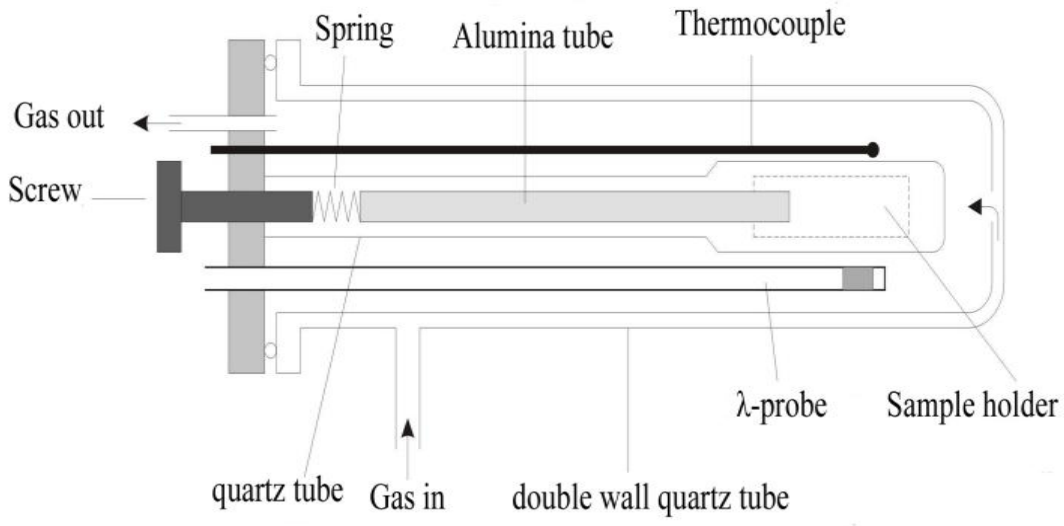

Figure 4.1: Schematic representation of the apparatus for electrochemical measurements under defined temperature and gas mixtures.

It can be used for measurements at temperatures up to 1000°C, and may accomplish nominal experimental conditions for long term measurements, thus providing suitable experimental conditions for investigations on electrochemical gas sensors. Kiel cell was placed and fastened in a tubular furnace with the steel support to be maintained outside the furnace. The temperature of the furnace was controlled with a temperature controller (Therm 3280-1). Inside the quartz tube one thermocouple (Pt/Pt-13%Rh or NiCr/Ni) was placed near to the sample or sensor under investigation, for reading the exact temperature. Platinum wires inside alumina tubes with small diameter were used to transfer the electrical signal from the electrochemical cell to the steel support base of the apparatus where it was further processed via BNC connectors to the electrical instruments. In the gas outlet a glycerin bubbler has been installed, and each time the apparatus has been assembled for measurements, its gas tightness has been individually checked before inserting the sample.

4.2 Preparation of cells and experimental setup

The details on preparation of individual materials and electrochemical cells as well as the experimental setup conditions for measurements will be presented in this section.

LiSIPO and Garnet have been employed as solid lithium ionic conductors. These two conductors were used as electrolytes of electrochemical sensors in this work.

LiSiPO is the solid solution of Li_3PO_4 with 50 mole % Li_4SiO_4 [1,2]. In Li_3PO_4 two kinds of tetrahedral lithium sites are present, and they are both fully occupied at room temperature, in Li_4SiO_4 there are 8 Li ions distributed over 18 sites [3]. As soon as Li_4SiO_4 is added to the Li_3PO_4, however, interstitial Li ions are introduced, which can contribute to the conductivity. In this work the composition has been prepared according to the solid state reaction.

Appropriate amounts of the starting materials Li_4SiO_4 (Aldrich-Chemie) and Li_3PO_4 (ChemPur, 99+%) were mixed and ball-milled in isopropanol using zirconia balls for 2 h, then sintered at 1000 °C in air for 2 h. Subsequently the powder mixture was ball-milled for 2 h again and isostatically pressed at 120 kN for 20 min and calcined at 1000 °C in air for 2 h once more and cut into the shape of a disk of 8 mm

in diameter and 1 mm in thickness. The pellet were prepared for using as solid electrolyte.

Garnets are orthosilicates with the general structural formula, $A_3^{II} B_2^{III} (SiO_4)_3$, where A and B refer to eight-coordinated and six-coordinated cation sites [4], respectively. SiO_4 tetrahedral are isolated and connected to each other through ionic bonds with the interstitial B-cations. A large variety of complex oxides have also been found to crystallize in garnet-like structures with other elements replacing silicon, for example, $A_3B_5O_{12}$ (A=Ca, Mg, Y, or Ln=La, or rare earth; B= Al, Fe, Ga, Ge, Mn, Ni, V). Compound with the chemical formula $Li_6ALa_2Ta_2O_{12}$ (A=Sr, Ba) were also found to have a garnet-like structure [5], whereas in this work the composition of $Li_6BaLa_2Ta_2O_{12}$ was prepared according to the solid state reaction process. Using appropriate amounts of high purity (>99.9%) La_2O_3 (pre-dried at 900°C for 24 h), $LiOH.H_2O$, $Ba(NO_3)_2$, and Ta_2O_5 obtained from Fluka or Aldrich. 10 wt% excess of $LiOH.H_2O$ was added to compensate loss due to volatilization of Li_2O during the preparation. The mixtures were heated in air and maintained at 700°C for 6 h and then annealed at 900°C for 24 h. Before and after the first step, the powders were ball-milled using zirconia balls for about 12 h in 2-propanol. For the second step of heat treatment, the reaction products were pressed into pellets by isostatic pressure and covered with powder of the same mother composition to reduce the loss of lithium because of volatilization.

Typically lithium carbonate with the formula Li_2CO_3 (Merck, 99%) is served as the sensing electrode. And Au paste (Product No.C5755A, Heraeus Inc.) is the conducting layer of the sensor. Because the powder of Li_2CO_3 is hard to press into pellet and has a low ionic conductivity in general working temperature range, in this work the mixture of Li_2CO_3 and Au paste were used as the sensing electrode. The volume ratio 6:4 of Li_2CO_3 powder and Au paste were mixed well in a glass tube, then paste on one side of the electrolyte with a soft brush. Put into the drying chamber at 120°C for 20 min, afterwards sintered into the furnace at 600°C for 2 hrs.

All used reference electrodes and preparation methods are listed in the following:

Lithium titanium oxide with the formula $Li_4Ti_5O_{12}$ was prepared according to the solid state reaction method [6]. The molar ratio of 5:4 of TiO_2 (Aldrich, 99.9%) and $LiNO_3$ (Aldrich, 99%) were mixed and ball milled for about 12 hrs in 2-propanol using zirconia balls then dried in air overnight. The first sintering step is to put the

dried mixture into the furnace and heating to 600°C for 6 hrs in air with heating and cooling rates of 5 °C/min. Then grained in a mortal and ball milled also for another 12 hrs. Following as heating to 800°C for 6 hrs in air with heating and cooling rates of 5 °C/min is the second sintering step. After that, the powder was isostatically pressed at 120 kN for 20 min, then calcined at 800°C for 10 hrs in air. It was also cut into the shape of a disk of 8 mm in diameter and 1 mm in thickness typically.

Alloy of lithium mercury shows a plateau when two phases coexist, which was prepared in the glove box. A proper amount of elemental lithium and liquid mercury were mixed in the crucible which was made by electrolyte material. Then the crucible and the mixture were heated to 200 °C and cooling to room temperature with heating and cooling rate of 2 °C / min for several times. During the heating and cooling time, one alumina rod was used for milling the mixture in order to react well.

Lithium tungsten oxide with the formula Li_xWO_3 is used well in electrochromic device. Because its good electronic conductivity and stable voltage plateau versus elemental lithium, in this work Li_xWO_3 (x=0.36) was used as the reference electrode. Li_xWO_3 (x=0.36) has the cubic structure [7], whereas in this work Li_xWO_3 (x=0.36) was prepared according to the solid state reaction process [8]. The following chemical reaction formula was used:

$$\frac{x}{2}Li_2WO_4 + \frac{3-2x}{3}WO_3 + \frac{x}{6}W \Rightarrow Li_xWO_3 \qquad (4.1)$$

take appropriate amounts of Li_2WO_4 (Strem, 98%), WO_3 (Alfa, 99.99+%) and W (Alfa, 99.9%), ball milling for 12 hrs used zirconia balls with 2-propanol, then dried in air overnight. The sintered step should finish in Argon gas at temperature of 750 °C for 2 hrs with heating and cooling rates of 1 °C/min. After that, the powder was isostatically pressed at 120 kN for 20 min, then calcined at 750 °C for 2 hrs in Argon. It was also cut into the shape of a disk of 8 mm in diameter and 1 mm in thickness typically.

Lithium manganese oxide with the formula $LiMn_2O_4$ (Aldrich, 99%) which was mainly selected as reversible cathode in lithium ion battery is always used as cathode material. The commercial lithium manganese oxide was isostatically pressed at 120 kN for 20 min, then calcined at 850 °C for 2 hrs in air. It was also cut into the shape of a disk of 8 mm in diameter and 1 mm in thickness typically.

Three phases mixture of $LiMn_2O_4$ (Aldrich, 99%), Li_2MnO_3 (Strem, 98%) and $LiMnO_2$ was also selected as the reference electrode. The molar ratio for $LiMn_2O_4$ -

Li_2MnO_3 - $LiMnO_2$ is 0.74 : 0.173 : 0.087. $LiMnO_2$ was prepared according to the solid state reaction method [9]. The molar ratio of 2:1 of MnO_2 (Aldrich, 99+%) and $LiCO_3$ (Merck, 99%) were mixed and ball milled for about 12 hrs in 2-propanol using zirconia balls then dried in air overnight. The sintering step is to put the dried mixture into the furnace and heating to 900°C for 12 hrs in argon atmosphere with heating and cooling rates of 2 °C/min. After that, the powder of the mixture $LiMn_2O_4$ - Li_2MnO_3 - $LiMnO_2$ was isostatically pressed at 120 kN for 20 min, then calcined at 900°C for 2 hrs in argon atmosphere. It was also cut into the shape of a disk of 8 mm in diameter and 1 mm in thickness typically.

Complete cells with solid reference electrode may be divided into two major cell structures namely those with Li_2CO_3 and Au paste sensing electrode and reference electrode which prepared in the glove box and those with Li_2CO_3 and Au paste sensing electrode and pellet reference electrode which prepared in air. For the first category, LiSiPO or Garnet has been employed as solid electrolyte for lithium ions in the electrochemical cell schematically shown in figure 4.2.

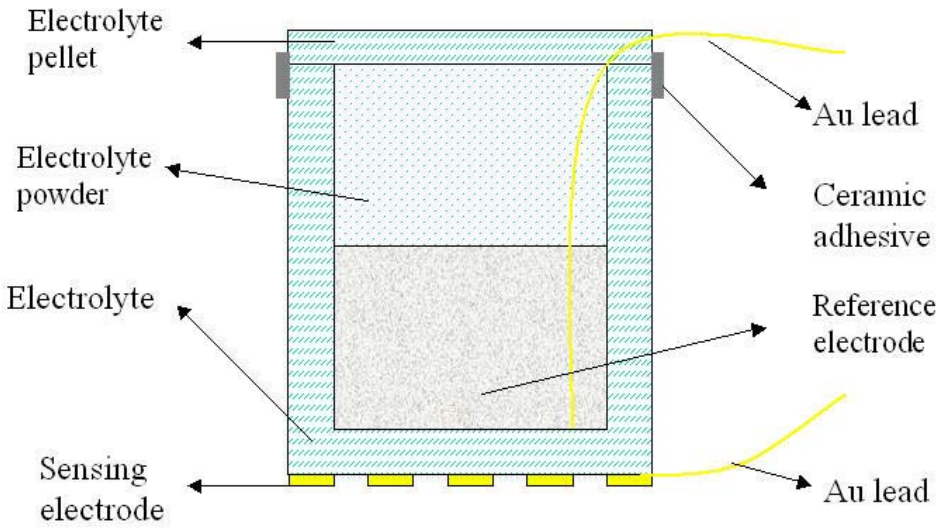

Figure 4.2: Schematic representation of the electrochemical cell under investigation in carbon dioxide atmospheres.

The electrolyte material, typically in form of crucibles of 9 cm length and 16 mm diameter with 2 mm wall thickness which were polished at bottom and the ringent. The reference material was put into the crucible which was made by the electrolyte material which was then painted inside of the electrolyte crucible with one Au wire used as metallic conductor, afterwards painted the sensing material of Li_2CO_3 and Au paste on the bottom of the crucible with another one Au wire. Then the cell was filled the left space inside of the electrolyte crucible with powder of the corresponding electrolyte material. One corresponding electrolyte disc was covered on the ringent side and sealed with high temperature ceramic adhesive (940 Cotronics Corp., N.Y.). Then the whole cell was leftover in the glove box for sufficient long time normally overnight for drying the ceramic glue. Afterwards the cell was taken out from the glove box and sintered at 600 °C for 2 hours.

For the second cell category, as shown schematically in figure 4.3, LiSiPO or Garnet electrolytes employed, in contact with the solid reference electrode. As gas sensitive compound Li_2CO_3 and Au paste have been used. The electrolyte disc typically 1-2 mm thick with a diameter of 6-10 mm was polished on both sides. Au paste needed to be heated up to 600 °C for 2 hrs during preparation because of the necessity to remove organic impurities in it and ensure adherent films on top of the solid electrolyte. The reference electrode material was in form of pellet, uniaxially pressed with 6-8 mm diameter. The reference and electrolyte discs were brought in contact using a self-made spring loaded accessory and peripherally encircled by a fast cure ceramic adhesive (940 Cotronics Corp., N.Y.). After applied Au paste on the reference side as electronic conducting layer, the high temperature ceramic adhesive was also painted on the top of the reference electrode for isolation from the surrounding atmosphere.

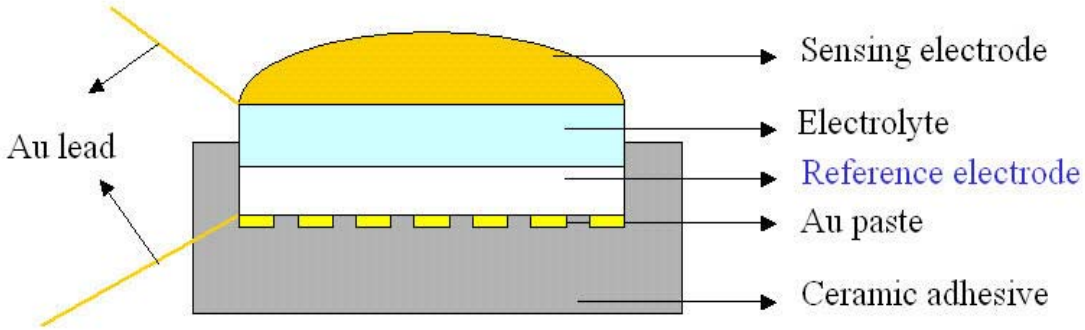

Figure 4.3: Schematic representation of the electrochemical cell under investigation in carbon dioxide atmospheres.

For the investigation on the kinetics of the Li_2CO_3 sensing electrode, experiments in electrochemical cells with elemental lithium as reference electrode were conducted. Metallic lithium is a reversible electrode for lithium ions, establishing lithium activity equal to unity. However, because of its high reactivity the preparation and sealing of the reference electrode were carried out carefully in an argon filled glove box. The schematic structure of the constructed electrochemical cell is shown in figure 4.4. The electrolyte material, typically in form of crucibles of 9 cm length and 16 mm diameter with 2 mm wall thickness employed. The tubes were then inserted in a glove box and filled with elemental lithium (Aldrich, 99.95%) whereas the open end was encapsulated by corresponding electrolyte disc and fixed by using high temperature ceramic seals (940 and Thermeez 7030, Cotronics Corp., N.Y.). Each tube left inside the glove box for at least 24 hrs allowing the seals to dry. The sensing electrode was always identical that is Li_2CO_3 and Au paste which is painted on the bottom of the electrolyte tubes and sintered at 600 °C for 2 hrs before hand.

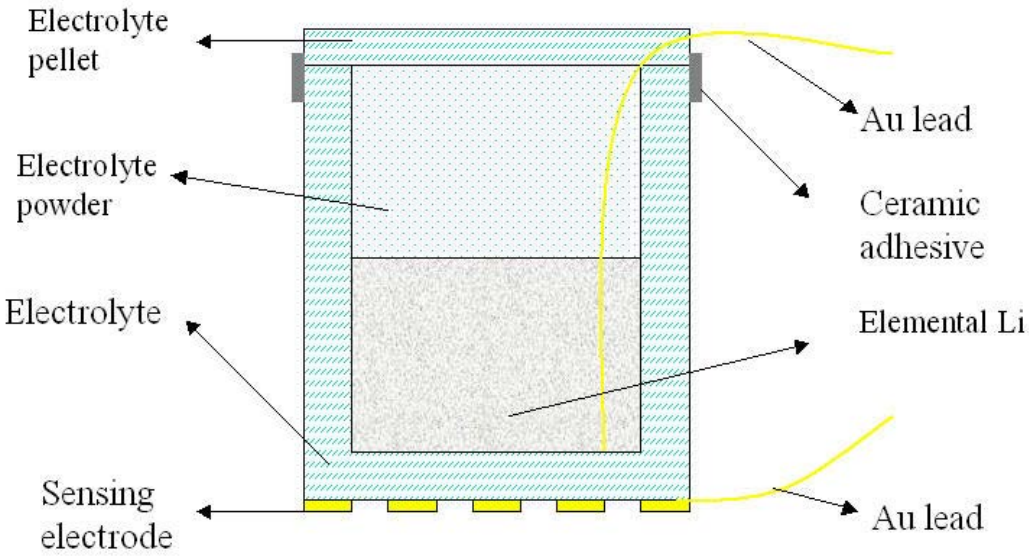

Figure 4.4: Schematic representation of the electrochemical cell under investigation in carbon dioxide atmospheres.

The experimental set up for the investigation on the electrolyte material stability against reactions with the electrodes consists of the following. As solid electrolyte for lithium ions, a LiSiPO (Li_3PO_4 with 50 mole % Li_4SiO_4) pellet was used. The pellet was 8 mm in diameter and 1 mm in thickness. Electrodes were made by painting Li_2CO_3 (Merck, 99+%) with Au paste (Product No.C5755A, Heraeus Inc.) on both sides of the electrolyte disc. The whole cell was annealed at 600 °C for 2 hrs in air. The average thickness of the electrode was 40 μm. The electrical signal was carried by using gold wires on sides of two electrodes. The cell was spring loaded with two Duran glass (EYDAM Inc.) on both sides. Two coniform plastic plugs were inserted into the open sides of Duran glass for sealing. Two stainless steel tubes were served as gas inlet and outlet respectively through plastic plugs. The construction of this experiment was schematic illustrated in figure 4.5. Then the apparatus was placed into a tubular furnace with a NiCr/Ni thermocouple placed around for measuring temperature. The oxygen partial pressure was maintained on both sides of electrodes by using synthetic air (21% O_2, 89% N_2). Varied partial pressures of CO_2 can be got by mixing synthetic air with 1% CO_2 (1% CO_2, 99% synthetic air) utilizing mass flow controllers (Tylan General FC 280 SA). The total flow rate for the mixture of synthetic air and 1% CO_2 was maintained constant at 70 sccm/min during the

experiment. The open circuit voltage of the concentration cell was measured with a high input impedance (> 10^{14} Ω) electrometer (EM 1.0, Ionic Systems, Germany) and the electrical signal was further proceeded to a PCI-DAS6014 card (Measurement Computing) which collects all the datas, then use LabView (National Instruments Inc.) to record the data.

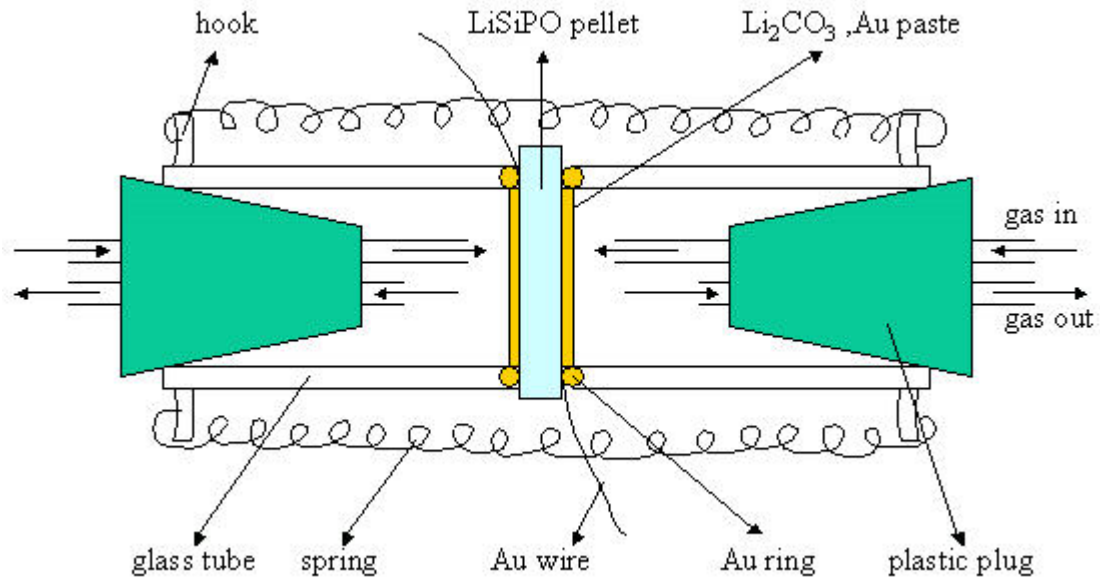

Figure 4.5: Schematic illustration of the experimental setup.

Measurements under CO_2 atmospheres were carried out in ``Kiel Cell`` where the temperature was controlled with either Pt/Pt-13% Rh thermocouples connected with THERM 3280-1 temperature controller or with NiCr/Ni thermocouples connected with Eurotherm 91E temperature controller. The desired carbon dioxide partial pressure was maintained by mixing synthetic air (synthetic air 5.5) with either pure CO_2 or diluted CO_2 (carbon dioxide 4.5) using mass flow controllers (Tylan FC-280 and Millipore 2900) with total flow rates 70 sccm/min, if otherwise not noted. All mass flow controllers used in this work have been calibrated using tables [10] in cases where those are applicable. Figure 4.6 shows the experimental arrangement for the investigations in CO_2 containing gas including the gas mixing system, tubular furnace for maintaining a certain temperature and instrument for measuring the electrical signal.

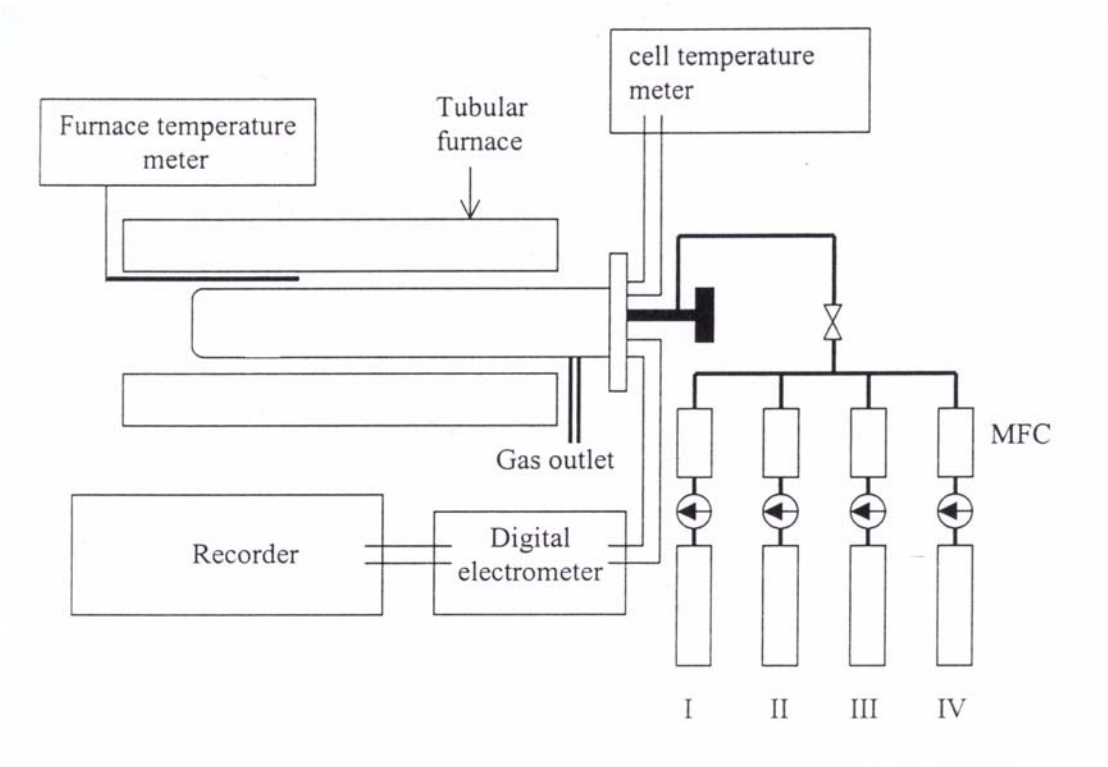

Figure 4.6: Schematic representation of the experimental setup for investigations under carbon dioxide atmospheres.

4.3 Experimental methods

Several experimental methods have been used in this work. A brief survey of impedance spectroscopy, scanning electron microscope, inductive coupling plasma, X-ray and thermal analysis will be presented in this paragraph.

Impedance measurements were carried out with two bridges. A 4192A LF Hewlett Packard Impedance Analyzer was used for the frequency region 13 MHz to 5 Hz while for lower frequencies down to 10^{-4} Hz an EIS-6416b impedance spectrometer utilized, combining a perturbation generator (PG-6416b) with a filter-amplifier (SR-640, Stanford Research Systems Inc.). The amplitude of the sinusoidal perturbation was in the range 40-100 mV. For electrochemical cells with an open circuit voltage under the experimental conditions when the complex impedance has been measured, compensation of the voltage was performed during the impedance measurements. The bridges were placed as close as possible to the experimental setup to minimize inductive or capacitive effects at high frequencies. Impedance

measurements were repeated to avoid any stray capacitive effects. The minimum frequency was chosen in order to fulfill the stability criterion for the electrochemical system under investigation.

Scanning electron microscope (SEM) was carried out with a computer controlled Philips XL30 microscope without coating the specimens. This instrument provides the possibility to look at topography of samples-interfaces and simultaneously determine the elemental compositions in distinct regions. The principle of SEM is based on the bombardment of a sample with a focused beam of electrons whereas the detected scattered electrons from the surface producing a highly magnified image. As a by-product of the interaction of the electron beam with the atoms in the sample surface x-rays are produced having energies which are characteristic of the atoms that produce them. Thus by attaching a energy-dispersive detector information for the elemental composition can be obtained.

A quantitative method of extracting information for the chemical composition of a sample provided by use of ICP. Inductively couple plasma (ICP) discharge is a source of atomic emission spectrometry. RF power is applied to a coil causing electric and magnetic fields to be set up in the surrounding area. With argon gas flowing through a spark, electrons are accelerated by the RF fields, causing further ionization and forming plasma. The sample typically in a solution form, is introduced through the induction region. Quantitative information obtained by comparing the emission spectrum of the sample to a reference one corresponding to a standard solution with known concentrations of the elements of interest. ICP measurements were performed using a computer driven instrument (Optima 3X00, Perkin Elmer Corp., Norwalk, USA).

Differential thermal analysis (DTA) is a dynamic technique where the temperature difference between the material under investigation and a reference material is measured at a function of temperature. The sample typically in fine powder form is inserted into a furnace where both substance and reference material are heated up to a certain temperature. Because this is a differential technique sensitive changes can be easily registered. Thermogravimetric analysis (TGA, TG) is a technique in which the mass of a substance is measured as a function of temperature or time while substance and reference material are subjected to a temperature program. For both differential thermal analysis and thermogravimetric analysis the temperature raise in typically linear. The reference substance should show no phase transitions within the

measured temperature range, have a similar heat conductivity and heat capacity s the measured one and should not react with the substance under study. A computer controlled thermal analyzer (STA 409 C NETZSCH) was used in this work, where simultaneously DTA and TGA/TG could be performed. The temperature raise with 5 °C/min if otherwise not noted. As reference material Al_2O_3 has been used. The temperature difference of substance and reference material registered with PtPh 10%-Pt thermocouples whereas the surrounding atmosphere could be controlled by having a special gas, or left open to air.

For cold pressing powder to form pellets or bars uniaxially or isostatic techniques have been used. Isostatically, the powder could be pressed to form bars of 6-10 mm diameter and up to about 15 min in length. Uniaxially the powder was pressed to form pellets of 6-10 mm diameter and 1-2 mm in length.

X-ray measurements were conducted with two diffractometers (SEIFERT XRD 3000 TT and 3000PTS) where Cu K_α radiation was used. X-ray analysis of the materials used in this work either in powder of in pellet form was performed as a preliminary investigation of the materials used.

Pellets were polished with a polishing machine (Potopol-V, Struers, Copenhagen, Denmark) using polishing discs of different roughness down to 1 μm.

Reference to Chapter 4

[1] Y – W. Hu, I. D. Raistrick, and R. A. Huggins, Mater. Res. Bull **11**, 1227 (1976)

[2] Y – W. Hu, I. D. Raistrick, and R. A. Huggins, J. Electrochem. Soc. **8**, 1240 – 1242 (1977)

[3] H.Völlenkle, A. Wittmann, and H. Nowotny, *Monatsh. Chem.,* **99**, 1360 (1968)

[4] A. F. Wells, Structural Inorganic Chemistry, 5th ed., Oxford Science Publications, Clarendon Press, Oxford, UK 1984.

[5] V. Thangadurai, W, Weppner, *Adv. Funct. Mater*. **15**, No. 1, January 2005

[6] Y.C.Zhang, H.Tagawa, S.Asakura, J.Electrochem.Soc., 144, 4345-4350 (1997)

[7] Q.Zhong, J.R.Dahn, and K.Colbow, *The American Physical Society*, **46** [4] 2554-2560 (1992)

[8] P.J.Wiseman, P.G.Dickens, *J. Solid State Chem.,* **17**, 91-100 (1976)

[9] I.J.Davidson, R.S.McMillan, J.J.Murray, J.E.Greedan, *J. Power Sources* **54**, 232 - 235 (1995)

[10] Tylan General Instruction Manual, Mass flow Controllers and Flowmeters

CHAPTER 5

Results

5.1 Performance of CO_2 gas concentration cell

The solid state CO_2 gas concentration cell has the following type:

$$O_2^{'}, CO_2^{'}, Au \overset{I}{|} Li_2CO_3 + Au(paste) \,|\, LiSiPO \,|\, Li_2CO_3 + Au(paste) \overset{II}{|} Au, O_2^{''}, CO_2^{''} \quad (5.1)$$

The following reaction takes place at electrode (I):

$$2Li^+ + 2e^- + \tfrac{1}{2}O_2^{'} + CO_2^{'} \leftrightarrow Li_2CO_3^{'} \quad (5.2)$$

The activity of Li at (I), a_{Li}^{I}, of this electrode (I) can be expressed as a function of $P_{CO_2}^{'}$ and $P_{O_2}^{'}$ as follows:

$$\ln a_{Li}^{I} = -\frac{\Delta G_{f(Li_2CO_3)}^{o} - \Delta G_{f(CO_2)}^{o}}{2RT} - \tfrac{1}{4}\ln P_{O_2^{'}} - \tfrac{1}{2}\ln P_{CO_2^{'}} \quad (5.3)$$

At electrode (II), the following reaction (5.4) takes place:

$$2Li^+ + 2e^- + \tfrac{1}{2}O_2^{''} + CO_2^{''} \leftrightarrow Li_2CO_3^{''} \quad (5.4)$$

The activity of Li at (II), a_{Li}^{II}, can be equally expressed as a function of $P_{CO_2}^{''}$ and $P_{O_2}^{''}$.

$$\ln a_{Li}^{II} = -\frac{\Delta G_{f(Li_2CO_3)}^{o} - \Delta G_{f(CO_2)}^{o}}{2RT} - \tfrac{1}{4}\ln P_{O_2^{''}} - \tfrac{1}{2}\ln P_{CO_2^{''}} \quad (5.5)$$

Mixtures of synthetic air containing no CO_2 (21% O_2, 89% N_2) and synthetic air containing 1% CO_2 (1% CO_2, 99% synthetic air) were applied to the two sides of the electrolyte. The oxygen partial pressures were always kept the same at the two interfaces,

$$P_{O_2^I} = P_{O_2^{II}} = P_{O_2} \quad (5.6)$$

Thus, according to equations (5.3), (5.5) and (5.6), the EMF of the CO_2 gas concentration cell (5.1) is given by

$$E = \frac{RT}{2F}(\ln P_{CO_2^{'}} - \ln P_{CO_2^{''}}) \quad (5.7)$$

R is the gas constant, T the absolute temperature and F the Faraday's constant.

5.1.1 Cell characteristics

The X-ray powder diffraction pattern of LiSiPO confirmed that a single phase was obtained. This is shown in figure 5.1.

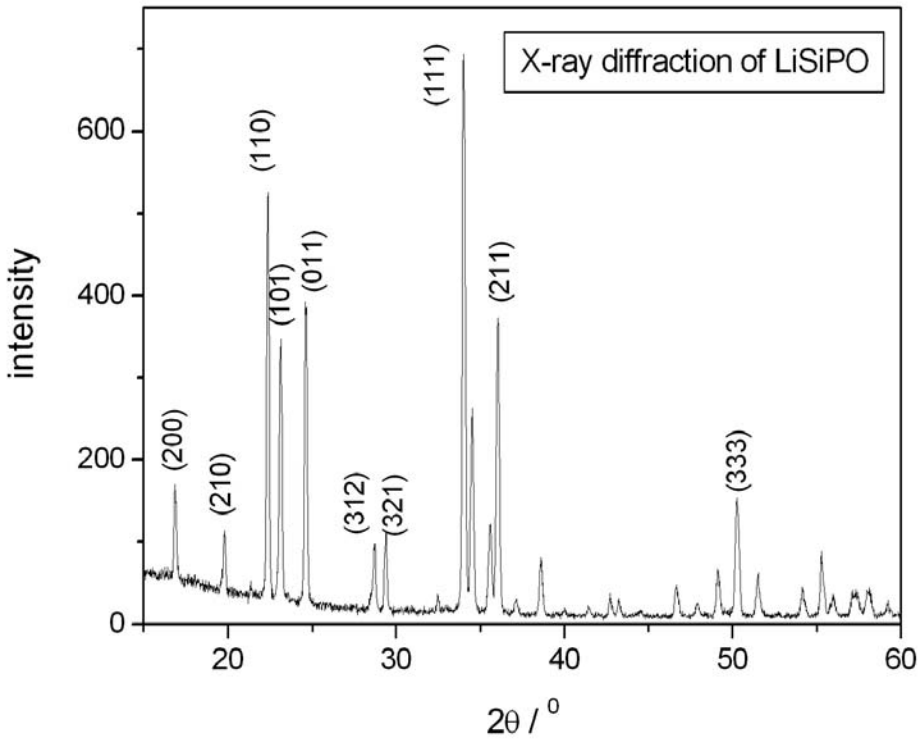

Figure 5.1: X-ray diffraction of LiSiPO.

A typical impedance plot for LiSiPO is shown in figure 5.2 for both sides with Au paste electrodes in air. For blocking electrodes, a sharp increase in the imaginary part is observed following the semicircle which corresponds to the bulk resistance. Figure 5.3 shows the experimental results of AC conductivity measurements of LiSiPO. The curvature in the Arrhenius plot at high temperature is attributed to experimental difficulties when the lead resistance becomes comparable in magnitude with the electrolyte resistance. For the straight line regime, the pre-exponential term (extrapolation of the conductivity to $T \to \infty$) is $\sigma_0 = 1.25 \times 10^6 \, Scm^{-1}K$. The activation energy E_a has a value of 0.4 eV.

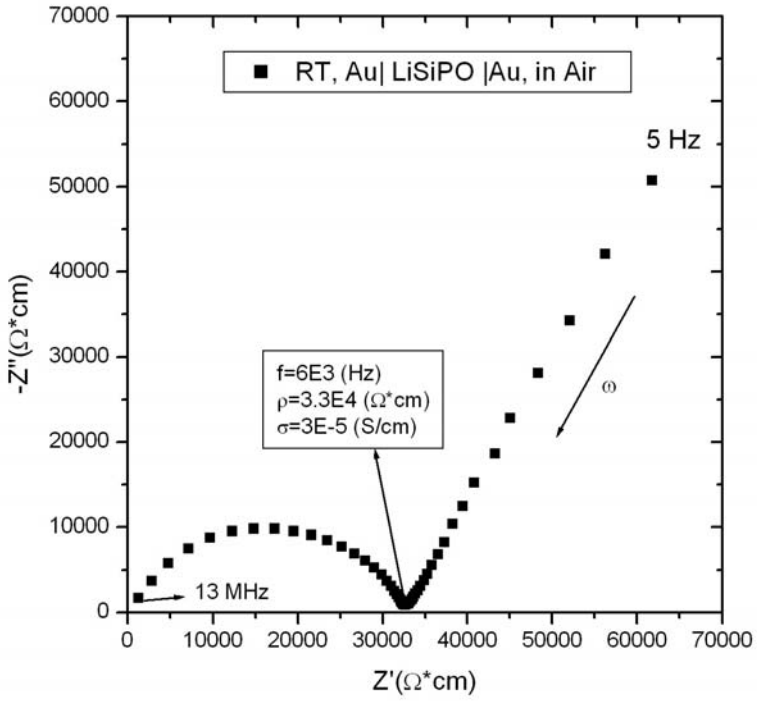

Figure 5.2: AC impedance spectra of LiSiPO both sides with Au paste electrodes in air at room temperature.

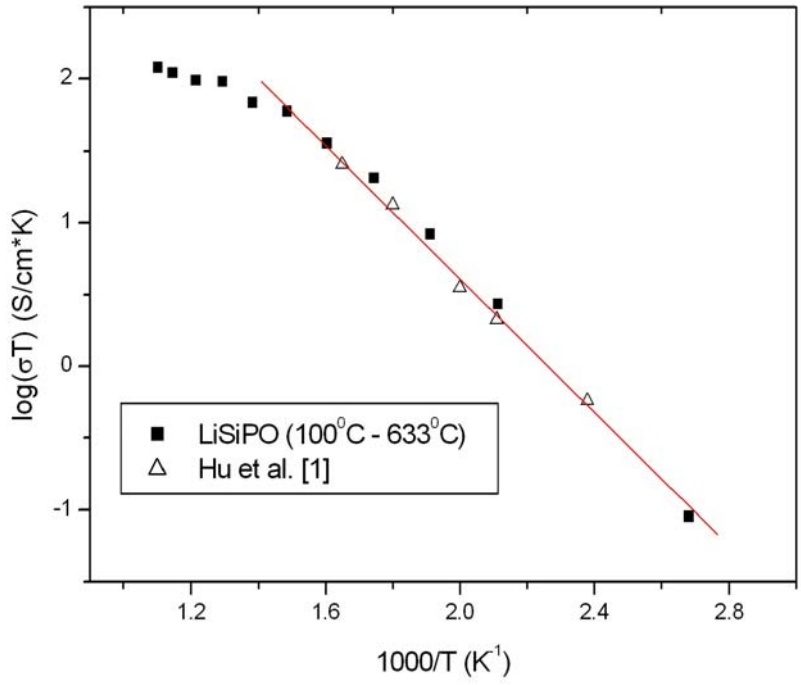

Figure 5.3: Arrhenius plot of the ionic conductivity of LiSiPO.

The SEM picture shown in figure 5.4 gives evidence of a good contact between the electrolyte and the electrode.

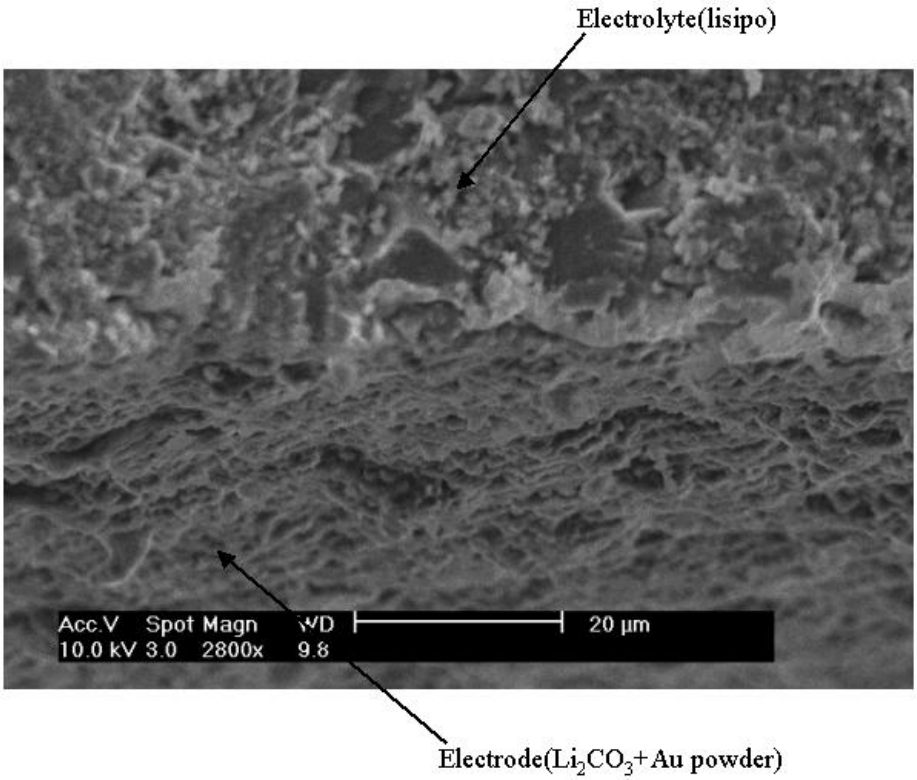

Figure 5.4: SEM picture of the interface between the electrode and the electrolyte.

5.1.2 EMF measurements

The cell has been heated up to the desired temperature with low heating rate (1°C/min). The mixture of lithium carbonate and Au paste was painted on both sides of LiSiPO. Before measurements were carried out, the cell was heated to 600°C for short time to ensure adequate adhesion of electrodes to the electrolyte. The desired carbon dioxide concentration was maintained by mixing pure or diluted carbon dioxide with synthetic air. EMF measurements were performed from 200 to 400 °C and by variable CO_2 concentrations of 100 ppm, 350 ppm (common air) and 1000 ppm with constant oxygen partial pressure of 0.205 bar at both electrodes and the total gas mixture flow rate equal to 70 sccm/min. The temperature variation of the emf of the cell (5.1) is shown in figure 5.5. It is observed from the diagram, that the measured EMFs have nearly the same values as calculated according to Eq. (5.7). The

maximum discrepancy is only 4 mV. In Eq. (5.7), at both sides, the Gibbs energies of formation of Li_2CO_3 are assumed to be the same. The results also confirmed that the two Li_2CO_3 layers at the both electrodes are identical and the reactions (5.2) and (5.4) are reversible. According to Eq. (5.7), the slope is $\frac{R}{2F}(\ln P_{CO_2'} - \ln P_{CO_2''})$. For comparison, the corresponding sensitivity according to Nernst's equation for a two electrons process is also shown in Table. 5.1 and Table 5.2. The dependence of the electromotive force of the cell (5.1) on the differences of the CO_2 partial pressure is shown in figure 5.6 from 200 °C to 400 °C. The open circuit voltage varies approximately linearly with the logarithm of CO_2 concentration, and increases with increasing CO_2 partial pressure at constant temperature, while it decreases with increasing temperature at fixed CO_2 partial pressure. According to Nernst's Equation, this is a two - electron process, from Table 5.2 the measured values are 1.95, 1.95, 1.94 at 200 °C, 300 °C, 400 °C, respectively.

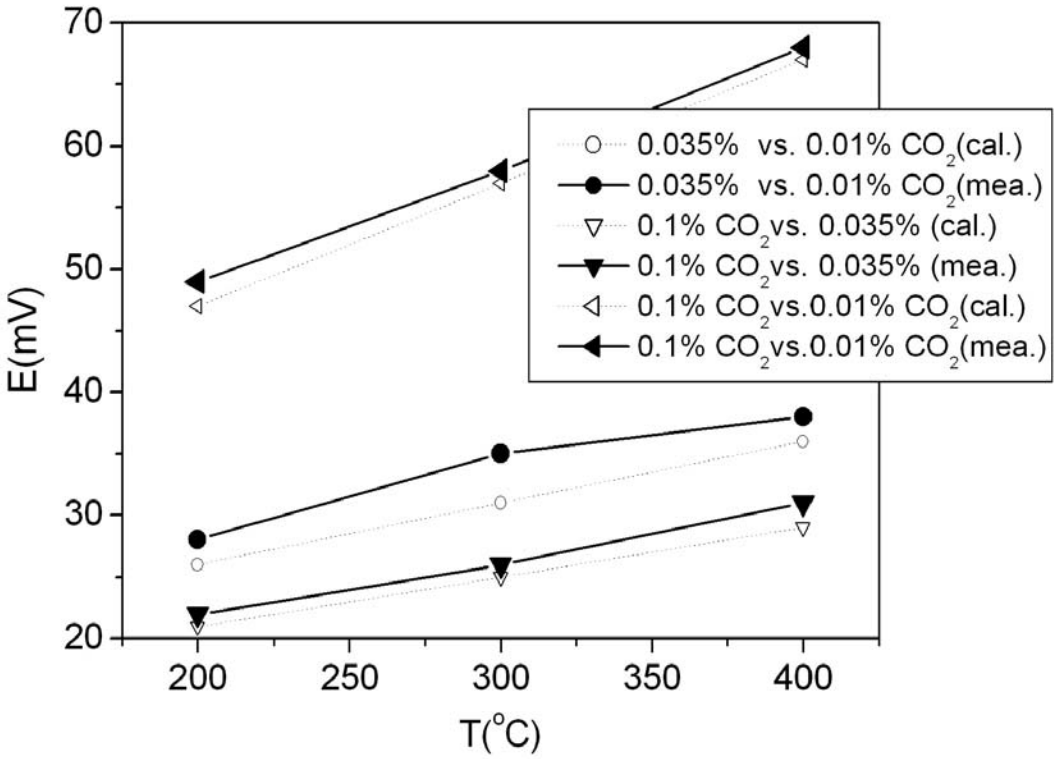

Figure 5.5: Experimental and calculated EMF as a function of temperature at various CO_2 concentrations.

CO_2 concentration	Measured slope (mV/K)	Calculated slope (mV/K)
100 ppm vs. 350 ppm (air)	5.3×10^{-2}	5.1×10^{-2}
1000 ppm vs. 350 ppm (air)	4.5×10^{-2}	4.4×10^{-2}
100 ppm vs. 1000 ppm	9.9×10^{-2}	9.8×10^{-2}

Table 5.1: Comparison of the slopes in different conditions.

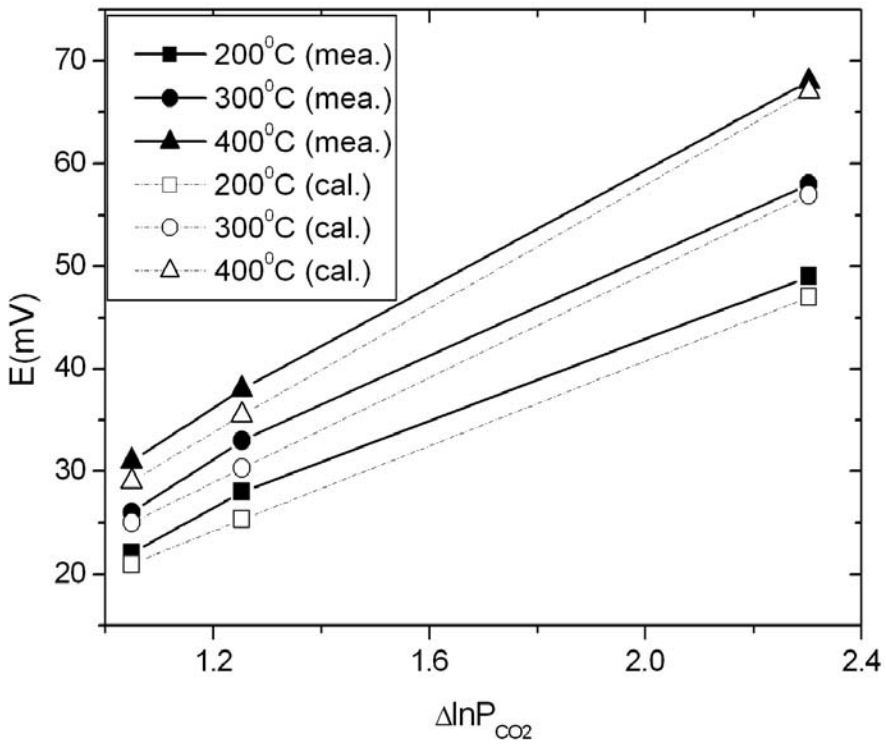

Figure 5.6: Experimental and calculated EMF as a function of $\Delta \ln P_{CO_2}$ at various temperatures.

Temperature (°C)	Measured slope (mV/decade)	Calculated slope (mV/decade)
200	20.5	21.0
300	24.7	25.3
400	29.2	30.1

Table 5.2: Comparison of the sensitivity at different temperature conditions.

Complex plane impedance plot of the gas concentration cell (5.1) at 400 °C is shown in figure 5.7. Impedance measurement was carried out with a perturbation amplitude of 50 mV in the frequency range 5 Hz to 13 MHz under carbon dioxide partial pressure of 0.1 atm. The evaluated capacitance for the interface LiSiPO – lithium carbonate and Au is 2.7×10^{-6} F at 400°C.

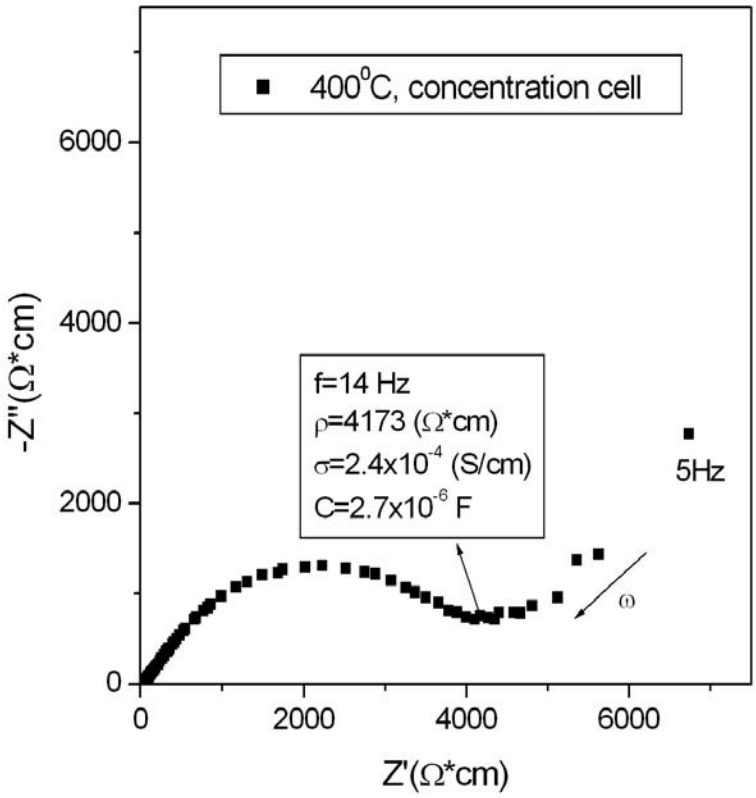

Figure 5.7: Complex plane impedance plot of the gas concentration cell (5.1) at 400 °C.

5.2 Solid reference electrodes for Potentiometric CO_2 sensor

This paragraph presents the results on the investigation of the kinetics of type III electrochemical cell with Li_2CO_3 and Au auxiliary compound under CO_2 atmospheres. The electrochemical cell under investigation may be written as:

Reference electrode | Lithium ion conductor | Sensing electrode, P_{O_2}, P_{CO_2} (5.8)

As reference electrode, in this work, seven different kinds of materials were selected and investigated.

5.2.1. Li as reference electrode

For the investigation of the kinetics and equilibration at the interface lithium carbonate sensing electrode – lithium ion conductor, elemental lithium has been used as reference electrode providing a lithium activity equal to unity. The electrochemical cell under investigation, which is schematically shown in figure 4.4 is written as:

$$Li \mid LiSiPO \mid Au, Li_2CO_3, CO_2, O_2 \qquad (5.9)$$

Because the elemental lithium is reactive in oxygen atmosphere, the electrolyte was made in the shape of a crucible in the glove box. The cell was heated up to the desired temperature with low heating rate (1°C/min). The lithium carbonate and Au paste was painted on the bottom of the electrolyte. Before measurements were carried out, the cell was heated to 200 °C and cooled to room temperature several times to ensure good adhesion of the elemental lithium to the electrolyte. The Schematic representation of the electrochemical cell under investigation in carbon dioxide atmospheres is shown in figure 4.4. The oxygen partial pressure was constant at 0.205 bar and the total gas mixture flow rate kept at 70 sccm/min. The working temperature was from 200 °C to 400 °C. For temperatures above 400 °C the sealing of elemental lithium was found to be inappropriate not allowing electrochemical measurements at higher temperatures. The dependence of the electromotive force of the cell (5.9) on the CO_2 partial pressure is shown in figure 5.8 from the temperature of 200 °C to 400 °C. The temperature variation of the emf response to CO_2 is shown in figure 5.9. Figure 5.10 shows the reproducibility and long time stability of the cell (5.9) voltages at 400 °C and CO_2 concentrations from 100 ppm to 10^6 ppm. When the temperature of 400 °C was reached, after nearly two minutes the cell voltage became 3079mV, it was only around 100mV lower than the calculated value (3168mV). But after two hours the value changed to 2640mV, nearly 600mV lower than the calculated one. When the cell was kept over a long time (≈22h), the voltage decreased slowly to 2588mV. Following changed the concentration of CO2 to 50000ppm (5%), resulted in 2658mV, 490mV lower than calculated value (3148mV). After 20 hrs the value decreased further to 2269mV. Subsequently change of the concentration of CO2 to 10000ppm (1%), resulted in 2238mV, 863mV lower than the calculated value (3101mV); after 20h it slowly decreased to 2133mV; using 1000ppm(0.1%) CO2, the observed emf was 2097mV, much lower (938mV) than

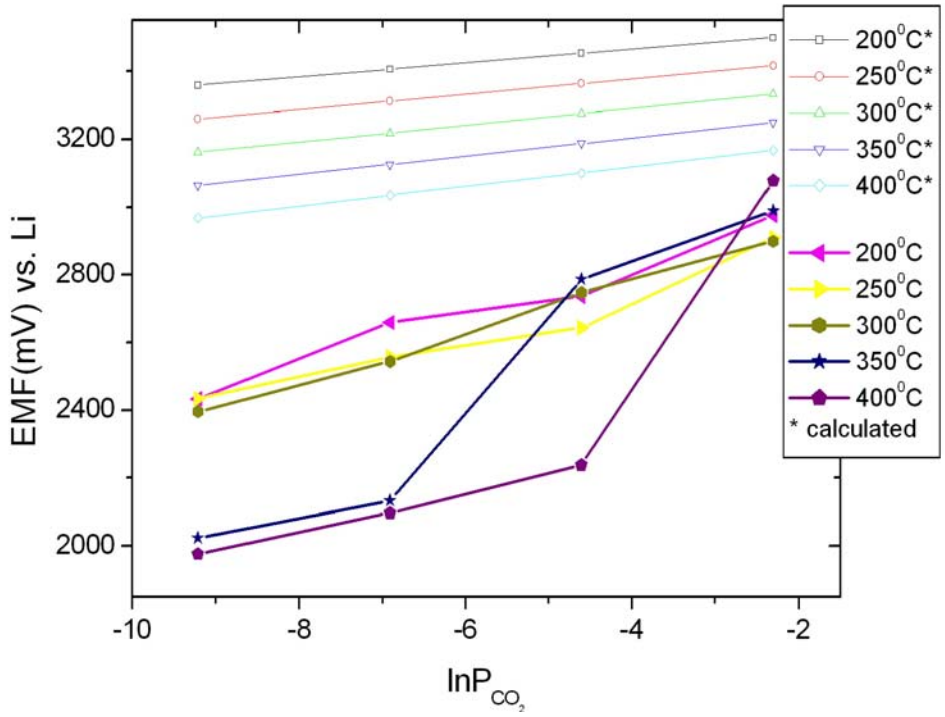

Figure 5.8: CO_2 partial pressure dependence of the cell (5.9) to EMF vs. elemental Li. * represents calculated values of the cell (5.9).

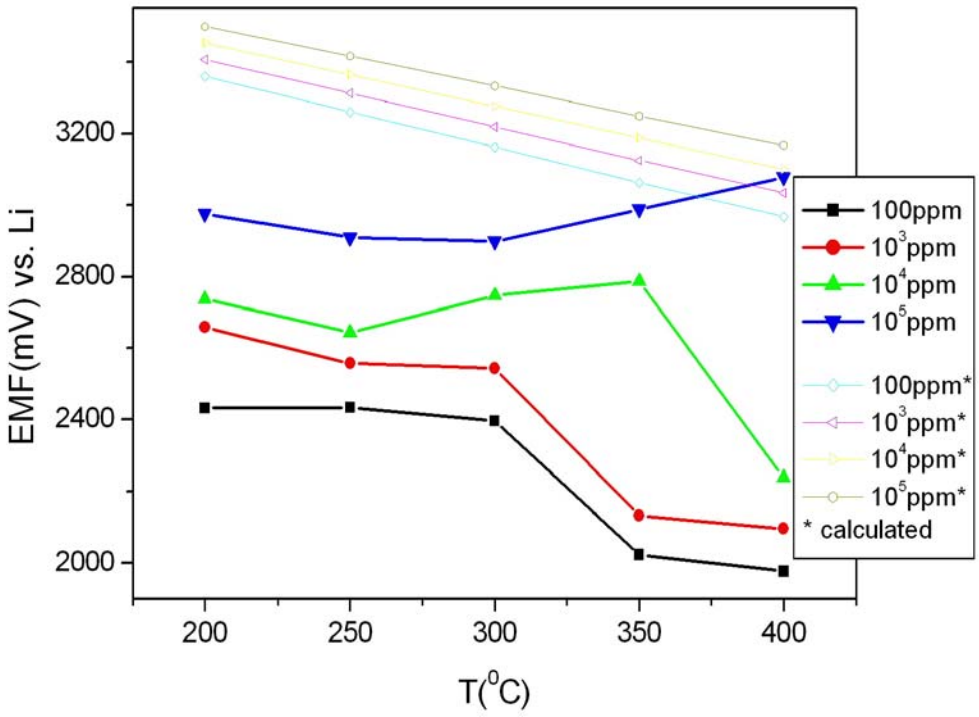

Figure 5.9: Temperature dependence of the EMF of cell (5.9) to CO_2. * The calculated values for a two – electron process are plotted for comparison.

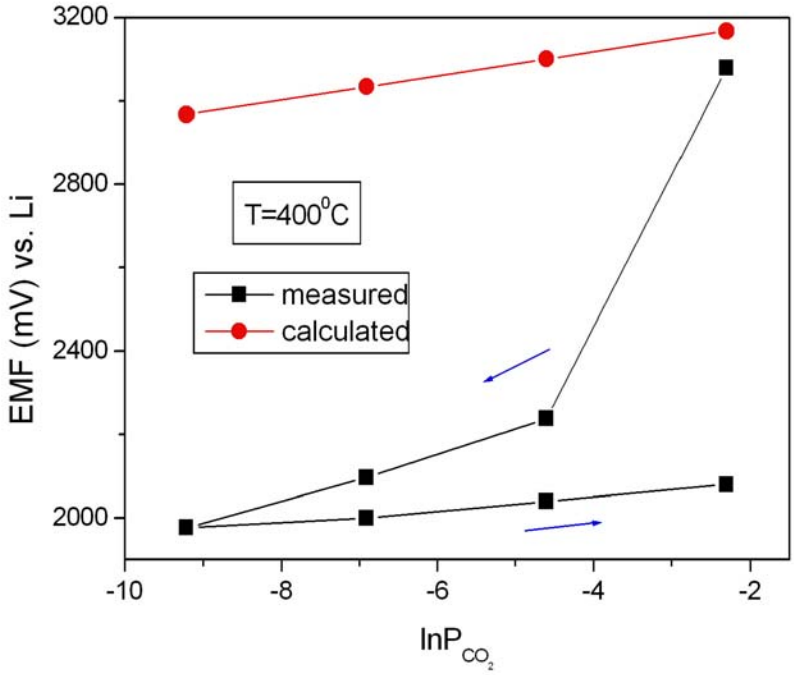

Figure 5.10: The reproducibility and long time stability measurement of the cell (5.9) at 400 °C at the CO_2 concentration from 100 ppm to 10^6 ppm.

calculated one (3035mV); when using 100ppm (0.01%) CO2, only 1977mV were left, 991mV lower than the theoretical value (2968mV). Increasing the concentration of CO2, resulted in 2000mV (1000ppm), 2040mV (10000ppm), and 2080mV (100000ppm). When the cells were taken out of the furnace, the ceramic glue, which was used for sealing, was always cracked. The complex impedance was measured in the frequency range from 200 mHz to 50 kHz employing a sinusoidal pertubation with 100 mV amplitude under 10^{-3} atm CO_2. The interfacial conductivities were 1 x 10^{-2} S / cm at 400 ° C and the corresponding interfacial capacitance was 1.8 μ F.

5.2.2 $Li_4Ti_5O_{12}$ as reference electrode

The prepared $Li_4Ti_5O_{12}$ electrode was checked by XRD diffraction through comparison with PCPDF data. The pure $Li_4Ti_5O_{12}$ phase was confirmed. This is schematically shown in figure 5.11. The electric conductivities of $Li_4Ti_5O_{12}$ remained nearly in the same range upon heating and cooling treatment from room temperature to 500 °C and the activation energy is 0.34 eV. This is shown in figure 5.12.

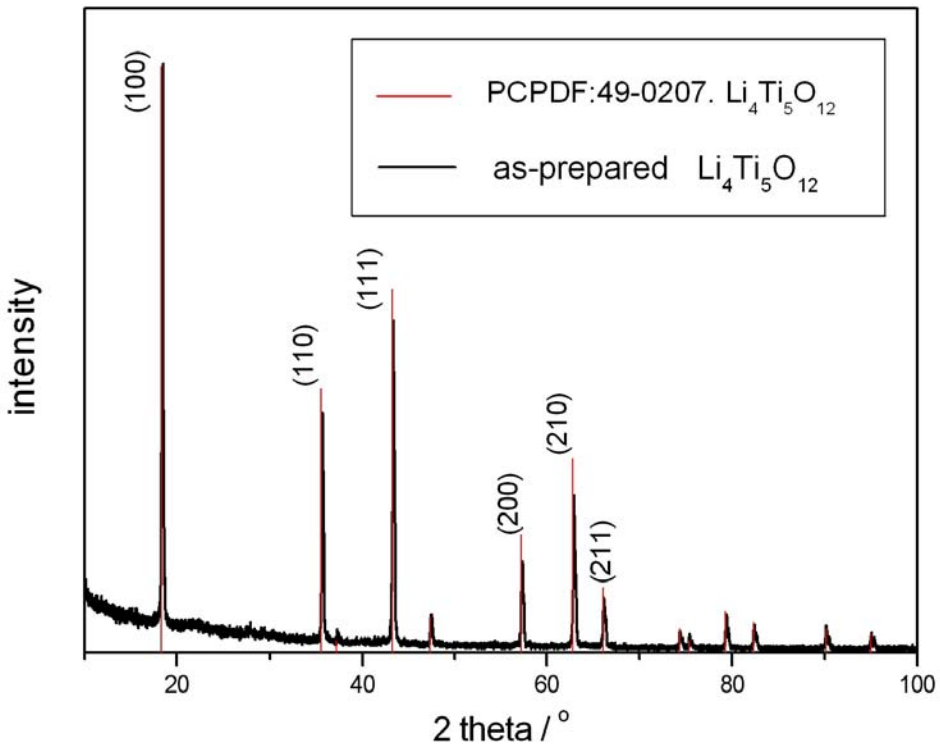

Figure 5.11: XRD pattern of as – prepared $Li_4Ti_5O_{12}$. The vertical red lines represent PCPDF (49-0207) data for $Li_4Ti_5O_{12}$.

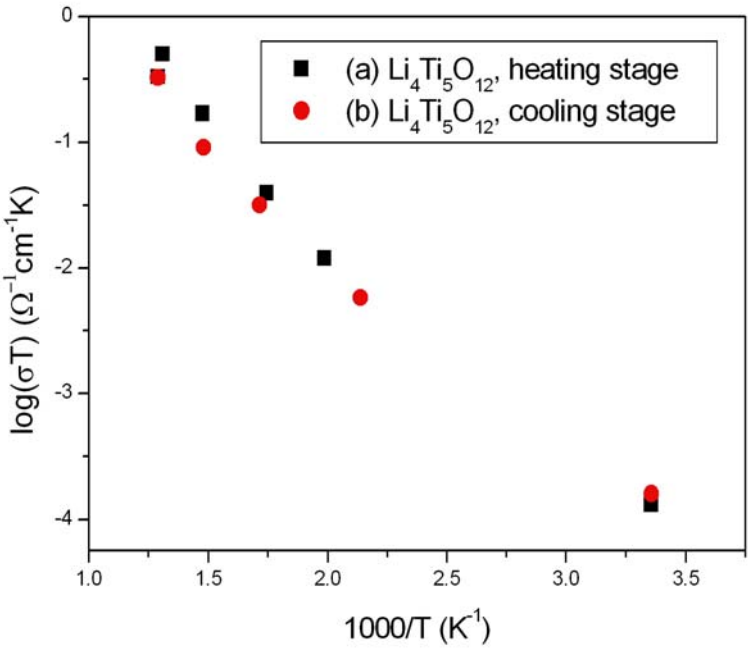

Figure 5.12: Arrhenius plot of $Li_4Ti_5O_{12}$ from room temperature to 500 °C. (a) represents heating data; (b) represents cooling data.

For the investigation of the characteristics of the electrochemical cell lithium titanate was used as reference electrode. The electrochemical cell under investigation under CO_2 atmospheres as schematically shown in figure 4.3 is written as:

$$Au, Li_4Ti_5O_{12} \mid LiSiPO \mid Li_2CO_3, Au, CO_2, O_2 \qquad (5.10)$$

The cell was heated to 400 °C and 450 °C in 1 % (10000 ppm) CO_2 with constant gas flow rate of 70 sccm/min. The transient response of the emf of cell (5.10) for various changes of the CO_2 partial pressure at 450 °C is shown in figure 5.13. The CO_2 partial pressure changed was: (a) from 0.01 atm to $1x10^{-3}$ atm, (b) from $1x10^{-3}$ atm to $8x10^{-4}$ atm, (c) from $8x10^{-4}$ atm to $5x10^{-4}$ atm, (d) from $5x10^{-4}$ atm to $3x10^{-4}$ atm, (e) from $3x10^{-4}$ atm to $1x10^{-5}$ atm, (f) from $1x10^{-5}$ atm to $3x10^{-4}$ atm, (g) from $3x10^{-4}$ atm to $5x10^{-4}$ atm, (h) form $5x10^{-4}$ atm to $8x10^{-4}$ atm, (i) from $8x10^{-4}$ atm to $1x10^{-3}$ atm, (j) from $1x10^{-3}$ atm to $8x10^{-4}$ atm, (k) from $8x10^{-4}$ atm to $5x10^{-4}$ atm, (l) from $5x10^{-4}$ atm to $3x10^{-4}$ atm, (m) from $3x10^{-4}$ atm to $1x10^{-5}$ atm. While varying the carbon dioxide partial pressure, the oxygen partial pressure was maintained to be equal to 0.205 bar.

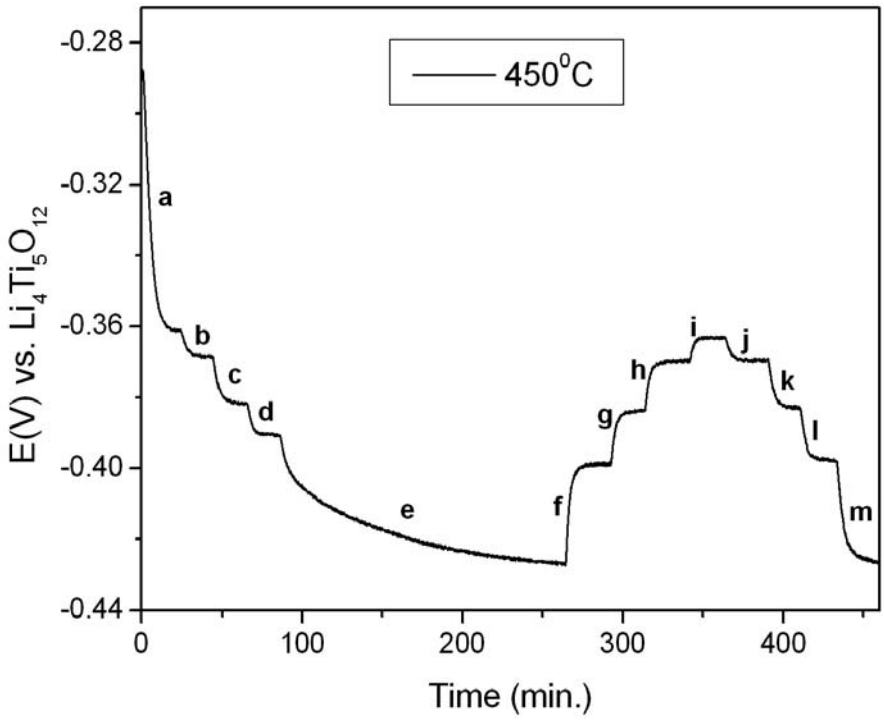

Figure 5.13: Transient responses to the cell (5.10) upon changes of the CO_2 partial pressure at 450 °C.

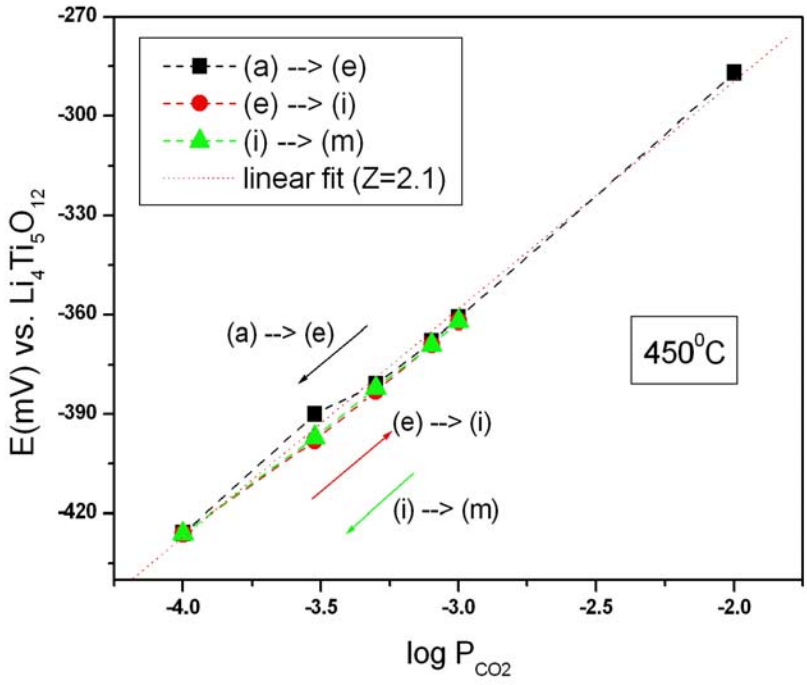

Figure 5.14: Open circuit voltage of the cell (5.10) vs. logarithm of CO_2 partial pressure at 450 °C.

Considering the experimental setup, the gas mixture was required to travel a certain distance until if reaches the sensor device. The time for providing another gas composition over the cell was about 7 min. Figure 5.14 shows the open circuit voltage as a function of the CO_2 partial pressure at 450 °C. The cell voltage varies linearly with the logarithm of CO_2 partial pressure; the sensitivity, that is the slope of the straight line agrees reasonably well with the excepted one for a two – electron process, providing an experimental value of Z = 2.1. Figure 5.15 shows the temperature dependence of the sensitivity of the emf of cell (5.10) in comparison to the calculated one from Nernst's equation for a two – electron process. The experimental evaluation of the sensitivity at different temperatures was carried out in the range from 10^{-4} to 10^{-3} atm CO_2. The experimental sensitivities are 65.8 mV/dec, 70 mV/dec and 76 mV/dec at 400 °C, 450 °C and 500 °C, correspondingly.

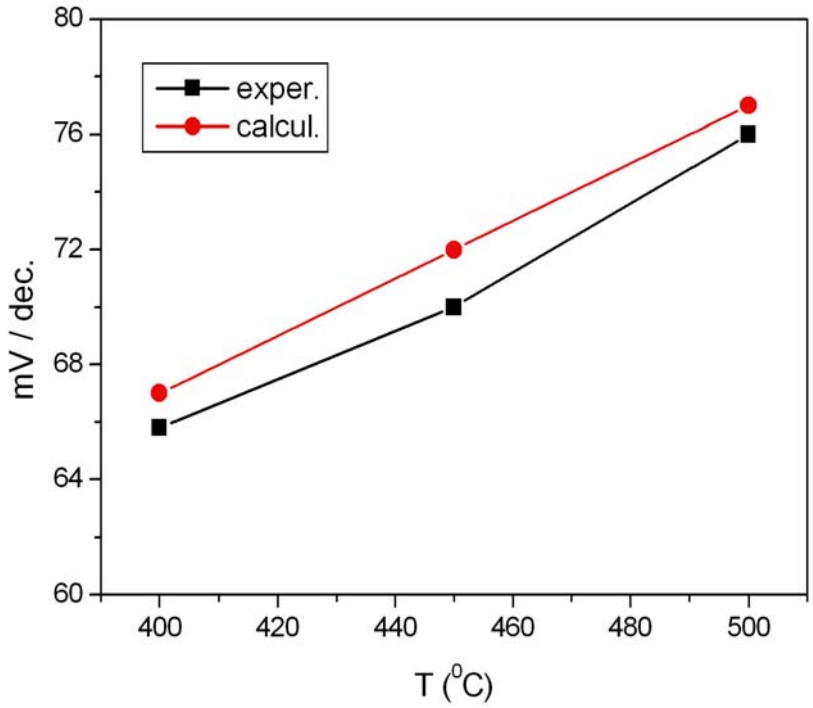

Figure 5.15: Temperature dependence of the experimental sensitivity of cell (5.10) to carbon dioxide, in comparison to the calculated one.

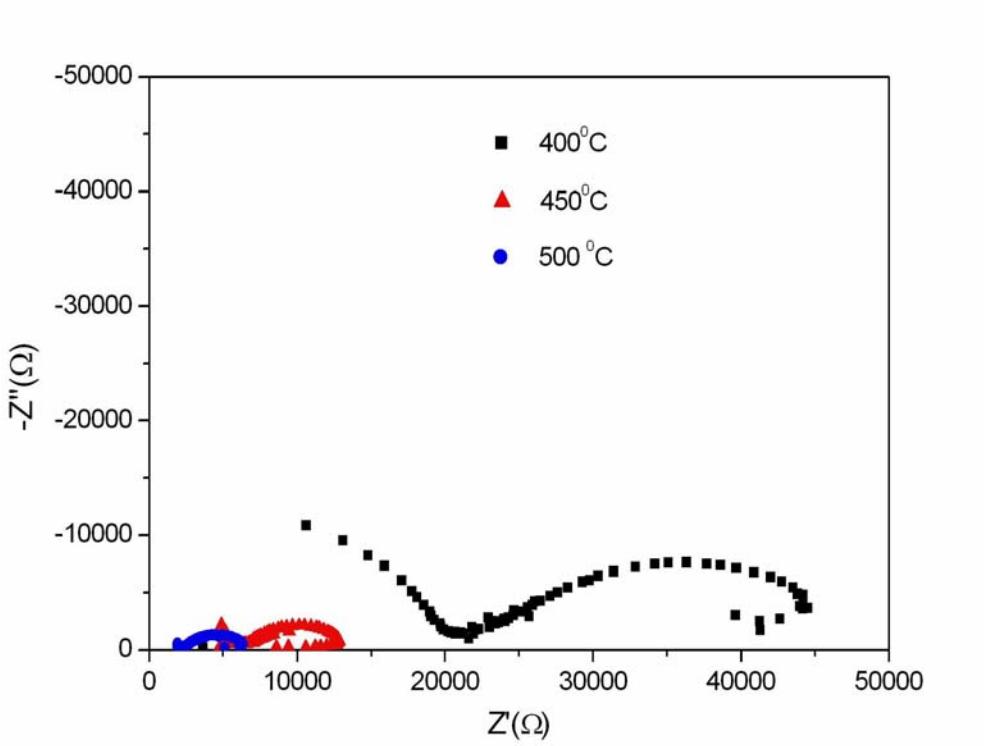

Figure 5.16: Complex plane impedance plots of the cell (5.10) at 400 °C, 450 °C and 500 °C.

To investigate the kinetic processes taking place at the interface during operating the cell at elevated temperatures and aging of the sensor, impedance spectroscopy was applied. The complex impedance was measured in the frequency range from 1 mHz to 50 kHz employing a sinusoidal pertubation with 100 mV amplitude under 10^{-3} atm CO_2. The frequency dispersion in the impedance plots consists of two semicircles. Figure 5.16 shows complex plane impedance plots of the sensor at 400 °C, 450 °C and 500 °C, respectively. During increasing the measuring temperatures, the interfacial resistances of the sensor were 20.7 kΩ, 6 kΩ and 2 kΩ at 400 °C, 450 °C and 500 °C, respectively. Figure 5.17 shows complex plane impedance plots of a freshly prepared sensor in dependent of the aging time. At 450 °C, the sensor shows the interfacial resistance of 6 kΩ at the first day and after 48 hrs it shows 2.6 kΩ of the interfacial resistance. The reproducibility of the open circuit voltage values of

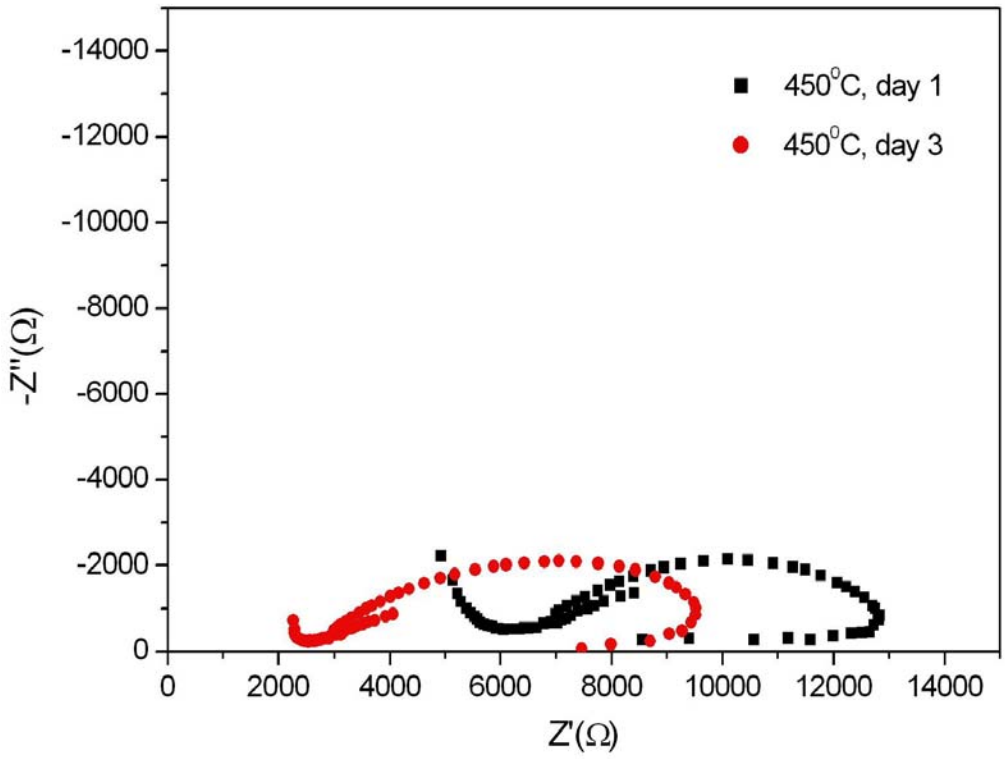

Figure 5.17: Complex plane impedance plots of the cell (5.10) during aging time at 450 °C.

cells at a fixed CO_2 concentration and temperature is within 40 mV. The long term stability test of several cells showed after aging of the sensors further shift of the open

circuit voltage absolute value between 1 – 6 mV per month independently on the composition employed for the auxiliary compound.

To further investigate the characteristics of the $Li_4Ti_5O_{12}$ as reference electrode, in situ prepared compound was used in this following test cell:

$$Au, Li_{4+\delta}Ti_5O_{12}(in \quad situ \quad formed) \mid Li_4Ti_5O_{12} \mid Li_2CO_3, Au, CO_2, O_2 \qquad (5.11)$$

In this cell, one pellet of $Li_4Ti_5O_{12}$ with 1.95 mm in thickness and 8.13 mm in diameter was selected as electrolyte. The cell was initially heated up to 450 °C in 10% CO_2 gas and a small current of 50 μA was passed through it moving lithium ions from the sensing electrode to the reference electrode side. The constant current of 50 μA was passed for 64 min which compounds to the formation of around 10 μm of

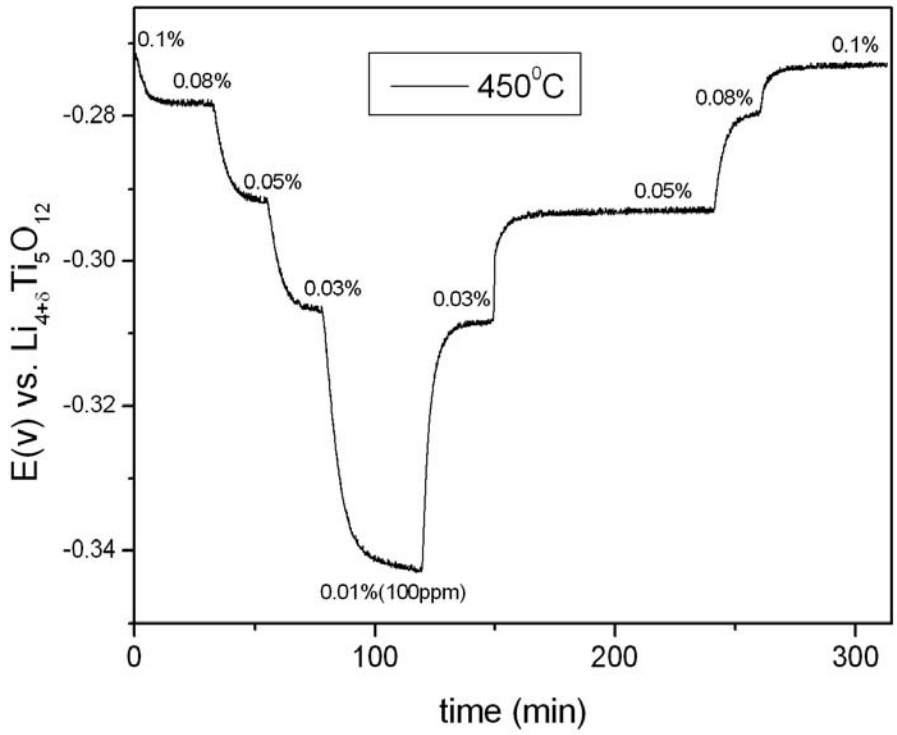

Figure 5.18: Transient responses to the cell (5.11) upon changes to the CO_2 partial pressure between 100 ppm and 1000 ppm at 450 °C.

$Li_{4+\delta}Ti_5O_{12}$ as reference electrode. Figure 5.18 shows the cell response to the CO_2 concentration which decreased from 0.1% (1000 ppm) to 0.01% (100 ppm) and increased from 0.01% (100 ppm) to 0.1% (1000 ppm). The response time t_{90} at 450 °C is 1 - 2 min. The open circuit voltage of cell (5.11) vs. logarithm of CO_2 partial

pressure at 450 °C is shown in figure 5.19. The experimental values agree with Nernst's law. The sensitivity to CO_2 translated to the number of electrons involved in the cell reaction at 450 °C, provides a value of 2.1 which is well in agreement with the expected value Z = 2. The small uncertainty in the reproducibility of the sensitivity to carbon dioxide observed in the experiments with other same prepared cells is within the agreement between the experimental and the calculated sensitivity.

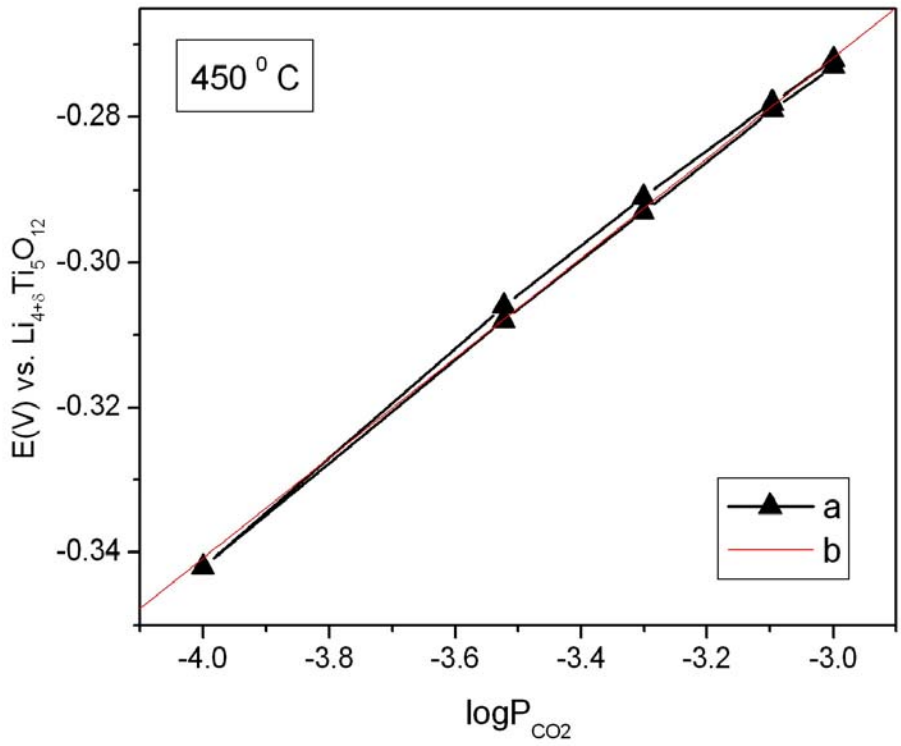

Figure 5.19: Open circuit voltage of cell (5.11) vs. logarithm of CO_2 partial pressure at 450 °C. (a) represents the experimental open circuit voltages from 100 ppm to 1000 ppm; (b) represents the linear fit of the experimental values and provides the experimental sensitivity of 69 mV/dec (calculated value is 72 mV/dec at 450 °C).

5.2.3 HgLi as reference electrode

Because HgLi is active in oxygen atmosphere, the electrolyte was made in the shape of a crucible and the preparation of the reference electrode was carried out in the glove box. Proper amounts of elemental lithium and mercury were mixed in the crucible which was made out of LiSiPO. The cell was heated up to the desired

temperature with low heating rate (1°C/min). The lithium carbonate and Au paste was painted on the bottom of the electrolyte. Before measurements were carried out, the cell was heated to 200 °C and cooled down to room temperature several times to ensure good adhesion of the reference electrode to the electrolyte. The schematic representation of the electrochemical cell under investigation in carbon dioxide atmospheres is shown in figure 4.2. The oxygen partial pressure was constant at 0.205 bar and the total gas mixture flow rate kept at 70 sccm/min. The electrochemical cell was written as:

$$HgLi \mid LiSiPO \mid Au, Li_2CO_3, CO_2, O_2 \tag{5.12}$$

The cell was heated up to 400 °C with a heating rate of 6 °C / min and a concentration of 50 % CO_2 gas. The open circuit voltage was stable at 2.38 V, then the concentration of the CO_2 gas was decreased to 0.1 %. Following, the CO_2 concentration was increased from 0.1 % to 20 %, decreased from 20 % to 0.5 %, increased from 0.5 % to 20 %. Transient responses of the cell for various changes of the CO_2 partial pressure at 400 °C are shown in figure 5.20. The cell was also tested at 350 °C and 300 °C. The temperatures sensitivities of the cell (5.12) were

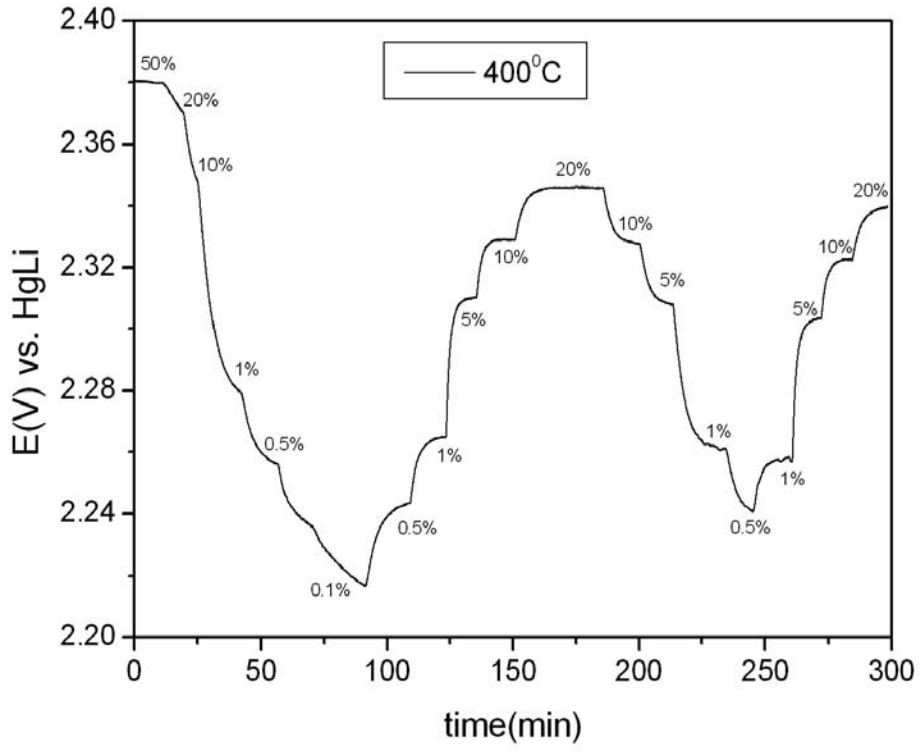

Figure 5.20: Transient response to the cell (5.12) upon changes to various concentrations of CO_2 gas at 400 °C.

47 mV/dec, 57 mV/dec and 63 mV/dec at 300 °C, 350 °C and 400 °C, respectively. Figure 5.21 shows the temperature dependence of the sensitivity of cell (5.12) in comparison to the calculated one from Nernst's equation for a two – electron process. The sensitivity to CO_2 translated to the number of electrons involved in the cell reaction, provides a value between 2.1 and 2.4. Figure 5.22 shows complex plane impedance plots of the cell (5.12) at different temperatures. The complex impedance was measured with an amplitude of 50 mV over the frequency range 1.5 Hz – 50 kHz at 400 °C and 350 °C and over the frequency range 20 mHz –50 kHz at 300 °C. The response time t_{90} is within 2 min at the measuring temperatures. The long term stability test of several cells after aging of the sensors showed a further shift of the open circuit voltage between 3mV and 10 mV per day independent of the sealing qualities of the ceramic glue.

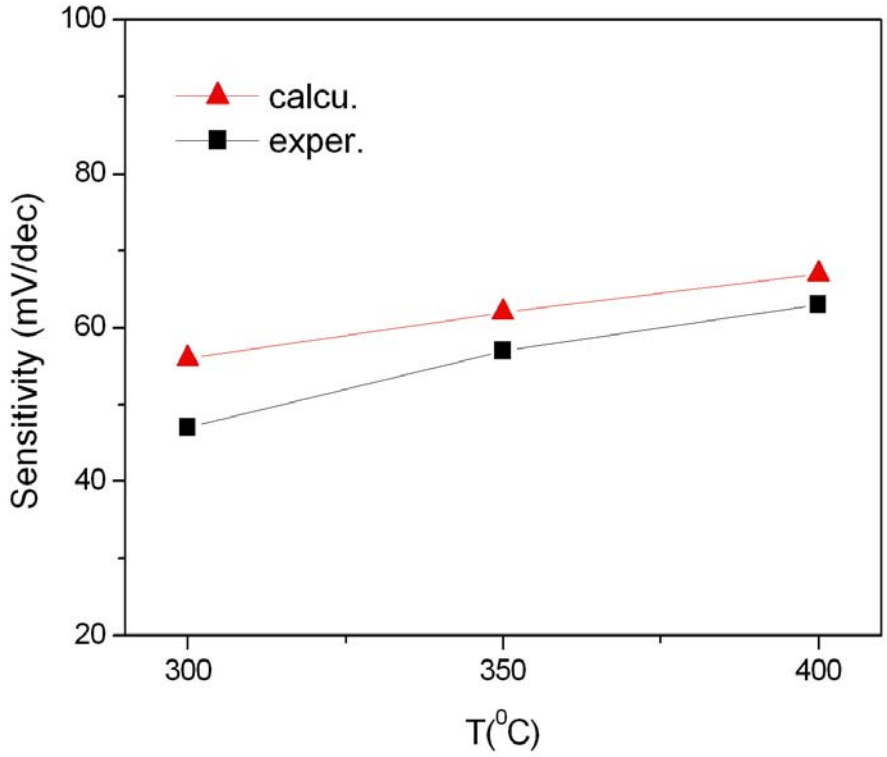

Figure 5.21: Temperature dependence of the experimental sensitivity of cell (5.12) to carbon dioxide in comparison to the calculated one.

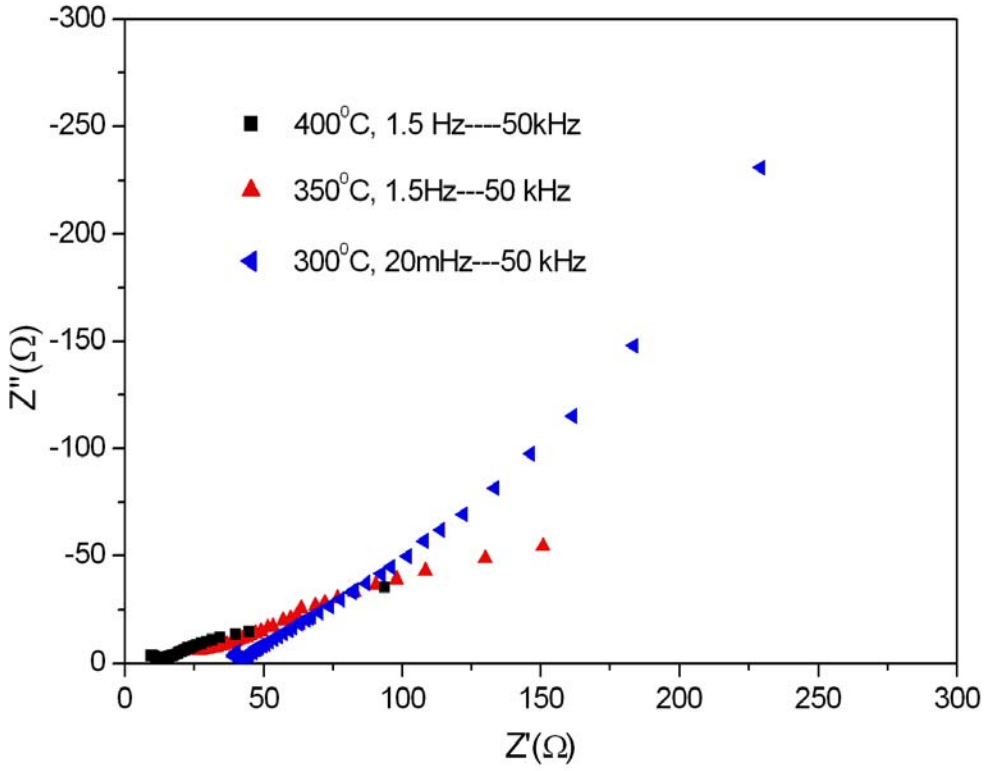

Figure 5.22: Complex plane impedance plots for the cell (5.12) at 400 °C, 350 °C and 300 °C.

5.2.4 Li_xWO_3 as reference electrode

For comparing Li_xWO_3 reference electrode, proper amounts of Li_2WO_4, WO_3 and W were mixed well and sintered in argon atmosphere at 750 °C for 2 hrs with heating and cooling rates of 1 °C / min. Figure 5.23 shows the X – ray powder diffraction pattern of as-prepared Li_xWO_3. The PCPDF data 76 –1497 correspond well to $Li_{0.36}WO_3$ to the as-prepared Li_xWO_3 powder. The lithium content was measured by use of ICP. It shows $x = 0.36 \pm 0.01$ which has a good agreement with the X – ray pattern of the as-prepared Li_xWO_3 with cubic structure. $Li_{0.36}WO_3$ shows good electronic conductivity. The value is 3.7 x 10^{-2} S/cm and the activation energy is 0.13 eV at 400 °C. The Arrhenius plot of $Li_{0.36}WO_3$ is shown in figure 5.24.

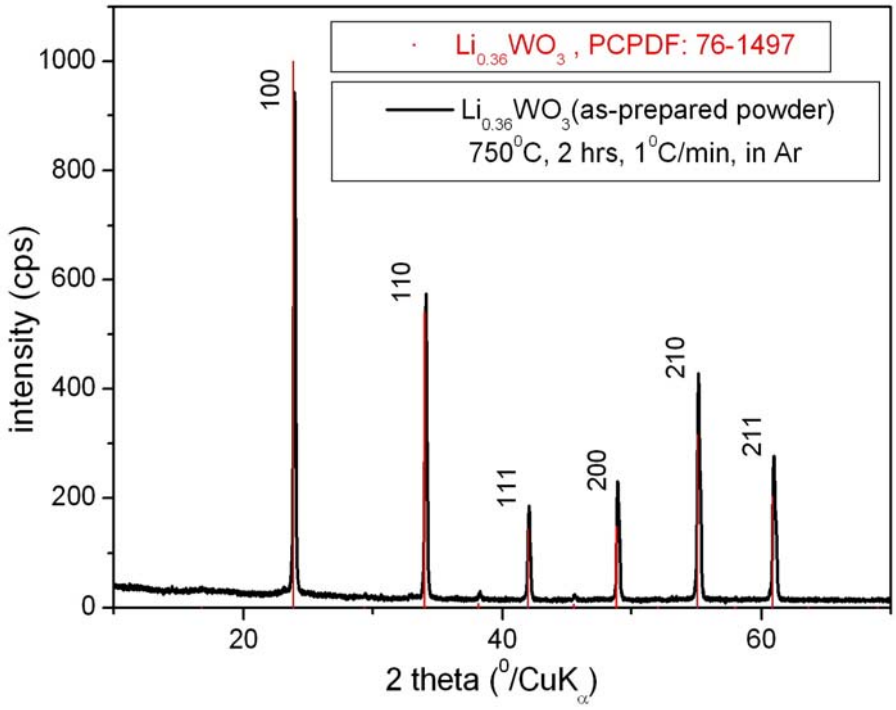

Figure 5.23: X – ray powder diffraction of as prepared $Li_{0.36}WO_3$ powder which agrees well with the PCPDF data of 76 –1497.

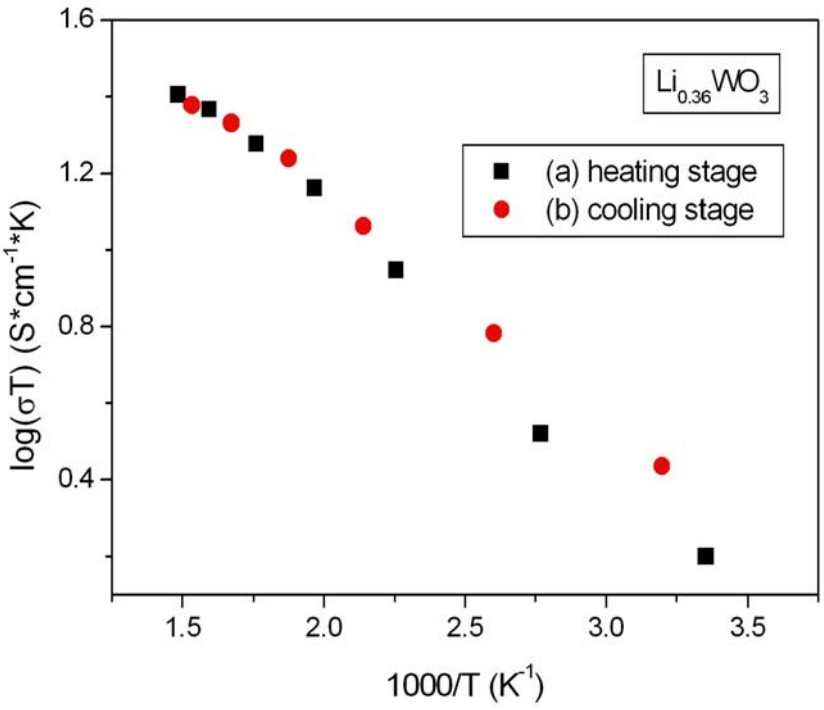

Figure 5.24: Arrhenius plot of $Li_{0.36}WO_3$ between 25 °C and 400 °C. (a) represents heating stage and (b) represents cooling stage.

When $Li_{0.36}WO_3$ was used as reference electrode, Garnet was selected as electrolyte. The electrochemical cell which is schematically shown in figure 4.3 was constructed as following:

$$Au, Li_{0.36}WO_3 \mid Garnet \mid Li_2CO_3, Au, CO_2, O_2 \qquad (5.13)$$

The cell was heated up to 450 °C initially with a heating rate of 6 °C / min in 10 % CO_2 gas concentration. During the experimental process, the oxygen partial pressure was kept at 0.205 bar and the total gas flow rate was kept 70 sccm / min. Figure 5.25 shows the transient responses of the cell (5.13) for various changes of the CO_2 concentration at 450 °C. The concentration of CO_2 gas changed from 10 % to 1 %, then from 1 % to 10 %, followed from 10 % to 0.01 %, then from 0.01 % to 10 %. Then the cell was heated to 500 °C. Figure 5.26 shows the transient responses of the cell for various concentrations of CO_2 at 500 °C. The concentration of CO_2 gas changed from 10 % to 0.01 %, then from 0.01 % to 10 %. The sensitivities of the cell (5.13) were 73 mV/dec (calculated sensitivity is 72 mV/dec) and 75 mV/dec (calculated sensitivity is 76 mV/dec) at 450 °C and 500 °C, respectively. The sensitivity to CO_2 translated to the number of electrons involved in the cell reaction,

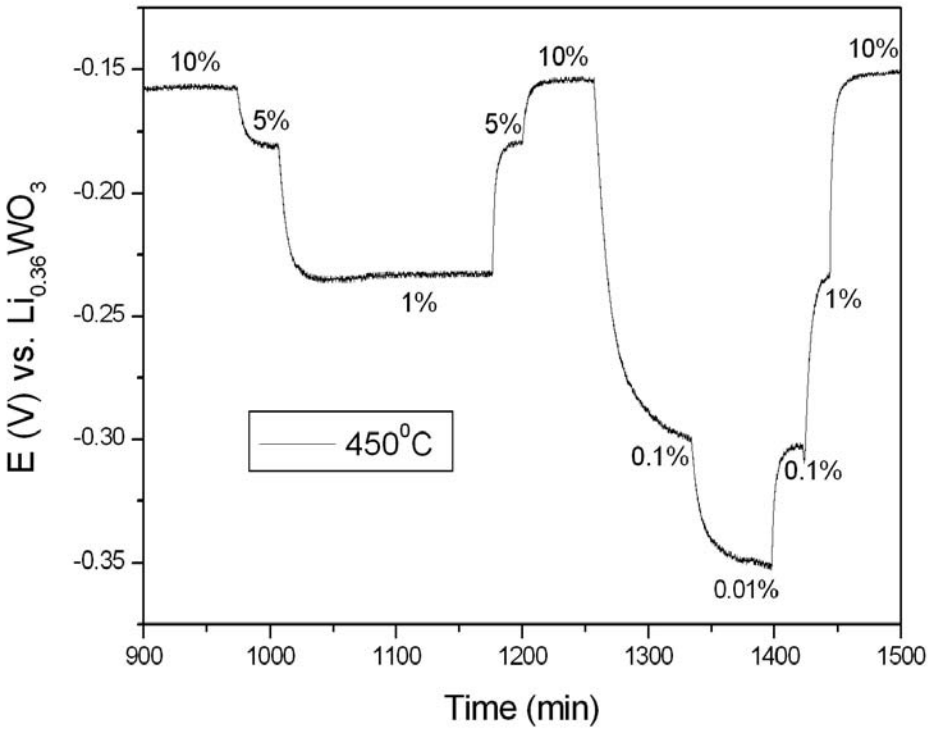

Figure 5.25: Transient responses to the cell (5.13) upon changes to the CO_2 partial pressure at 450 °C.

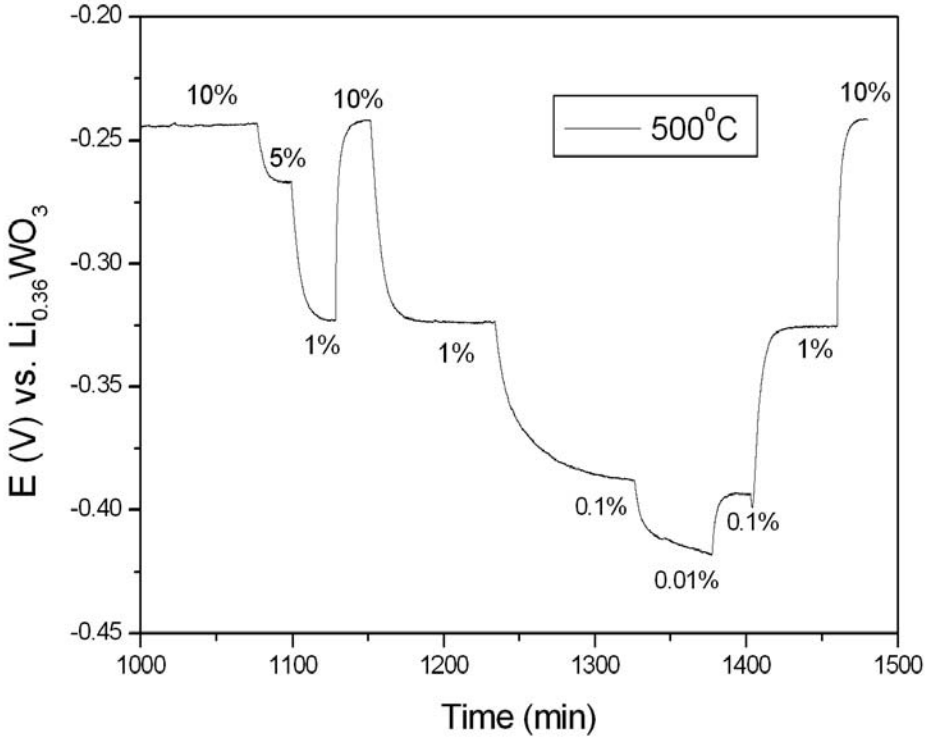

Figure 5.26: Transient responses to the cell (5.13) upon changes to the CO_2 partial pressure at 500 °C.

provides a value 1.9 at 450 °C and 2.0 at 500 °C. During operating the cell at elevated temperatures, impedance spectroscopy was applied. The complex impedance was measured in the frequency range from 5 Hz to 13 MHz employing a sinusoidal perturbation with 100 mV amplitude under 10^{-2} atm CO_2. The frequency dispersion in the impedance plots consists of a semicircle with its value on the real axis to be the interfacial resistance. Figure 5.27 shows the complex impedance plots at 450 °C and 500 °C. The interfacial conductivities were 3.8 x 10^{-5} S / cm at 450 °C and 2 x 10^{-4} S / cm at 500 °C. The corresponding interfacial capacitances as evaluated from the complex impedance plots were 11 nF and 13 nF at 450 °C and 500 °C, respectively. The response time t_{90} is within 1 min at measuring temperatures. The long term stability test of several cells showed after aging of the sensors, further shift of the absolute value of the open circuit voltage between 2 –8 mV per month independently on the sealing qualities of the ceramic glue.

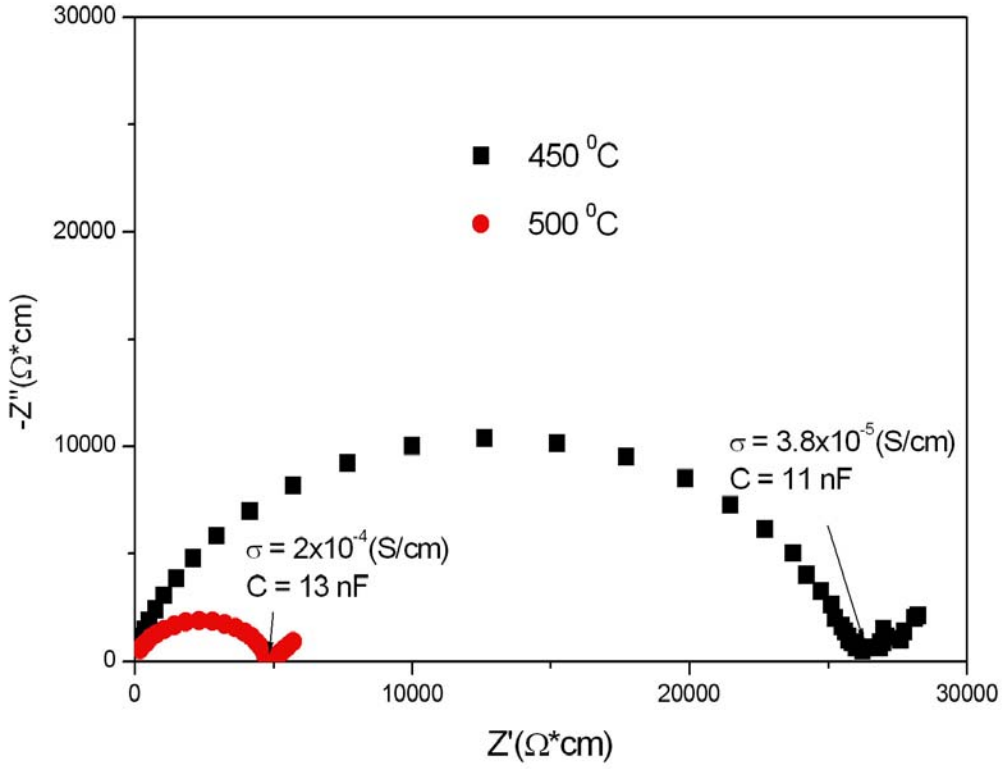

Figure 5.27: Complex plane impedance plots of the cell (5.13) at 450 °C and 500 °C.

5.2.5 $LiMn_2O_4$ as reference electrode

The results of investigation of electrochemical cells with $LiMn_2O_4$ reference electrode and Li_2CO_3 mixed with Au as auxiliary compound under CO_2 atmospheres are presented in this paragraph. The experimental cell which is schematically shown in figure 4.3 may be represented as:

$$Au, LiMn_2O_4 \mid Li^+ conductor \mid Au, Li_2CO_3, CO_2, O_2 \qquad (5.14)$$

LiSiPO and Garnet were used as electrolyte for lithium ions conductors. The cell assembly is shown in figure 4.3 in the experimental section.

(i) LiSiPO as electrolyte:

The cell was heated up to 450 °C initially with a heating rate of 6 °C / min at a CO_2 partial pressure of 10^{-2} atm. During the experimental process, the oxygen partial pressure was kept at 0.205 bar and the total gas flow rate was kept at 70 sccm / min. Figure 5.28 shows the transient responses of the cell (5.14) for various changes of the CO_2 concentration at 450 °C. The concentration of CO_2 gas changed from 1 % to 10 %, then from 1 % to 10 %, followed from 10 % to 0.1 %, then from 0.1 % to 10 %.

Subsequently, the cell was tested at 400 °C and 500 °C. The measured sensitivities of the cell (5.14) were 66 mV/dec (calculated sensitivity is 67 mV/dec) at 400 °C; 73 mV/dec (calculated sensitivity is 72 mV/dec) at 450 °C and 76 mV/dec (calculated sensitivity is 76 mV/dec) at 500 °C. The temperature variation of the sensitivity of cell (5.14) to CO_2 is shown in figure 5.29. The experimental points were evaluated from measurements of the steady state open circuit voltage vs. $\log P_{CO_2}$ at 400 °C, 450 °C and 500 °C, when the CO_2 partial pressure was varied between 10^{-3}– 0.1 atm. For comparison, the corresponding sensitivity according to Nernst's equation for a two – electron process is also shown. Complex impedance was measured in 10^{-2} atm CO_2 gas atmosphere with a perturbation amplitude of 100 mV while the frequency varied from 1 mHz to 50 kHz. This is shown in figure 5.30. The corresponding interfacial capacitances as evaluated from the complex impedance plots were 1.8 x 10^{-7} F at 450 °C and 2 x 10^{-7} F at 500 °C. The response time t_{90} is within 1 min at measuring temperatures. The long term stability test of several cells showed after aging of the sensors, a further shift of the absolute value of the open circuit voltage between 3 –10 mV per month independently on the sealing qualities of the ceramic glue.

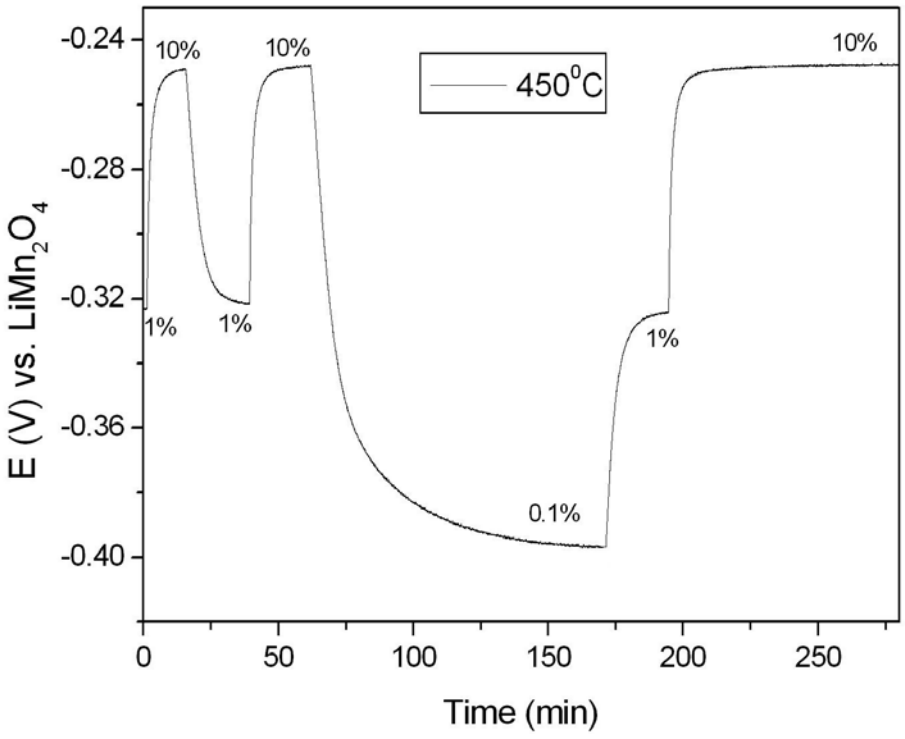

Figure 5.28: Transient responses to the cell (5.14) upon changes to the CO_2 partial pressure at 450 °C.

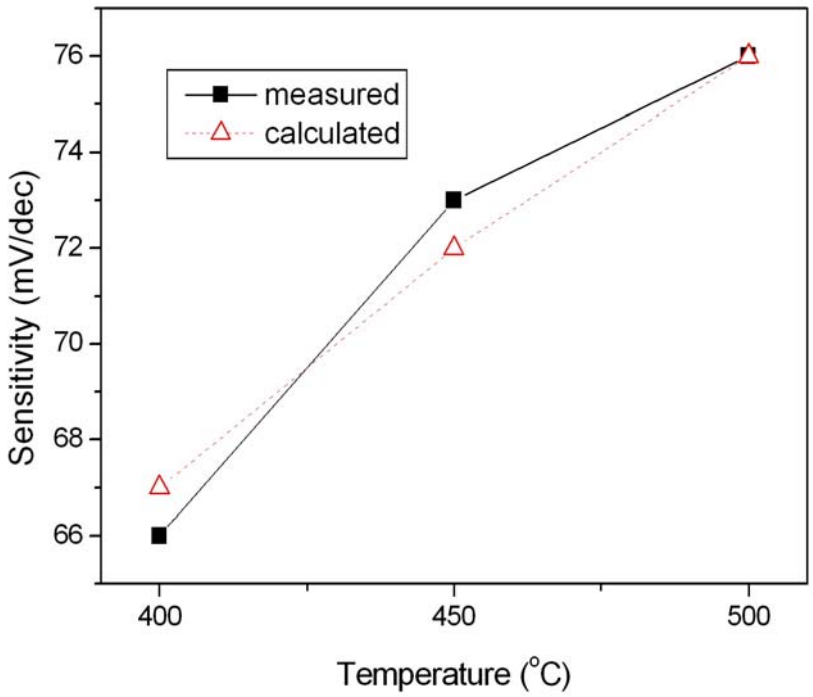

Figure 5.29: Temperature dependence of the sensitivity of cell (5.14) to CO_2. The calculated values for a two – electron process are plotted for comparison.

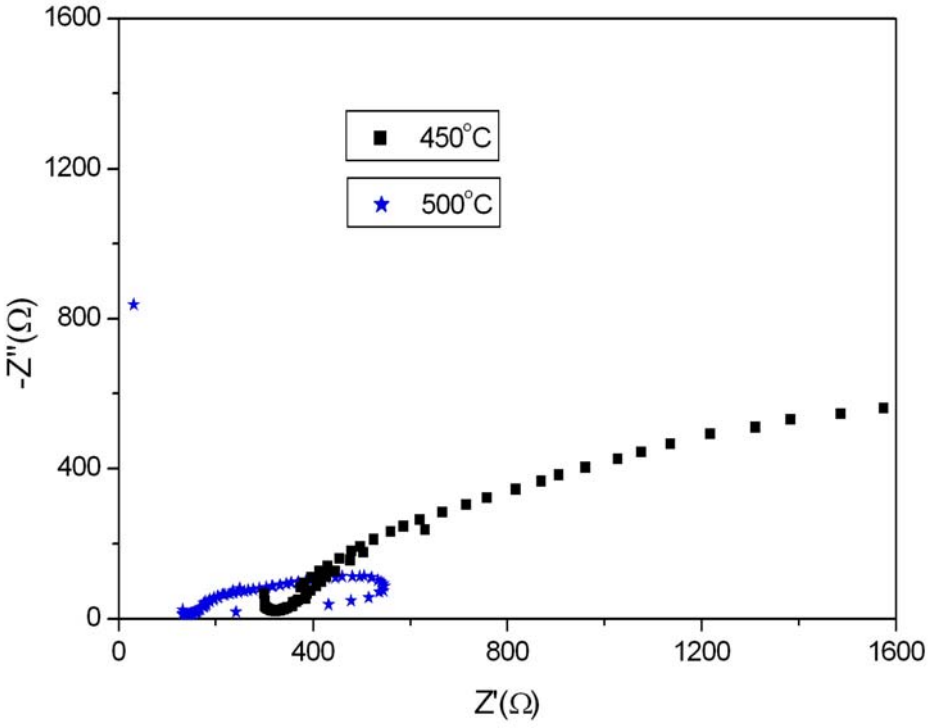

Figure 5.30: Complex plane impedance plots for cell (5.14) at 450 °C and 500 °C. The frequency range is from 1 mHz to 50 kHz.

(ii) Garnet as electrolyte:

The cell was heated up to 450 °C initially with a heating rate of 6 °C / min at a CO_2 partial pressure of 10^{-2} atm. During the experimental process, the oxygen partial pressure was kept at 0.205 bar and the total gas flow rate was kept at 70 sccm / min. Figure 5.31 shows the transient responses of the cell (5.14) with Garnet as electrolyte for various changes of the CO_2 concentration at 450 °C. The concentration of CO_2 gas changed from 1 % to 10 %, then from 10 % to 0.1 %, followed from 0.1 % to 10 %, then from 10 % to 1 %. Subsequently, the cell was tested at 500 °C. The measured sensitivities of the cell (5.14) with Garnet as electrolyte were 64 mV/dec (calculated sensitivity is 72 mV/dec) at 450 °C and 64 mV/dec (calculated sensitivity is 76 mV/dec) at 500 °C. The sensitivity to CO_2 translated to the number of electrons involved in the cell reaction, provides values of 2.2 at 450 °C and 2.4 at 500 °C. During operating the cell at elevated temperatures, impedance spectroscopy was applied. The complex impedance was measured over the frequency range from 5 Hz to 13 MHz employing a sinusoidal perturbation with 100 mV amplitude under 10^{-2} atm CO_2. The frequency dispersion in the impedance plots consists of a semicircle with its value on the real axis to be the interfacial resistance. This is shown in figure 5.32. The corresponding interfacial capacitances as evaluated from the complex impedance plots were 29 nF at 450 °C and 27 nF at 500 °C. The response time t_{90} is 1 -2 min at measuring temperatures. The long term stability test of several cells showed after aging of the sensors, a further shift of the absolute value of the open circuit voltage between 4mV and 15 mV per day independently on the sealing qualities of the ceramic glue.

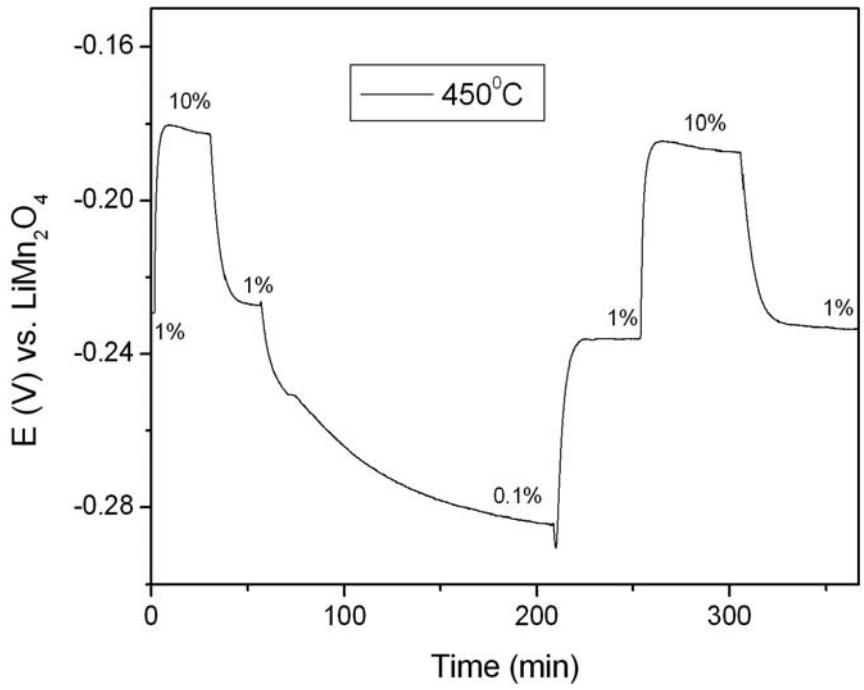

Figure 5.31: Transient responses to the cell (5.14) with Garnet as electrolyte upon changes to the CO_2 partial pressure at 450 °C.

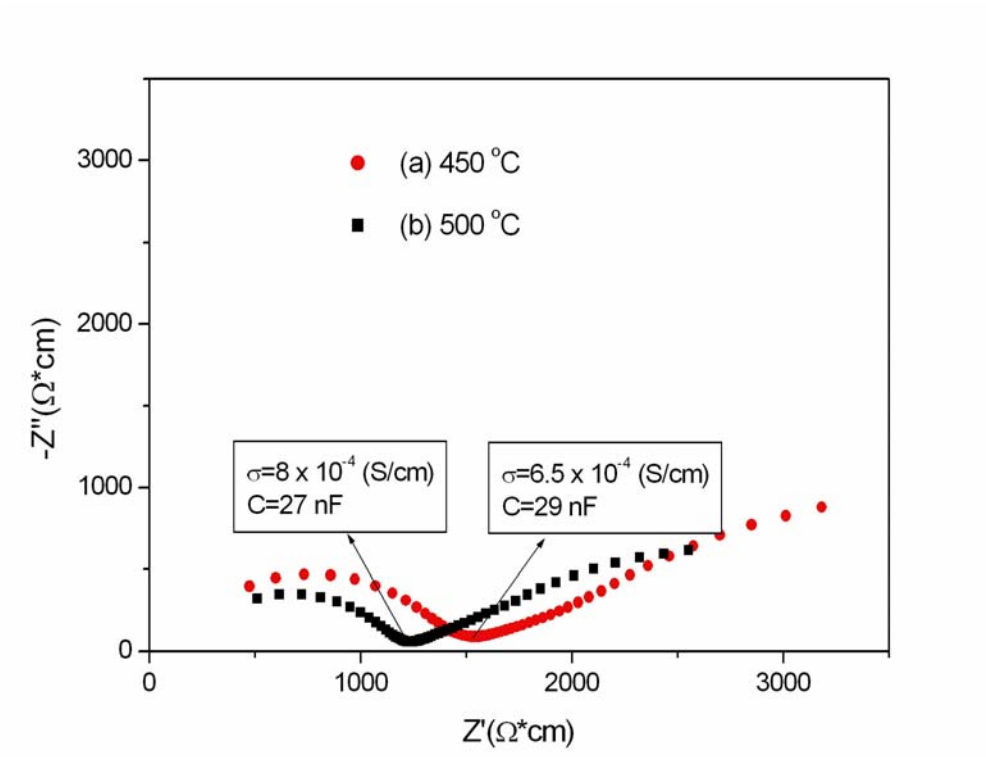

Figure 5.32: Complex plane impedance plots for cell (5.14) with Garnet as electrolyte at (a) 450 °C and (b) 500 °C. The frequency range is from 5 Hz to 13 MHz.

5.2.6 3PE ($LiMn_2O_4$ - Li_2MnO_3 - $LiMnO_2$) as reference electrode

This paragraph presents the results on the investigation of the electrochemical cell with $LiMn_2O_4$ - Li_2MnO_3 - $LiMnO_2$ (abbreviated by 3PE) reference electrode under CO_2 atmosphere. The electrochemical cell under investigation, which is schematically shown in figure 4.3, is written as:

$$3PE, Au \mid LiSiPO \mid Li_2CO_3, Au, CO_2, O_2 \qquad (5.15)$$

The molar ratio of $LiMn_2O_4$: Li_2MnO_3 : $LiMnO_2$ is 0.74 : 0.173 : 0.087. The mixture has a highly content of $LiMn_2O_4$ which has good electronic conductivity. Figure 5.33 shows the Arrhenius plot of 3PE from 40 °C to 450 °C. For comparison, the electronic conductivities of $LiMn_2O_4$ is also shown in figure 5.33. The activation energy for 3PE is 0.36 ± 0.02 eV and for $LiMn_2O_4$ is 0.34 ± 0.17 eV.

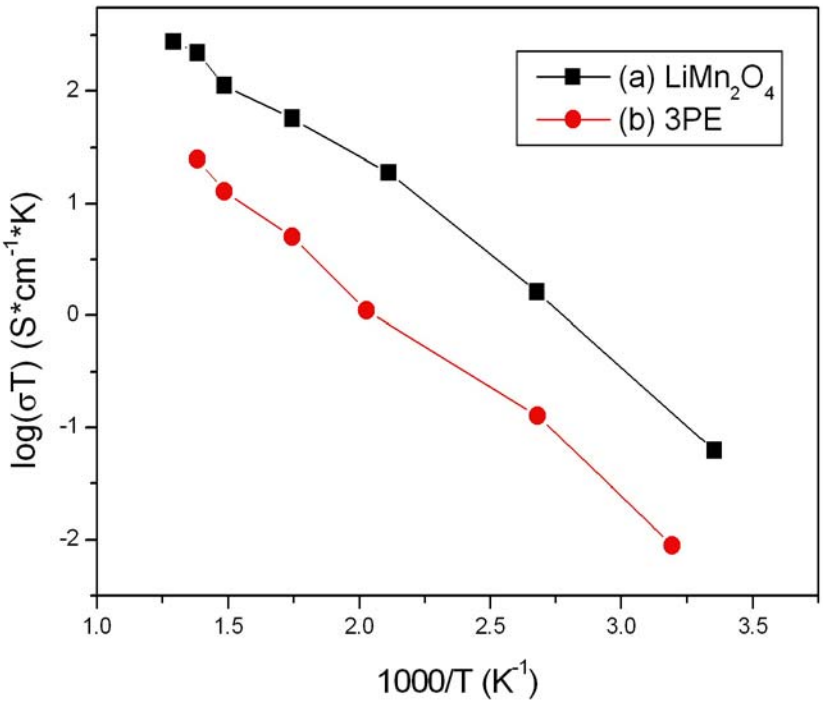

Figure 5.33: Arrhenius plot of $LiMn_2O_4$ - Li_2MnO_3 - $LiMnO_2$ (3PE) from 40 °C to 450 °C. (a) $LiMn_2O_4$ for comparison and (b) represents 3PE.

The cell (5.15) was heated up to 500 °C initially with a heating rate of 6 °C / min at CO_2 partial pressure of 10^{-2} atm. The oxygen partial pressure was always kept at 0.205 bar and the total gas flow rate was kept at 70 sccm / min. Figure 5.34 shows the transient responses of the cell (5.15) for various changes of the CO_2 concentration at 500 °C. The concentration of CO_2 gas was changed from 10 % to 1 %, then from 1 % to 10 %, then from 10 % to 0.1 %, then from 0.1 % to 1 % following to 10 %, at finally from 10 % to 1 %. The cell was also tested at 450 °C. The measured sensitivities of the cell (5.15) were 70 mV/dec (calculated sensitivity is 72 mV/dec) at 450 °C and 76 mV/dec (calculated sensitivity is 76 mV/dec) at 500 °C. The sensitivity to CO_2 translated to the number of electrons involved in the cell reaction, provides a value 2.1 at 450 °C and 2.0 at 500 °C. During operating the cell at variable times, impedance spectroscopy was applied. The complex impedance was measured over the frequency range from 5 Hz to 13 MHz employing a sinusoidal perturbation with 100 mV amplitude under 10^{-2} atm CO_2. The vales at days 3 –19 when the cell remain under open circuit voltage at 500 °C are shown in figure 5.35. The frequency dispersion in the impedance plots consists of a semicircle with its value on the real axis which are interpreted as interfacial resistance. The corresponding interfacial capacitances as evaluated from the complex impedance plots were 21 nF at day 3 and 9.4 nF at day 19. The response time t_{90} is within 1 min at measuring temperatures. The cell was kept measuring at 500 °C in 1 % CO2 concentration for open circuit voltage for 20 days. The long term stability test of the cell (5.15) is shown in figure 5.36. Further shift of the absolute value of the open circuit voltage between 3mV and 10 mV per month independently on the sealing qualities of the ceramic glue.

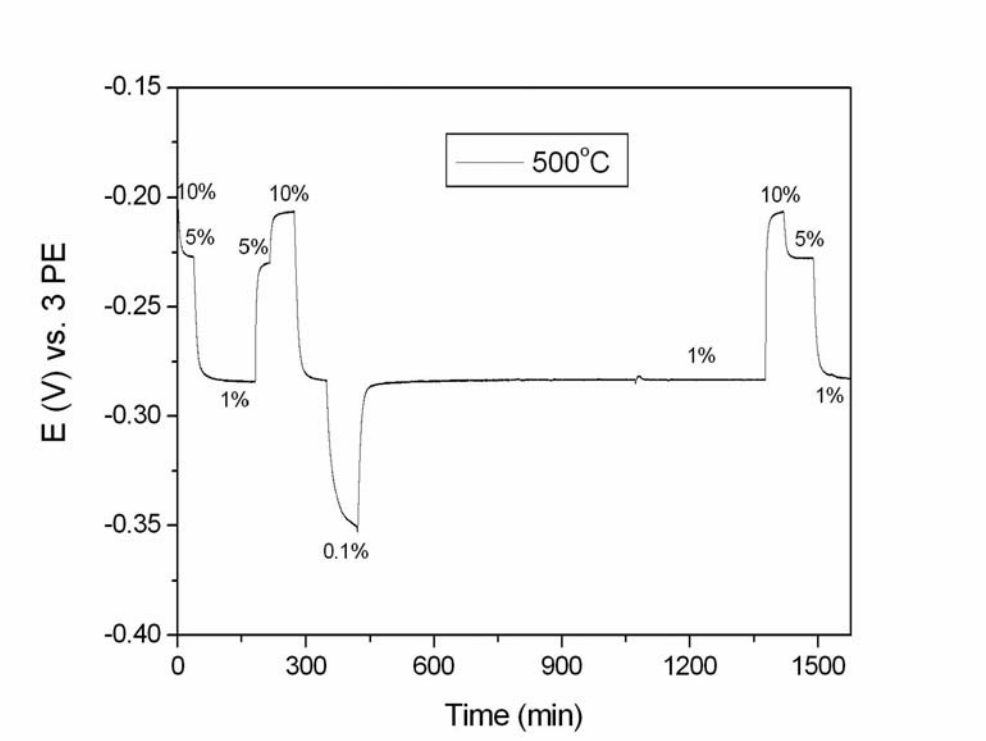

Figure 5.34: Transient responses to the cell (5.15) upon changes to the CO_2 partial pressure at 500 °C. The range of CO_2 partial pressure is from 10^{-3} atm to 0.1 atm.

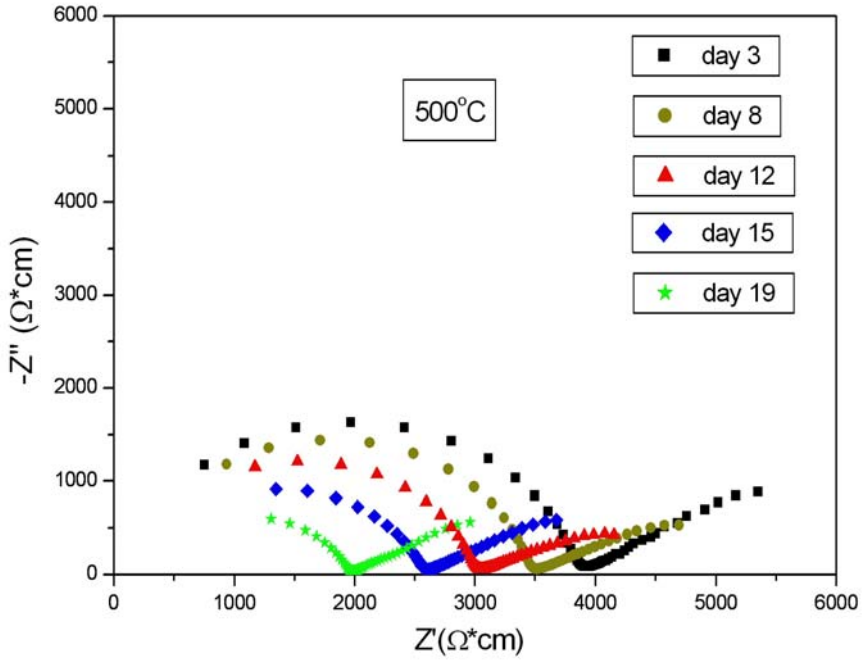

Figure 5.35: Complex plane impedance plots for the cell (5.15) for different times at 500 °C under CO_2 partial pressure of 10^{-2} atm.

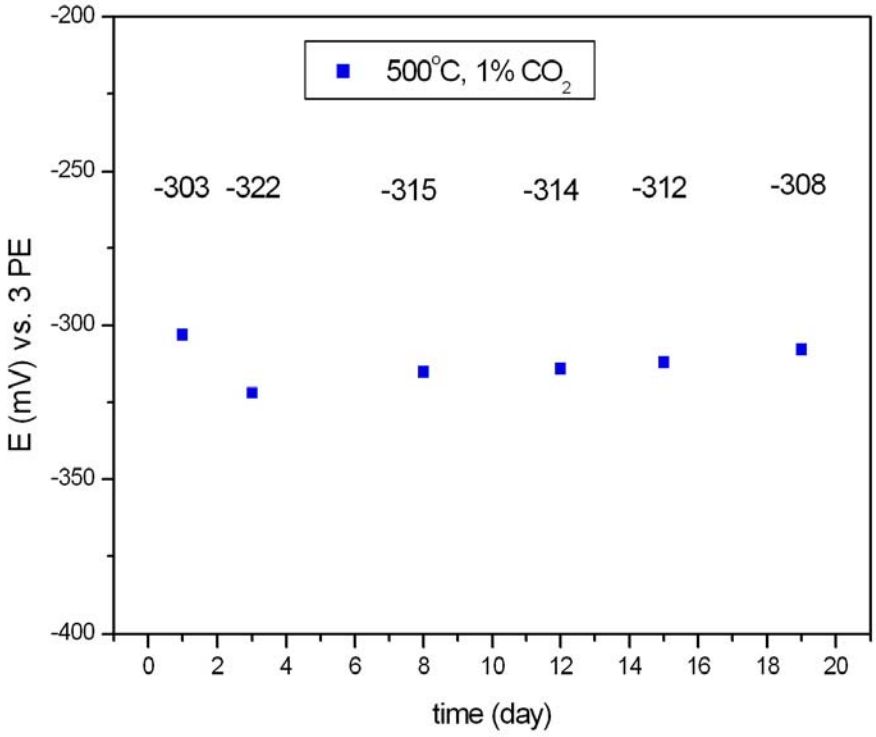

Figure 5.36: The long time stability test for cell (5.15) at 500 °C, 1 % CO_2 for 20 days.

References to Charpter 5

[1] Y – W. Hu, I. D. Raistrick, and R. A. Huggins, *J. Electrochem. Soc.* **8**, 1240 – 1242 (1977).

CHAPTER 6

Discussion

6.1 Discussion on the sensing electrode

When the electrolyte is initially just covered with a porous electronic lead, such as Au, the sensing reaction starts at the triple phase boundary (TPB). This process involves oxygen and carbon dioxide from the gas phase as schematically represented in figure 6.1. This process may be split into the following steps:

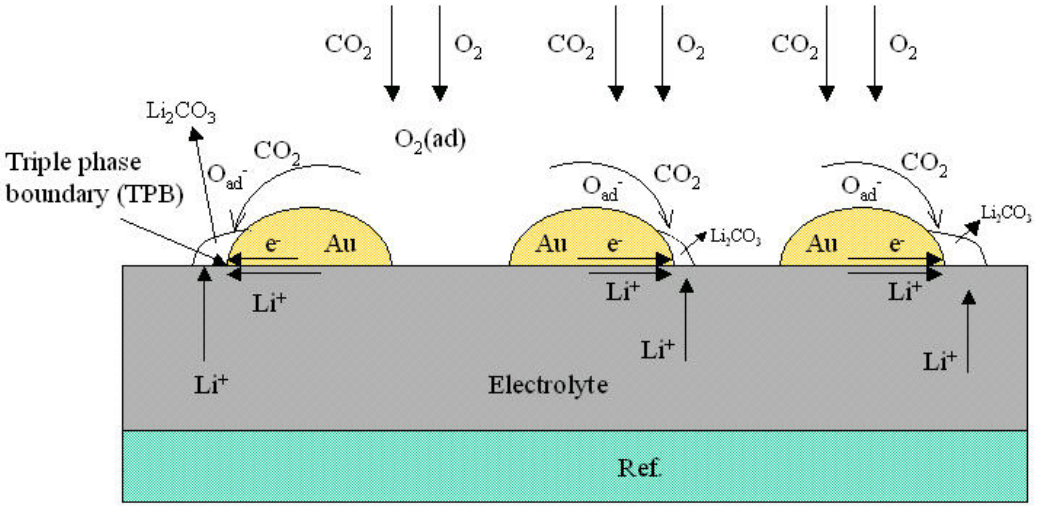

Figure 6.1: Schematic representation of the galvanic cell reaction of the formation of Li_2CO_3 in a CO_2 sensor.

(a) Oxygen and carbon dioxide diffusion in the gas phase or along the surface of Au and the uncovered surface area of the electrolyte.

(b) Transfer of electrons from the gold to form CO_3^{2-} from O_2 and CO_2.

(c) Migration of lithium ions in the electrolyte to the triple phase boundary and formation of Li_2CO_3.

Assuming that a sufficiently thick layer of Li_2CO_3 is present. There are several possible reasons causing the delay in the response to the sensing gas upon abrupt changes of the gas partial pressure:

- Chemical equilibration between the sensing gas and Li_2CO_3 layer delayed.
- The surface activity of the detectable gaseous species only slowly equilibrated with the interface lithium electrolyte / Li_2CO_3 by slow diffusion of lithium ions.
- When Au is in contact with the electrolyte, the interface is locally not uniform, i.e. the lithium activity shows a gradient along the interface.

Li_2CO_3 has a low ionic conductivity in the general working temperature range. A volume ratio 6 : 4 of Li_2CO_3 powder and Au paste was mixed as sensing electrode to enhance the electrical conductivity, thus permitting faster equilibration. The conductivity of pure Li_2CO_3 sample is 10^{-4} S/cm [1] and that of LiSiPO is 0.1 S/cm at 400 °C. The conductivity of cell (5.1) is 2.4 x 10^{-4} S/cm at 400 °C. The sensitivity of cell (5.1) agrees within the experimental error with the calculated one from Nernst's equation for a two – electron process. The sensitivity to CO_2 translated to the number of electrons involved in the galvanic cell reaction, provides values of 1.95, 1.95, 1.94 at 200 °C, 300 °C, 400 °C, respectively. The differences may originate from the lack of thermodynamic equilibrium at the sensing electrode is not achieved instantaneously. The sensing electrode reaction (3.87) requires the reaction of lithium ions from the electrolyte, electrons from the electronic lead, carbon dioxide from the gas phase and oxygen from a dissociated oxygen molecule in the gas phase, in a single reaction step [2]:

$$2Li^+ + 2e^- + \frac{1}{2}O_2 + CO_2 \rightarrow Li_2CO_3 \qquad (6.1)$$

At lower temperatures this reaction is not kinetically favorable and intermediate products with less negative Gibbs energies of formation may be formed. Only the reaction step that involved electrons from the metallic conductor contributes to the cell voltage. Purely chemical reactions at the interface occurring electrolyte - gas do not contribute. This may cause the sluggish response, especially at lower temperatures, where the formation of lithium carbonate is impeded by slow electrode kinetics. The sensitivity to carbon dioxide increased gradually with temperature suggesting that the formation of lithium carbonate is kinetically favorable only at high temperature whereas at intermediate or low temperatures the intermediate compound lithium oxide is formed at the measuring side:

$$2Li^+ + 2e^- + \frac{1}{2}O_2 \rightarrow Li_2O \qquad (6.2)$$

Li_2O reacts further with CO_2 to form Li_2CO_3 without involving electrons as shown in equation (6.3):

$$Li_2O + CO_2 \rightarrow Li_2CO_3 \quad (6.3)$$

At 450 °C, the calculated open circuit voltage of Li_2CO_3 versus elemental Li from Barin's literature data [3] is 3087mV, 3015 mV and 2943mV under 10^{-1}, 10^{-2} and 10^{-3} atm CO_2 in air, respectively. An open circuit voltage of $LiMn_2O_4$ versus elemental Li was measured to be 3325 mV at 450 °C. An open circuit voltage for the formation of Li_2O versus elemental Li [3] was calculated to be 2590 mV at 450 °C. This is shown in figure 6.2. If we compare the measured open circuit voltage of cell (5.14) at 450 °C in figure 5.27 with the calculated values in figure 6.2, we can conclude the reaction of CO_2 and O_2 occurs in one step at 450 °C and no intermediate compound Li_2O is being formed, as shown in figure 6.3. When Miura et al. [4] constructed sensors based on MgO – ZrO_2 (MSZ) as electrolyte and Li_2CO_3 as sensing electrode, he assumed Li_2ZrO_3 was formed between the sensing electrode and electrolyte, in the course of the galvanic cell reaction of the mobile Li^+, electrons and ZrO_2. Thermodynamic data are in good agreement with the experimental data, while large discrepancies result when the formation of Li_2O is assumed. Lee et al. [5] reported that when the CO_2 concentration is changed from 500 ppm to 50 % with fixed 10 % O_2 at 500 °C, Li_2CO_3 is thermodynamically stable and does not decompose at this temperature. Then, Li_2O formation is not responsible for the observed deviation from the Nernst equation at 500 °C. This is contrary to the studies with Na_2CO_3 electrode [6-8], explaining the deviation due to the presence of a Na_2O layer. In this work, when the mixture of the electrolyte (LiSiPO) and sensing electrode material (Li_2CO_3) with the molar ratio 1:1 was investigated through DTA measurement under 0.1 atm CO_2 atmosphere, there is no peak observed during heating and cooling time at the temperature range of 200-500 °C, which is the operating temperature range in this work. There is one peak at 720 °C during heating which is believed to be related to the decomposition of the molten Li_2CO_3 into CO_2 and Li_2O [9]. This is shown in figure 6.4. The observed final voltage values of cell (5.9), including error bars are lower than those calculated from Barin's literature data [3]. At 400 °C, a value of $-611.38\frac{kJ}{mol}$ is calculated while a value of $-594.15 \pm 5.42\frac{kJ}{mol}$ has been measured at 400 °C.

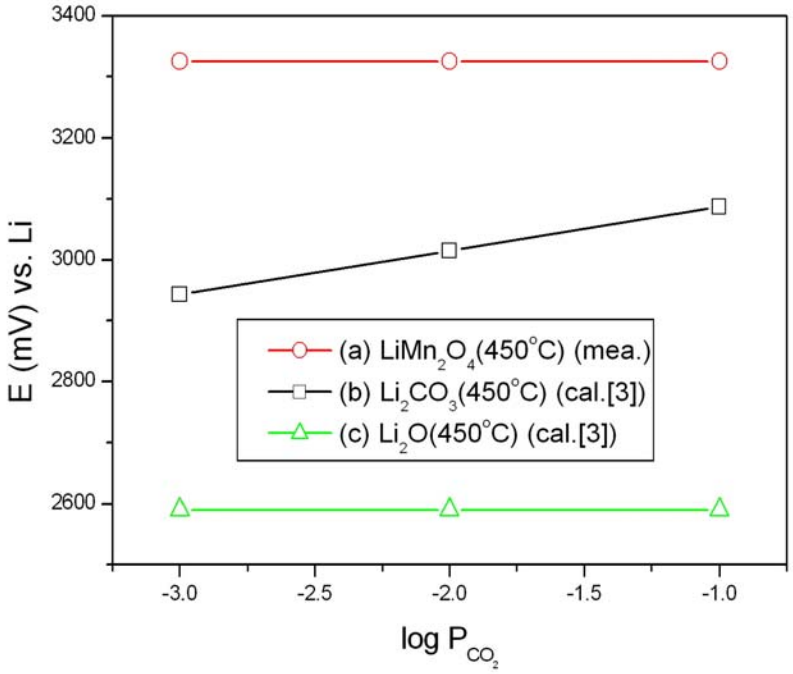

Figure 6.2: At 450 °C, the open circuit voltage of (a) $LiMn_2O_4$ measured in glove box, (b) Li_2CO_3 calculated according to [3] and (c) Li_2O calculated according to [3] versus elemental lithium.

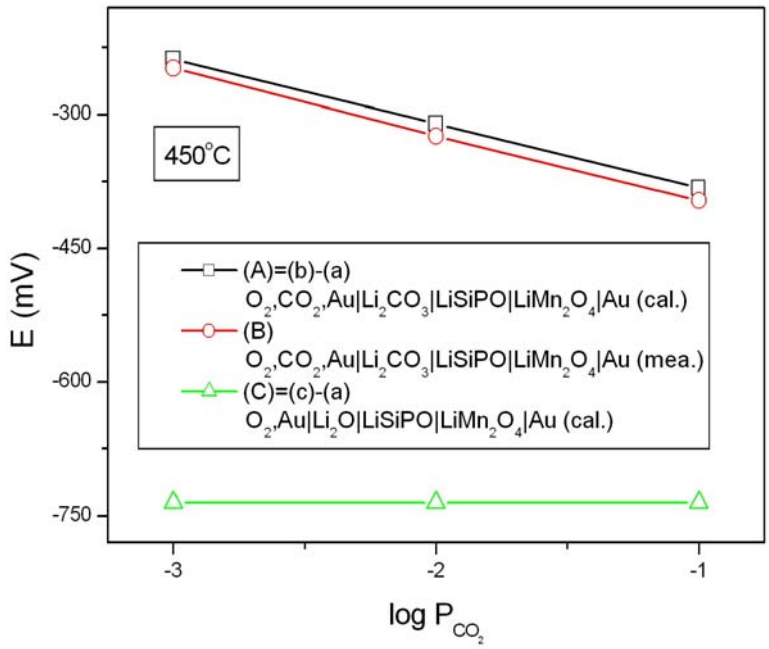

Figure 6.3: Comparison of the values in figure 6.2. (A) represents the calculated emf of Li_2CO_3 versus $LiMn_2O_4$, (B) represents the measured emf of the cell (5.14) and (C) represents the calculated emf of Li_2O versus $LiMn_2O_4$.

To see whether the temperature measurement error has an effect on this discrepancy, the variation of Gibbs energy of formation with temperature was compared with the experimentally observed values. Such a comparison yields: $318.63\frac{J}{K \cdot mol}$ from the literature [3] and $343.48 \pm 2.01\frac{J}{K \cdot mol}$ for the experimental values. The corresponding uncertainty would be about 25 K. From the above comparison, the discrepancy is due to incomplete equilibration at the sensing electrode and temperature uncertainties.

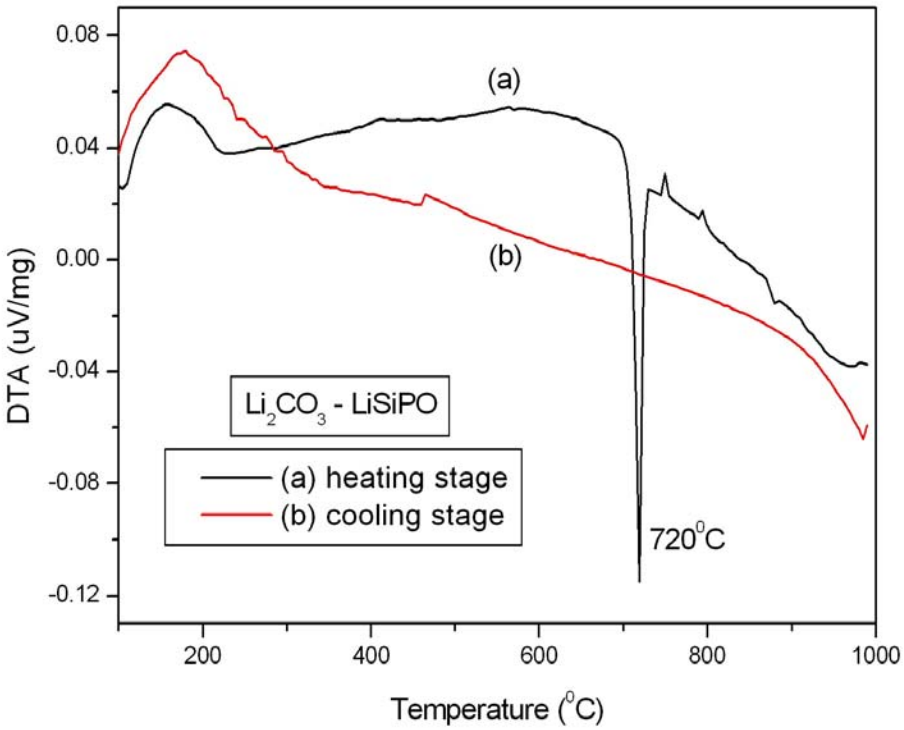

Figure 6.4: Differential thermal analysis (DTA) of Li_2CO_3 – LiSiPO mixture under 0.1 atm CO_2 atmosphere. The mixture was heated and cooled with a rate of 2 K/min. (a) represents the heating stage and (b) represents the cooling stage.

6.2 Discussion on reference electrodes

The calculation of the cell voltage as a function of the CO_2 partial pressure involves thermodynamic data for the gas sensitive Li_2CO_3 compound and the reference electrodes. The thermodynamic data of the Li_2CO_3 sensing electrode have been discussed in section 6.1. Regarding the performance of the cells in section 5.2, the open circuit voltage is lower than the calculated one using thermodynamic properties of the sensing electrode and measured value of the reference electrode. The results of the impedance spectroscopy suggest a reaction between the electrolyte and the solid reference electrodes at elevated temperatures. That is proposed to explain the discrepancy between calculated and observed values of the cell measurements presented in section 5.2. The formation of a new blocking phase in - between the reference electrode and the electrolyte introduces a change in the interface, which is therefore not well defined and thus does not allow to establish a constant potential. At 450 °C, the calculated open circuit voltage of Li_2CO_3 versus elemental Li is 3015 mV under 10^{-2} atm CO_2 and the measured open circuit voltage of $LiMn_2O_4$ versus elemental Li is 3025 mV in the glove box. The measured open circuit voltage of the cell (5.14) at 450 °C under 10^{-2} atm CO_2 is –320 mV in figure 5.28 compared with – 10 mV (3015-3025 mV) of the experimental results which was investigated in the glove box. A similar observation was reported by Zhang [10]. In order to avoid the reaction between the electrolyte and reference electrode a dense Li^+ conducting glass ceramics pellet was used. The measured and calculated open circuit voltage at 500 °C shows a difference of around 60 mV. But this reaction develops with time dependent on the operating temperature. Figure 5.35 shows the impedance spectroscopy of the cell (5.15) at 500 °C under 10^{-2} atm CO_2 partial pressure. The aging time ranged from 3 to 19 days. The impedance spectra consist of a high – frequency semicircle and a low frequency tail. The corresponding interfacial capacitances were 21 nF at day 3 and 9.4 nF at day 19. The interfacial impedance is strongly dependent on the time of the heat treatment and the interfacial impedance decreased substantially with aging time. This is shown in figure 6.5. After the measurements with the complete cell, the ceramic glue showed several cracks, maybe due to mechanical stresses as a result of different thermal expansion between the reference electrode and the electrolyte during heat treatment. Compared to all reference electrodes, the electrolyte material LiSiPO has a rather large expansion coefficient which is 2.9 x 10^{-5} 1/K. These stresses result

in a crack formation. This is proposed to explain the relative poor reproducibility of cells. With regard to reference electrodes, an essential property is that the electrostatic potential should not change if the stoichiometry of the alkali species is slightly changed. When some cracks form, the gas will penetrate through the cracks and reduce or oxidize the reference electrode. This results in the changes of the electrostatic potential of reference electrodes.

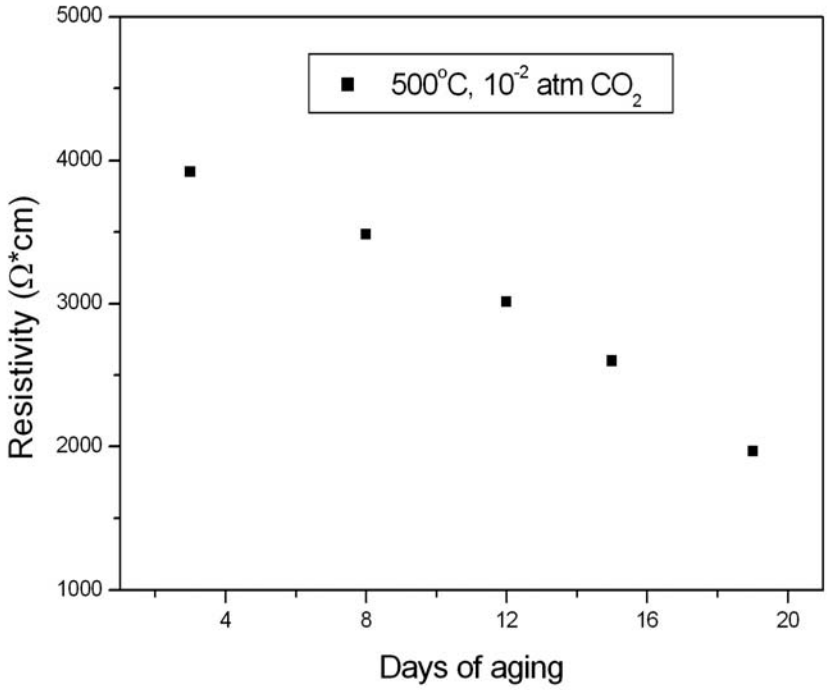

Figure 6.5: Changes of the interfacial resistivity of the cell (5.15) at 500 °C under 10-2 atm CO_2 partial pressure for 3, 8, 12, 15 and 19 day, respectively.

6.3 Discussion on cell performance

When the fresh cell was under evaluation, the emf has always been equilibrated for an initial period of time on average of 5 – 10 hours, it reached steady state value. Under the experimental conditions, the cell was short - circuited for 10 seconds, and the emf has recovered in 15 minutes. We assume that several monolayers were formed by the current. Porosity and cracks of the sealing material are considered to affect the lithium activity of the reference electrode because of the uptake of gas. In this case, oxygen can diffuse through the cracks and porosities until a steady state is

reached. The activity of the lithium ions will decrease or increase according to the change of the oxygen activity. In order to get good contact between electrode and electrolyte pellets, they were always polished to the μm roughness range. During aging, the contact between the electrode and electrolyte was improved considerably. This was observed when electrode and electrolyte were separated after some time and the total conductivities increased with aging time. This phenomena was also reported by Song et al. [11]. This better contact between electrode and electrolyte results in enhanced interfacial adherence and improved charge transfer kinetics. The decrease of the cell resistivity, as shown in figure 6.5, may be due to this reason. The other possible reason for the differences in the emf between the calculated and experimentally observed ones can be a mixed ionic and electronic conduction of the electrolyte. If the electrolyte is not a perfect ionic conductor, the mass transport of lithium occurs in the electrolyte due to a gradient of the chemical potential between the sensing and the reference electrode [12]. Therefore, the lithium activities at the electrodes are important because the leakage current during mass transport through the electrolyte induces the deviation from the Nernst emf. When the equilibrium was reached during the aging processes, the cell has achieved a steady state.

Comparing all the cells, which were used in this work, they all show good sensitivities. Only at 300 °C, when HgLi was used as reference electrode and LiSiPO as electrolyte, and at 500 °C, when $LiMn_2O_4$ was employed as reference electrode and Garnet as electrolyte, Z=2.42 and Z=2.40 were observed, respectively. Cells with $Li_4Ti_5O_{12}$ as reference electrode and LiSiPO as electrolyte showed relatively good sensitivities at 10^{-4} to 10^{-2} atm CO_2, but the response time is slower than the cells in which $LiMn_2O_4$ works as reference electrode. The cell with 3PE as reference electrode and LiSiPO as electrolyte also shows rather fast response time. Comparing all sensors, which were evaluated in this work, $LiMn_2O_4$ reference electrode and LiSiPO as electrolyte has shown the best performance. The comparison is shown in Table 6.1.

Electrolyte	Ref. Electrode	T (°C)	Exper. Sensitivity (mV/dec)	Z	Calcu. Sensitivity (mV/dec)	CO_2 Range (atm)	Resp. Time (min)
LiSiPO	$Li_4Ti_5O_{12}$	400	65.8	2.03	67	10^{-3}-10^{-2}	2-3
		450	70	2.05	72	10^{-4}-10^{-2}	1-2
		500	76	2.00	76	10^{-4}-10^{-2}	~1
	HgLi	300	47	2.42	56	10^{-2}-0.2	2-3
		350	57	2.17	62	$5x10^{-3}$-0.2	2-3
		400	63	2.12	67	10^{-3}-0.5	1-2
	3PE	450	70	2.05	72	10^{-2}-10^{-1}	<1
		500	76	2.00	76	10^{-3}-10^{-1}	<1
	$LiMn_2O_4$	400	66	2.02	67	10^{-3}-10^{-1}	~1
		450	73	1.96	72	10^{-3}-10^{-1}	<1
		500	76	2.00	76	10^{-3}-10^{-2}	<1
Garnet	$LiMn_2O_4$	450	64	2.24	72	10^{-3}-10^{-1}	1-2
		500	64	2.40	76	10^{-3}-10^{-1}	1-2
	$Li_{0.36}WO_3$	450	73	1.96	72	10^{-4}-10^{-1}	1-2
		500	75	2.02	76	10^{-4}-10^{-1}	~1

Table 6.1: Comparison of the cells which were used in this work.

References to Charpter 6

[1] Z.Y.Can, H.Tagawa, S.Asakura, J.Mizusaki and M.Narita, *J. Electrochem. Soc.,* **144**, 4345 (1997)

[2] E.D.Tsagarakis, W.Chu, T.Metzing and W.Weppner, Solid State Ionics Devices II Ceramic Sensors, pp. 270-284, Proceedings of the 198th Electrochemical Society Meeting, Phoenix, Arizona, USA (2000)

[3] I.Barin, Thermochemical Data of Pure Substances, VCH, Weinheim – New York (1993)

[4] Norio Miura, Yongtie Yan, Masaki Sato, Sheng Yao, Seijiro Nonaka, Youichi Shimizu, Noboru Yamazoe, *Sensors and Actuators B,* **24-25**, 260-265 (1995)

[5] Chonghoon Lee, Prabir K. Dutta, Ramasamy Ramamoorthy, Sheikh A. Akbar, *J. Electrochem. Soc.,* **153** (1) H4-H14 (2006)

[6] Y.Sadaoka, Y.Sakai, and T.Manabe, *Sens. Actuators B*, **13-14**, 532 (1993)

[7] M.Alonso-Porta and R.V.Kumar, *Sens. Actuators B,* **71**, 173 (2000)

[8] J.Ramirez-Salgado and P.Fabry, *Solid State Ionics,* **158**, 297 (2003)

[9] B.G.Kale, *Indian J. of Pure and Appl.Phys.,* **29**, 738 (1991)

[10] Y.C.Zhang, M.Kaneko, K.Uchida, J.Mizusaki and H.Tagawa*, J. Electrochem. Soc.,* **148** (8) H81-H84 (2001)

[11] Scung-Wan Song, L.Peter Martin, Robert S. Glass, Erica P. Murray, Jaco H. Visser, Richard E. Soltis, Robert F. Novak and David J. Kubinski*, J. Electrochem. Soc.*, **153** (9) H171-H180 (2006)

[12] C.O.Park, C.Lee, S.A.Akbar, J.Hwang, *Sensors and Actuators B,* **88**, 53-59 (2003)

CHAPTER 7

Summary and Outlook

7.1 Summary

Solid state electrochemical sensors are attractive because the chemical quantities, which are measured, are directly transduced in electrical signals and the responses obey thermodynamic laws. All solid state electrochemical sensors require a combination of materials with appropriate electrical properties. These properties include electrolytes with predominantly ionic conduction and electrodes with mixed ionic – electronic conductivity. At the interface between the electrolyte and the electrodes, a junction forms generating strong electrical fields. The potential drop is within a narrow regime at the interface where both ions and electrons are equilibrating. Thus the performance of electrochemical gas sensors depends on the engineering of appropriate interfaces. The electrode reaction is based on the interaction of species from the galvanic cell and the gas phase. Under equilibrium conditions, thermodynamic laws provide the sensing properties of the sensor device. During the transition from one to another gas concentration, the kinetics of the interface solid – gas controls or limits the performance of the sensor. Type III Potentiometric sensors are particularly attractive because of large ranges of measuring gas pressure and no limitations for the materials with specific electrical properties at the desired operating temperatures. The essential precaution for potentiometric sensors is to use a very high input impedance of the measuring setup to avoid any polarization effect and any change in the internal reference system.

The equilibration of the interface between LiSiPO and Li_2CO_3 with Au paste plays a major role in the response behavior of the concentration cell. Using a constant oxygen partial pressure (0.205 bar), the concentration cell showed good agreement with Nernst's laws under different CO_2 partial pressure at the measuring temperatures. The experimental results show that Li_2CO_3 with Au paste sensing electrode worked well for detecting CO_2 gas.

While concentration cell are based on the formation of the interface between LiSiPO and Li_2CO_3 with Au paste, different types of interfaces (solid – gas and solid -

solid) were employed. The engineering of junction formation and the electrode kinetics with respect to gas sensing has been investigated in electrochemical cells based on LiSiPO and Garnet electrolyte. The overall cell performance is a combination of processes occurring at the sensing and the reference side. It was shown that the kinetics at the interface between the gas and solid ionic conductor plays a major role with respect to the sensing characteristics under CO_2 atmospheres. Furthermore, the formation of interfacial compounds at both sensing and reference sides resulted in sluggish response times, deviations from the equilibrium cell voltage and voltage shifts with time.

7.2 Outlook

It has been shown that in type III potentiometric CO_2 sensors based on lithium ion conductors, Li_2CO_3 and Au paste form a proper sensing electrode. Further investigations should focus on the reference electrodes and preparation technology. Also cross sensitivity investigation should be done in the future. Multicomponent solid electrolytes which contain many elements show reactions with the cell electrodes in which also a variety of elements is present. Interfacial compounds of high thermodynamic stability or kinetically favorable ones are thus formed in between the electrolyte and the electrodes. Chemically stable interfaces are difficult but have to be achieved especially for long terms.

List of symbols

The following principal symbols have been used throughout in this work.

a_i	Activity of species i
$A_{i,}B_i$	Constant phase angle impedance coefficients
A	Electrode area
c_e	Concentration of electrons
c_i	Concentration of species i
C	Capacitance
C_{dl}	Overall double layer capacitance
C_D	Diffuse layer capacitance
C_g	Geometric capacitance
C_H	Helmholtz layer capacitance
d	Determinant of stoichiometric numbers, thickness
d_{ij}	Minor of determinant d
D_i	Diffusion coefficient of species i
$\tilde{D}_i$	Chemical diffusion coefficient of species i
D_i^T	Tracer diffusion coefficient of species I
E	Electromotive force (emf)
$\vec{E}$	Electrical field
E_F	Fermi energy
f_j	Correlation factor
F	Faraday's constant
G	Gibbs energy
ΔG_f^0	Standard Gibbs energy of formation
ΔH	Change in enthalpy
I	Electrical current
I_0	Exchange current density
J_i	Flux density of particle i
K	Ratio of adsorption to desorption specific rate constants
k	Boltzmann's constant
k_{ad}	Adsorption specific rate constant
k_{des}	Desorption specific rate constant
L	Diffusion length, inductance
L_{Deb}	Debye length
m_i	Mass of species i
M_i	Molecular weight of species i
n_i	Number of species i
P_i	Partial gas pressure of the component i

q	Electron charge
Q	Charge to form a monolayer of adsorbed intermediates
R	Gas constant, electrical resistance
S	Entropy
t	Time
T	Absolute temperature
t_i	Transference number of species i
u_i	Electrical mobility of species i
U	Applied voltage
U_0	Amplitude of applied voltage
$\vec{v}_i$	Mean velocity of particle i
V	Volume
W	Enhancement factor
x	Distance coordinate
$\vec{Y}$	Complex admittance
$\vec{Z}$	Complex impedance
Z'	Real part of complex impedance
Z''	Imaginary part of complex impedance
$\vec{Z}_w$	Complex Warburg impedance
α	Transfer coefficient
ε	Dielectric constant
ε_0	Permitivity of vacuum
η_i	Electrochemical potential of species i
θ	Surface coverage due to adsorption
μ_{e^-,h^+}	Chemical potential of electrons and holes, respectively
μ_i	Chemical potential of species i
μ_i^0	Chemical potential of species i in the standard state
ρ	Charge density
σ	Electrical conductivity
σ_i	Partial electrical conductivity of species i
τ	Relaxation time
$\upsilon_{ad}, \upsilon_{des}$	Adsorption – desorption rates
φ	Phase shift between input voltage and output current
ϕ	Electrostatic potential
ω	Angular frequency

Abbreviations

DTA	Differential thermal analysis
IAQ	Indoor air quality
ICP	Inductively coupled plasma
MAK	Maximale Arbeitsplatzkonzentration
MFC	Mass flow controller
SAW	Surface acoustic wave
SEM	Scanning electrons microscope
TGA	Thermogravimetric analysis
TPB	Triple phase boundary
YSZ	Yttria stabilized zirconia
XRD	X – ray diffraction

List of Figures

Figure 3.1: Schematic representation of the classification of electrochemical gas sensors.
Figure 3.2: Schematic arrangement of a type I gas sensor for measurement of the partial pressure of gas A.
Figure 3.3: Measurement of the partial pressure of gas B employing a type II gas sensor.
Figure 3.4: Schematic arrangement of a type III gas sensor for the measurement of partial pressure of gas C.
Figure 3.5: Principle of the limiting-current sensor.
Figure 3.6: Solid electrolytes as intermediate between normal crystalline solids and liquids [50].
Figure 3.7: Concentration profiles according to the solution of diffusion equation subjected to the conditions given above.
Figure 3.8: Complex plane representations of impedance and admittance vectors.
Figure 3.9: Equivalent circuits for the frequency dispersion of a solid ionic conductor with single time constant in between a) reversible (left-hand side) and b) blocking electrodes (right hand-side).
Figure 3.10: Complex plane representation of the impedance of the Randles equivalent circuit for the electrochemical interface.
Figure 3.11: a) The region $A_xB_yC_z$ of a hypothetic ternary phase diagram A-B-C is shown enlarged 1ϕ, 2ϕ and 3ϕ indicate one, two or three phase regions. and b) variation in the activity of species i along the path a to b to c to d.
Figure 3.12: Crystal structures of typical garnet $Y_3Fe_5O_{12}$. For clarity, the positions of Y in $Y_3Fe_5O_{12}$ is not shown [90].

Figure 4.1: Schematic representation of the apparatus for electrochemical measurements under defined temperature and gas mixtures.
Figure 4.2: Schematic representation of the electrochemical cell under investigation in carbon dioxide atmospheres.
Figure 4.3: Schematic representation of the electrochemical cell under investigation in carbon dioxide atmospheres.

Figure 4.4: Schematic representation of the electrochemical cell under investigation in carbon dioxide atmospheres.
Figure 4.5: Schematic illustration of the experimental setup.
Figure 4.6: Schematic representation of the experimental setup for investigations under carbon dioxide atmospheres.

Figure 5.1: X-ray diffraction of LiSiPO.
Figure 5.2: AC impedance spectra of LiSiPO both sides with Au paste electrodes in air at room temperature.
Figure 5.3: Arrhenius plot of the ionic conductivity of LiSiPO.
Figure 5.4: SEM picture of the interface between the electrode and the electrolyte.
Figure 5.5: Experimental and calculated EMF as a function of temperature at various CO_2 concentrations.
Figure 5.6: Experimental and calculated EMF as a function of $\Delta \ln P_{CO_2}$ at various temperatures.
Figure 5.7: Complex plane impedance plot of the gas concentration cell (5.1) at 400 °C.
Figure 5.8: CO_2 partial pressure dependence of the cell (5.9) to EMF vs. elemental Li. * represents calculated values of the cell (5.9).
Figure 5.9: Temperature dependence of the EMF of cell (5.9) to CO_2. * The calculated values for a two – electron process are plotted for comparison.
Figure 5.10: The reproducibility and long time stability measurement of the cell (5.9) at 400 °C at the CO_2 concentration from 100 ppm to 10^6 ppm.
Figure 5.11: XRD pattern of as – prepared $Li_4Ti_5O_{12}$. The vertical red lines represent PCPDF (49-0207) data for $Li_4Ti_5O_{12}$.
Figure 5.12: Arrhenius plot of $Li_4Ti_5O_{12}$ from room temperature to 500 °C. (a) represents heating data; (b) represents cooling data.
Figure 5.13: Transient responses to the cell (5.10) upon changes to the CO_2 partial pressure at 450 °C.
Figure 5.14: Open circuit voltage of the cell (5.10) vs. logarithm of CO_2 partial pressure at 450 °C.
Figure 5.15: Temperature dependence of the experimental sensitivity of cell (5.10) to carbon dioxide, in comparison to the calculated one.

Figure 5.16: Complex plane impedance plots of the cell (5.10) at 400 °C, 450 °C and 500 °C.
Figure 5.17: Complex plane impedance plots of the cell (5.10) during aging time at 450 °C.
Figure 5.18: Transient responses to the cell (5.11) upon changes to the CO_2 partial pressure between 100 ppm and 1000 ppm at 450 °C.
Figure 5.19: Open circuit voltage of cell (5.11) vs. logarithm of CO_2 partial pressure at 450 °C. (a) represents the experimental open circuit voltages from 100 ppm to 1000 ppm; (b) represents the linear fit of the experimental values and provides the experimental sensitivity of 69 mV/dec (calculated value is 72 mV/dec at 450 °C).
Figure 5.20: Transient response to the cell (5.12) upon changes to various concentrations of CO_2 gas at 400 °C.
Figure 5.21: Temperature dependence of the experimental sensitivity of cell (5.12) to carbon dioxide in comparison to the calculated one.
Figure 5.22: Complex plane impedance plots for the cell (5.12) at 400 °C, 350 °C and 300 °C.
Figure 5.23: X – ray powder diffraction of as prepared $Li_{0.36}WO_3$ powder which agrees well with the PCPDF data of 76 –1497.
Figure 5.24: Arrhenius plot of $Li_{0.36}WO_3$ between 25 °C and 400 °C. (a) represents heating stage and (b) represents cooling stage.
Figure 5.25: Transient responses to the cell (5.13) upon changes to the CO_2 partial pressure at 450 °C.
Figure 5.26: Transient responses to the cell (5.13) upon changes to the CO_2 partial pressure at 500 °C.
Figure 5.27: Complex plane impedance plots of the cell (5.13) at 450 °C and 500 °C.
Figure 5.28: Transient responses to the cell (5.14) upon changes to the CO_2 partial pressure at 450 °C.
Figure 5.29: Temperature dependence of the sensitivity of cell (5.14) to CO_2. The calculated values for a two – electron process are plotted for comparison.
Figure 5.30: Complex plane impedance plots for cell (5.14) at 450 °C and 500 °C. The frequency range is from 1 mHz to 50 kHz.
Figure 5.31: Transient responses to the cell (5.14) with Garnet as electrolyte upon changes to the CO_2 partial pressure at 450 °C.

Figure 5.32: Complex plane impedance plots for cell (5.14) with Garnet as electrolyte at (a) 450 °C and (b) 500 °C. The frequency range is from 5 Hz to 13 MHz.
Figure 5.33: Arrhenius plot of $LiMn_2O_4$ - Li_2MnO_3 - $LiMnO_2$ (3PE) from 40 °C to 450 °C. (a) $LiMn_2O_4$ for comparison and (b) represents 3PE.
Figure 5.34: Transient responses to the cell (5.15) upon changes to the CO_2 partial pressure at 500 °C. The range of CO_2 partial pressure is from 10^{-3} atm to 0.1 atm.
Figure 5.35: Complex plane impedance plots for the cell (5.15) for different times at 500 °C under CO_2 partial pressure of 10^{-2} atm.
Figure 5.36: The long time stability test for cell (5.15) at 500 °C, 1 % CO_2 for 20 days.

Figure 6.1: Schematic representation of the galvanic cell reaction processed for the formation of Li_2CO_3 in a CO_2 sensor.
Figure 6.2: At 450 °C, the open circuit voltage of (a) $LiMn_2O_4$ measured in glove box, (b) Li_2CO_3 calculated according to [3] and (c) Li_2O calculated according to [3] versus elemental lithium.
Figure 6.3: Comparison of the values in figure 6.2. (A) represents the calculated emf of Li_2CO_3 versus $LiMn_2O_4$, (B) represents the measured emf of the cell (5.14) and (C) represents the calculated emf of Li_2O versus $LiMn_2O_4$.
Figure 6.4: Differential thermal analysis (DTA) of Li_2CO_3 – LiSiPO mixture under 0.1 atm CO_2 atmosphere. The mixture was heated and cooled with a rate of 2 K/min. (a) represents the heating stage and (b) represents the cooling stage.
Figure 6.5: Changes of the interfacial resistivity of the cell (5.15) at 500 °C under 10-2 atm CO2 partial pressure for 3, 8, 12, 15 and 19 day, respectively.

List of Tables

Table 3.1: Basic electrical elements of equivalent circuit representation.

Table 5.1: Comparison of the slopes in different conditions.

Table 5.2: Comparison of the sensitivity at different temperature conditions.

Table 6.1: Comparison of the cells which were used in this work.

Physical constants

$F = 96485.3415$	C Mol^{-1}	Faraday's constant
$k = 1.38066 \times 10^{-23}$	J K^{-1}	Boltzmann's constant
$q = 1.60218 \times 10^{-19}$	C	Electron charge
$R = 8.314472$	J K^{-1} Mol^{-1}	Gas constant
$\varepsilon_0 = 8.85418 \times 10^{-12}$	F m^{-1}	Permittivity of vacuum